MILJØMINISTERIET

Miljøstyrelsen

Polymerer i anlæg med CO_2 som kølemiddel

Marcin B. Andreasen & Klaus Frederiksen
Teknologisk Institut

Nicolas von Solms, Jakob Kristensen & Vasu Neela
Institut for Kemiteknik
Danmarks Tekniske Universitet

Miljøprojekt Nr. 1278 2009

Indhold

Forord

I et forsøg på at finde kølesystemer med minimal miljømæssig påvirkning er CO_2 igen kommet i søgelyset. Det viser sig dog, at det er et problem at opretholde tætheden i køleanlæg med CO_2, idet polymerbaserede pakninger har en større evne til at optage CO_2 end traditionelle kølemidler. Selvom små lækager i CO_2-baserede køleanlæg ikke direkte udgør en fare for miljøet, kan de være årsag til driftsproblemer.

Baseret på projektgruppens erfaring er der udvalgt en række polymertype, hvis fysiske egenskaber er blevet undersøgt i dette projekt. Polymerernes styrke og CO_2 permeabiliteten gennem polymermaterialerne er blevet testet, med det formål at kunne afklare, hvilke polymer er bedst anvendelige i anlæg med CO_2.

Der er i projektet bygget en teststand med det formål at kunne måle polymerernes styrkeegenskaber, mens de er udsat i CO_2-miljøet (både under- og overkritisk). Desuden har Danmarks Tekniske Universitet, DTU, udlånt deres testfaciliteter, hvor opmåling af solubilitet og diffussivitet kunne foretages.

Projektet har modtaget økonomisk støtte fra Miljøstyrelsen, Kontoret for renere produkter.

Projektets organisation består af følgende:

Teknologisk Institut, Center for Køle- og Varmepumpeteknik
- Marcin B. Andreasen
- Klaus Frederiksen
- Lars Reinholdt

Danmarks Tekniske Universitet, Institut for kemiteknik
- Nicolas von Solms

Union Engineering
- Jan Flensted Poulsen

Johnsons Controls
- Alexander Cohr Pachai

Parker Hannifin Danmark A/S
- Dorthe Pedersen
- Christian Burmester

Danfoss A/S
- Niels Vestergaard

Der skal fra projektlederens side rettes en tak til projektgruppen og naturligvis til Miljøstyrelsen.

Marcin B. Andreasen
Projektleder
Teknologisk Institut, Center for Køle- og Varmepumpeteknik
September 2008

Sammenfatning og konklusioner

Formål med projektet

Formålet med projektet var at afklare, hvilke polymertyper (til både pakninger og konstruktionselementer), der er anvendelige i anlæg med CO_2 som kølemiddel, samt hvilke materialeparametre, der er kritiske i forhold til CO_2.

De testede polymertyper er blevet udvalgt på baggrund af projektdeltagernes erfaringer på området. Polymerernes styrke, solubilitet og diffusion er blevet testet med det formål at bestemme, hvilke polymertyper, der udviser mindst påvirkning i CO_2-miljøet, samt hvilke parametre (som tryk og temperatur), der påvirker polymererne mest. Selvom det er blevet påpeget af projektgruppen, at olien (foruden tryk og temperatur) også kan have indflydelse på polymerernes fysiske egenskaber, så har man valgt at se bort fra denne parameter.

Resultat af projektet

Der er blevet opbygget en forsøgsstand, hvor polymerernes brudstyrke kunne bestemmes i underkritisk og overkritisk CO_2. Brudstyrke er blevet bestemt på følgende polymermaterialer:

EPDM, FKM, HNBR, PTFE, PVDF, PEEK

Opløselighed og diffusion er blevet målt ved hjælp af højtryksvægten på følgende polymermaterialer:

EPDM, HNBR

Permeabilitet er blevet direkte målt ved hjælp af 2D permeationscelle på følgende polymermaterialer:

PTFE, PTFE + 10% Ekonol, PTFE + $PPSO_2$ + grafit,
FKM
TFM, TFM + 10% glas

Konklusion

Permeabilitet

På basis af permeabilitetsmålingerne kan man sige, at polymererne ligger i følgende rækkefølge fra ”bedst” til ”værst”, dvs. mindst permeabel til mest:

- TFM,
- PTFE,
- TFM + 10% glas,
- FKM,
- PTFE + 10% Ekonol,
- PTFE + $PPSO_2$ + grafit.

Der er dog ikke en stor forskel mellem de første fem. Den sidste (PTFE + $PPSO_2$ + grafit) er væsentligt værre end de øvrige fem. Endvidere kan man sige, at polymererne bliver mere permeable, når man tilsætter noget (fx glas, ekonol, grafit, $PPSO_2$).

Opløselighed og diffusion

Generel opløselighed af CO_2 i HNBR er omkring dobbelt så stor som i EPDM, derimod er diffusion ca. en størrelsesorden mindre. Selvom opløselighed er højere i HNBR, så er diffusionskoefficienten betydelig mindre, hvilket medfører at permeabiliteten er mindre i HNBR. Dette gælder for alle temperatur og tryk spand.

Polymerernes mekaniske egenskaber:

Alle testede elastomertyper (EPDM, FKM, HNBR) ser ud til at være kraftigt påvirket af CO_2. Fælles for dem alle var, at deres brudstyrke viste en stor afhængighed af både CO_2-temperatur og tryk. Brudforlængelsen for disse materialer ser ud til at falde, og det gør brudstyrken også. Ved overkritisk drift skal man forvente styrkereduktion med over 60 %. Litteraturstudiet har bekræftet måleresultaterne. Forsøgene udført i 1999 på University of Wales i Swansea i Storbritannien på fluorelastomer, silikoneelastomer og nitril viste samme tendenser dvs. faldende brudstyrke og brudforlængelse.

PTFE viste gode tendenser, idet dens brudstyrke så ud til at være stort set uafhængig af trykket. Derimod faldt brudstyrken, når CO_2-temperaturen blev øget.

PVDF og PEEK - Det har været svært at få gode resultater i hus for de to plastmaterialer pga. meget kort brudforlængelse især for PEEK. Dog var det betegnende for de to materialer (PVDF og PEEK) at deres egenskaber ændres ved højere tryk og temperatur, hvor brudforlængelsen bliver betydelig længere. PVDF-brudstyrken ser også ud til at være påvirket af både CO_2 tryk og temperatur.

1 Baggrund

1.1 Generelt om køleanlæg med CO_2

Anvendes CO_2 som kølemiddel i et køleanlæg vil processen afhænge af kondenseringstemperaturen. Ved temperaturer på under 31ºC kan CO_2 kondensere, og køleprocessen forløber som ved andre kølemidler (Carnot-processen), hvorimod der ved temperaturer over 31ºC blot kan køles på gassen. Denne proces kaldes transkritisk (Lorentz-processen).

- Figur 1 viser et h,log(p)-diagram med et konventionelt R134a kølesystem samt et CO_2-system ved transkritisk og underkritisk drift.
- Det ses, at CO_2-systemet ved samme høje og lave temperatur opererer ved et langt højere tryk end et R134a kølesystem.

I dag er der to typer CO_2-kølesystemer på markedet:

CO_2-kølesystemer, der kun kører subkritisk ved at kondenseringstemperaturen holdes under 31 ºC, og transkritiske systemer, hvor der køres transkristisk, når det er nødvendigt.

Som det ses i nedenstående figur, opererer et køleanlæg med CO_2 ved væsentligt højere tryk og temperatur for den transkritiske proces. Så specielt for disse anlæg udsættes pakninger for væsentligt højere tryk og også for højere temperaturer end i traditionelle køleanlæg. Dette skærper kravene til paknings- og konstruktionsmaterialer til CO_2-anlæg.

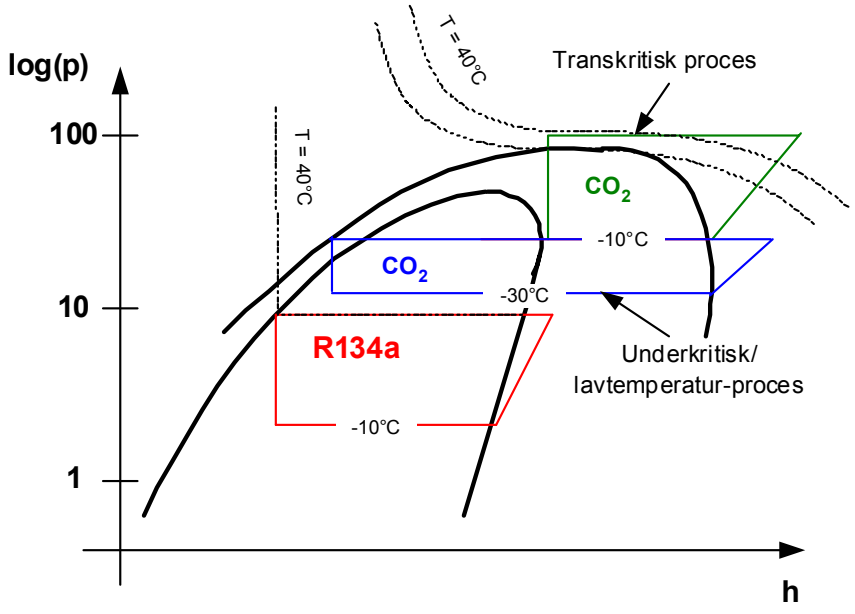

Figur 1: Kredsprocessen for R134a og CO_2.

1.2 Polymertyper

Polymerer anvendes i vid udstrækning overalt i samfundet. Plastik og gummi er således dannet af polymerer. I industrien og kølebranchen er polymerer specielt anvendt som pakningsmateriale og som konstruktionselementer i fx ventiler og pumper.
I typiske køleanlæg bruges i dag forskellige typer polymerer. Som pakningsmaterialer i fx topstykke på kompressor, mellem kompressor og motor i en åben kompressor og mellem flangesamlinger anvendes typisk elastomerer, der er deformerbare og kan pakke tæt på en overflade. Som konstruktionselementer i ventiler, pumper og styringer anvendes typisk plasttyper, der er stærkere end elastomererne, men som ikke er deformerbare.

En polymer er en naturlig eller syntetisk forbindelse, der er dannet ved sammenkædning af identiske eller næsten identiske enheder. Denne proces, hvor enhederne sammenkædes, kaldes polymerisering. Polymer referer altså til en lang molekylekæde, men bruges også som navn på selve materialet.

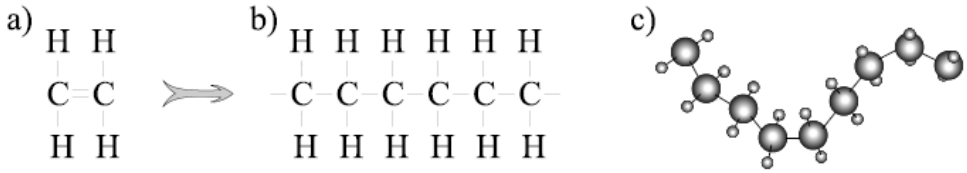

Figur 2: Polymerisering af etylen til polyetylen a) etylen, b) polyetylen c) kuglemodel af etylen[45].

Fælles for alle polymerer er den lange kæde af kulstofatomer, som er bundet sammen af kovalente bindinger. I denne lange kæde kan forskellige andre molekyler og sidegrene koble sig på, og polymerkæden kan gennem forskellige bindinger koble sig sammen med andre polymerkæder. Dette giver et utal af muligheder for forskellige polymerer med forskellige egenskaber. Endvidere kan forskellige fyldestoffer opløses i polymeren mellem de lange molekyler, således at polymeren opnår de ønskede egenskaber[46].

Disse fyldestoffer kan fremelske eller forstærke polymerens egenskaber fx polymerens styrke eller dens kemikaliebestandighed.

De lange polymerkæder holdes sammen af forskellige interatomare kræfter, og det er muligt at dele polymerer op efter, hvilke af disse kræfter, der virker. Der kan opdeles i følgende:

- Termoplast
- Hærdeplast
- Elastomerer

Termoplastiske polymerer er en plast, hvor de lange polymerkæder holdes sammen af en række svage interatomare kræfter som fx Van der Waalske kræfter og brintbindinger. Disse bindinger er relativt svage, og ved temperaturer typisk mellem 70 °C og 300 °C smelter polymeren, og den kan udstøbes i fx et ekstruderingsværktøj.

Termohærdende plast består af polymerer, hvor der er kovalente bindinger mellem molekylekæderne. Derfor kan denne type polymerer ikke smeltes, men blot brændes ved opvarmning. Termohærdende plast skal således være formet, som det ønskes, før den opvarmes, og de kovalente bindinger mellem kæderne dannes. Hærdeplast er fx epoxy.

Elastomer indeholder (som termohærdende polymerer) kovalente bindinger mellem molekylekæderne. Til forskel fra de termohærdende polymerer ligger bindinger mellem kæderne og polymerkæderne langt fra hinanden. Dette gør materialet elastisk, da den store afstand mellem de kovalente bindinger og de manglende svage bindinger gør det muligt at trække kæderne lange. De kovanlente bindinger kan dog ikke brydes uden videre og vil ofte vende tilbage til en tidligere uorden, når trækket på kæderne slippes. Dette betyder, at en elastomer er meget fleksibel, og derfor kan den deformeres uden at kæderne brydes, og elastomeren går i stykker.

Atomstrukturen, sammenhænge mellem molekylerne, har betydning for materialets mekaniske egenskaber. Elastomererne og de termohærdende plasttyper er materialer, hvor molekylekæderne hægter sig sammen vha. af kovalente bindinger. I elastomeren er der relativt langt mellem disse kovalente bindinger, og derfor er materialet meget fleksibelt og finder tilbage til sit udgangspunkt, efter det har været udsat for en belastning.
Der kan også skelnes mellem amorfe polymerer og delkrystallinske polymerer. I en amorf polymer ligger polymerkæderne i fuldstændig uorden. En amorf plast er typisk gennemsigtig. Elastomererne har en amorf struktur.
I en delkrystallinsk polymer danner polymerkæderne krystallinske områder, hvor molekylerne danner ordnede strukturer indbyrdes. At materialet danner krystallignende områder, vil øge dets styrke[45].

En polymers glastemperatur har også betydning for en polymers egenskaber. Der kan skelnes mellem polymerer, hvis egenskaber udnyttes over glastemperaturen eller under glastemperaturen. Når en polymer er koldere end glastemperaturen, mindskes den indbyrdes bevægelighed mellem molekylekæderne, og polymeren får glasegenskaber. Den bliver stivere og kan svært deformeres uden brud. Dette er typisk for de fleste hårdere plasttyper. Dette er ønskeligt for de stærkere plasttyper, der herved opnår en stor styrke men ikke kan deformeres uden brud.
Over glastemperaturen er polymeren læderagtig og således sejere og lettere deformerbar. Dette er typisk for elastomerer, der således kan deformeres, hvilket fx er ønskeligt, når det anvendes i pakninger mellem fx 2 overflader.

1.3 Typiske problemer med polymererne i CO_2

En række direkte problemer kom frem i lyset i forbindelse med anvendelsen af polymerer i anlæg med CO_2, og de er følgende:

- CO_2 gennemtrængningsevne – et stort problem i forbindelse med at anvende polymermaterialerne i anlæg med CO_2 er, at CO_2 kan trænge igennem materialet og skabe lækage. Mængden af CO_2, der lækker gennem pakningen, afhænger af solubilitet og diffussivitet, altså polymerernes evne til at optage CO_2 og til at slippe CO_2 igennem materialet.

- Eksplosiv dekompression kan indtræffe, når trykket i CO_2-systemet reduceres hurtig. Den opløste CO_2 i polymeren kan ikke diffusere hurtig nok til omgivelserne, hvormed der dannes bobler i materialet, som kan ødelægge polymerernes struktur.

- Dimensionsændring - ved systemets tryksætning kan polymererne udvide som resultat af optagelse af CO_2. Polymeren optager simpelthen CO_2 og ændrer sin fysiske størrelse. Dette er specielt et problem for konstruktionselementer af plast. Disse er ofte forarbejdet meget nøjagtigt, og ved en udvidelse kan de fx spærre en ventil.

- Ændring af egenskaber – CO_2 evne til at blive opløst i polymererne bevirker, at polymerernes egenskaber ændres. Den polymer, der skulle have en given styrke, kan fx under påvirkning af CO_2 miste sin mekaniske styrke og derved gå i stykker.

1.4 Tidligere udført arbejde omhandlende de mekaniske egenskaber af polymerer i CO_2

I 1999 blev der udført træktest af elastomerer i CO_2-atmosfære på University of Wales i Swansea i Storbritannien[1]. Testene blev udført i en trækprøvemaskine, der er bygget sammen med en trykbeholder. Der arbejdes med tryk på op til 40 bar i denne beholder. Kraften, som prøven optager, måles af en indbygget specialvejecelle i tanken.

Baggrunden for arbejdet er et ønske om at kunne bestemme materialets E-modul og styrke, mens elastomeren stadig befinder sig i CO_2-atmosfæren. Sammen med værdierne for opløselighed og diffusion af CO_2 i elastomeren skal disse data danne baggrund for at simulere, hvilke elastomerer, der egner sig bedst, hvis eksplosiv dekompression skal undgås.

Materialerne, der testes, er fluorelastomerer, nitrilelastomerer og en siliconeelastomer. Testene er alle udført ved 23 °C, og der er udført test, hvor CO_2 er erstattet af nitrogen.

For test i 40 bars nitrogen-atmosfære ses ingen ændring i elastomerernes egenskaber. De bibeholder deres E-modul og styrke i forhold til test, foretaget i almindelig luft.

For trækprøver, udført i CO_2,ses derimod, at elastomerens styrke og brudforlængelse falder. Dette gælder for alle 3 elastomertyper se figur 3 og 4. Det største fald i styrke ses for fluorelastomeren, der taber over 50% i styrke, og det samme gør sig glædende for siliconeelastomeren. Nitrilen klarer sig bedst og mister kun i størrelsesordenen 25% af sin brudstyrke. Det samme gør sig gældende for brudforlængelserne.
Interessant er det også at se, at for alle 3 elastomerer er der tale om et lavere E-modul i starten af trækprøveforsøget i forhold til testene, udført i luft.

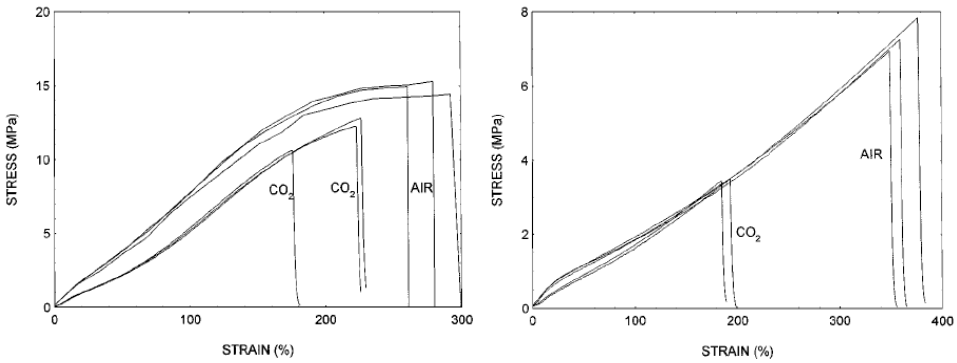

Figur 3: Til venstre nitrilgummi (shore 80) i 40 bar CO_2; til højre siliconegummi (shore 65) i 40 bar CO_2.

[1] The mechanical properties of elastomers in high-pressure CO_2, Department of Materials Engineering, University of Wales, Swansea.

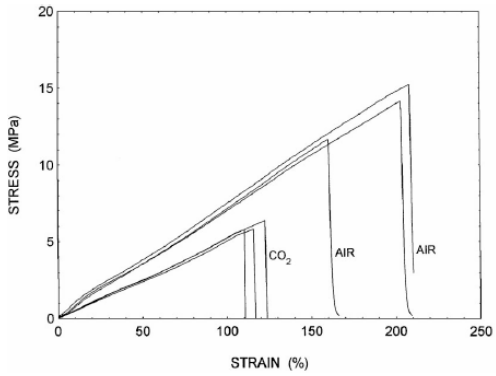

Figur 4: Fluorgummi (shore 80) i 40 bar CO_2.

Alle brudflader underkastes nærmere undersøgelse. For brudfladerne gælder, at de ved CO_2-forsøget er plane og præcise. I modsætning til dette er brudfladerne ved en trækprøve i luft mere ru.

Bortset fra dette konstateres det, at der ikke direkte kan ses andre grunde til faldet i de mekaniske værdier.

Det formodes, at det højere E-modul for testene, udført i atmosfære luft over de første 20% af trækket, opstår, fordi polymerkæderne og fyldestofferne påvirker hinanden indbyrdes, således at elastomeren er stivere over de første 20% af trækket. Denne effekt ses ikke ved forsøgene udført i CO_2.

Dette sammenfattes i arbejdet til, at CO_2 har gjort elastomeren blødere, og at den er blevet plastificeret. Dette formodes at være fordi, CO_2 har påvirket den måde, kæderne hænger sammen på. CO_2 har svækket bindingerne mellem kæderne, og CO_2 har svækket fyldestofferne.
Dette vil ifølge forfatterne resultere i mindre brudstyrke, mindre brudforlængelse og et fald i E-modul, som det ses i forsøgene.

1.5 Udvælgelse af polymer til test

Til forsøgene er følgende materialer valgt:

- Plastmateriale: PVDF, PTFE og PEEK
- Elastomer: EPDM, FKM og HNBR.

I det følgende gives en kort beskrivelse af hvert materiale:

PVDF er en delkrystalinsk termoplast med en høj krystallinitet, der tilhører familien af fluorplaster. PVDF bruges inden for den kemiske industri og andre steder, hvor der bruges aggressive væsker og høje temperaturer. Det anvendes til fremstilling af ventiler, pakninger, pumpedele, tanke, fittings og rørføringer. PVDF har en glastemperatur på -35 ºC.

PTFE er en delkrystalinsk termoplast med en høj krystallinitet, der tilhører familien af fluorplast. PTFE er kendt under navnet teflon og anvendes således ofte som en sliplet overflade. I øvrigt anvendes polymeren bredt, da den har gode mekaniske egenskaber og kan modstå aggressive miljøer og høje temperaturer.
PTFE har en glastemperatur på 126 ºC.

PEEK er en delkrystallinsk termplast. PEEK er en teknisk plast, der anvendes bredt til konstruktionselementer, som fx ventiler, pumpedele, tandhjul, lejer, snekkehjul, hydraulikdele og slidringe.
PEEK har en glastemperatur på 145 ºC.

EPDM er en elastomer, der er kendt for sin ældnings-, sollys- og ozonbestandighed, og har en god bestandighed mod varmt vand og damp. Ikke-bestandig mod mineralolieprodukter. Temp. -50 ºC til +120 °C.
EPDM har en glastemperatur på -54 ºC.

FKM er en elastomer, der også er kendt under navnet viton. Den finder anvendelse i forskellige industrielle applikationer. Polymeren indeholder fluor. Har god bestandighed mod mineralolier, alifatiske, aromatiske og klorerede kulbrinter, koncentrerede og fortyndede syrer. Temp. -30 °C til +200 °C.

HNBR er en elastomer. Elastomeren er en hydreret nitrilgummi. Elastomeren har god oliebestandighed. Temp. -30 °C til +150 °C.

2 Permeabilitet, opløselighed og diffusion

2.1 Opløselighed og diffusion

I det følgende bestemmes opløselighed og diffusion af CO_2 på gasfase i HNBR, EPDM, som er bløde polymerer, der bruges som tætningsmateriale (bl.a. O-ringe). Resultaterne heraf skal efterfølgende bruges til at bestemme modelparametre til den termodynamiske model PC-SAFT, således at det er muligt at bestemme opløseligheden af CO_2 i den pågældende polymer ved en given betingelse af tryk og temperatur.

2.1.1 Opløselighed

Hvor nemt gasser diffunderer gennem polymerer er bestemt af permeabiliteten. Permeabilitet er en proces i 2 trin. Opløsning af gas i polymeren og diffusion af gassen gennem polymeren. For at forstå permeabilitet er det derfor vigtigt at have viden omkring begge disse trin. Permeabilitet kan udtrykkes som produktet af opløselighed og diffusion. Man ønsker naturligvis en meget lav permeabilitet, da det giver længere levetid. Dette gælder både rør i offshore-industrien og kølecyklusser i køleindustrien. Tidligere studier har vist, at opløseligheden af CO_2 i forskellige polymermaterialer er faldende med stigende temperatur. Diffusionen derimod er altid stigende med temperaturen. Disse 2 tendenser modvirker hinanden mht. permeabiliteten. Af samme årsag er det et stort ønske at kunne opstille modeller for opløselighed og diffusion og deraf beregne permeabiliteten. Når et polymermateriale placeres i et system med overtryk af f.eks. CO_2, vil gassen absorberes i polymeren. Derved vil vægten af polymerprøven stige, indtil der er opnået en mætningsligevægt. Figur 5 viser et typisk forløb, hvor en gas opløses i en polymer og det omvendte forløb, hvor en gas desorberes. Polymerprøven har samme facon som en flad cylinder eller en disk.

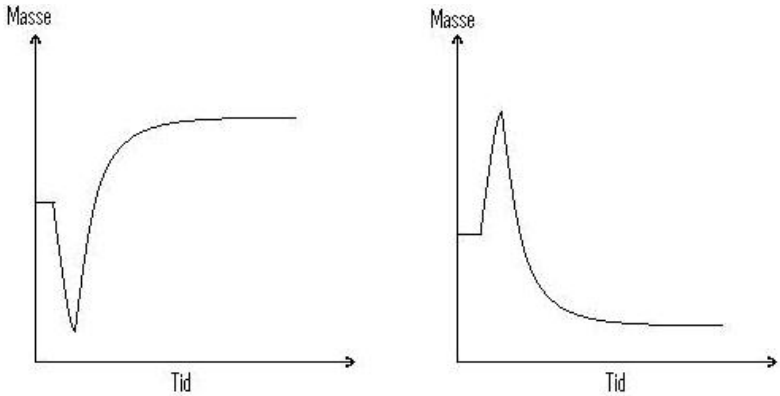

Figur 5: Masseændring af polymer som funktion af tid ved absorption/desorption af en gas.

På den første del af figuren ses, at ved trykstigning vil massen først falde for derefter at stige indtil ligevægt. Det virker meget fornuftigt, at ændringen i

massen er størst fra starten. Reduktionen i vægten fra starten skyldes opdriftseffekten. Når trykket stiger, stiger opdriften, og vægten vil derfor reduceres. Efter effekten af opdriften har vist sig, øges vægten som forventet. Det samme gør sig gældende på den anden del af figuren. Bare omvendt. Masseændringen bestemmes som forskellen mellem massen ved "toppunktet" og massen ved ligevægt. Denne masse må naturligvis være massen af gas. Opløseligheden S beregnes som:

$$S = \frac{Massen\ af\ \ gas\ [mg]}{Massen\ af\ \ polymer\ [mg]} \tag{1}$$

2.1.2 Diffusion

Masseændringen viser sig at være lineær afhængig af kvadratroden af tiden, for den første tidlige del af forsøget. "Toppunktet" skal da vælges som nyt 0-punkt for x-aksen. Dette skyldes, at en ændring på x-aksen (på f.eks. 1) ikke svarer til den samme ændring i tid overalt.

$$\sqrt{t_2} - \sqrt{t_1} \neq \sqrt{t_2 - t_1} \tag{2}$$

Jo højere værdierne er for kvadratroden af tiden, desto større er forskellen i "rigtig" tid.

Da den lineære sammenhæng mellem masseændringen og $\sqrt{t}$, kun er gældende i det første korte tidsrum, er det derfor vigtigt at "toppunktet" vælges som nyt 0-punkt mht. x-aksen. Havde den lineære sammenhæng været gældende under hele forsøget, havde det ikke været nødvendigt at vælge nyt "toppunkt". I den første korte tidsperiode kan en disk/plade med rette antages at være et halvuendeligt emne. For et halvuendeligt emne gælder følgende:

$$Q = A\sqrt{\frac{4Dt}{\pi}}(c_{græn,0} - c_{cent,0}) \tag{3}$$

hvor Q er masseændringen [mg], A er det tilgængelige overfladeareal [cm^2], D er diffusionskoefficienten [cm^2/s], t er tiden [s], $c_{græn,\ 0}$ er gaskoncentrationen af CO_2 i overfladen af prøven i det første korte tidsrum [mg/cm^3] og $c_{cent,0}$ er gaskoncentrationen af CO_2 i centrum af prøven i det første korte tidsrum [mg/cm^3]. $C_{græn,0}$ antages at være lig gaskoncentrationen overalt i emnet ved ligevægt. Dvs.:

$$c_{græn,0} = Opløseligheden\left[\frac{mg_{gas}}{mg_{polymer}}\right] \cdot Densitet\ af\ \ polymer\left[\frac{mg}{cm^3}\right] = \left[\frac{mg_{gas}}{cm^3{}_{polymer}}\right]$$

Ved omskrivning af ligning (3) fås:

$$Q = (c_{græn,0} - c_{cent,0}) \cdot 2A\sqrt{\frac{D}{\pi}} \cdot \sqrt{t} \tag{4}$$

Plottes Q som funktion af kvadratroden af tid fås en ret linie med hældningen

$$(c_{græn,0} - c_{cent,0}) \cdot 2A\sqrt{\frac{D}{\pi}} \qquad (5)$$

Af dette kan diffusionskoefficienten D bestemmes. I figur 6 og figur 7 ses masseændringen som funktion af kvadratroden af tid for et af de udførte forsøg. Som tidligere beskrevet ses den lineære sammen hæng mellem masseændringen og $\sqrt{t}$ for den første del af kurven.

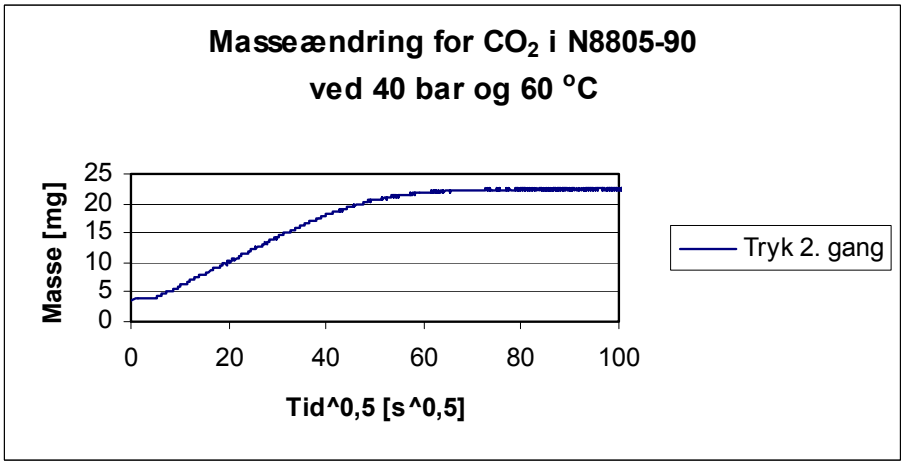

Figur 6 Masseændringen som funktion af $t^{0,5}$ for N8805-90 ved 40 bar og 60 ºC.

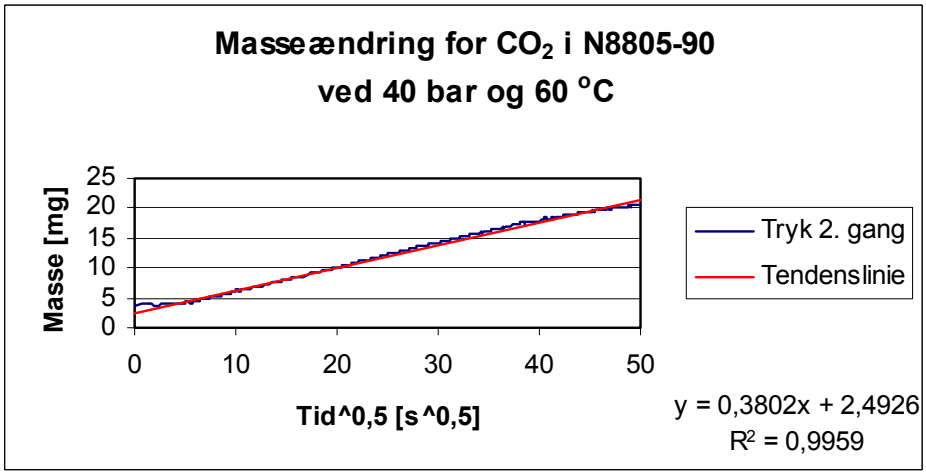

Figur 7 Masseændringen som funktion af $t^{0,5}$ for N8805-90 ved 40 bar og 60 ºC.

Diffusionskoefficienten følger en Arrhenius afhængighed:

$$D = D_0 \cdot e^{-E_D/RT}, \qquad (6)$$

hvor D_0 er den preeksponentielle faktor [cm^2/s], E_D er aktiveringsenergien [J/mol] for diffusion, R er gaskonstanten [J/(mol·K)] og T er temperaturen i kelvin. Ved omskrivning fås:

$$\log D = \log D_0 - \frac{E_D}{R} \cdot \frac{1}{T} \qquad (7)$$

Ved at plotte log D som funktion af 1/T, fås en ret linie, hvor hældningen er bestemt som $-E_D/R$, og log D_0 er skæringen med y-aksen. Heraf er det muligt

at bestemme E_D og D_0. Der er i dette projekt ikke lavet beregninger på E_D og D_0, da disse værdier ikke er væsentlige for projektet. Log D er dog stadig plottet med 1/T for at vise den lineære tendens.

2.1.3 Beskrivelse af forsøgsudstyr

Udstyret til bestemmelse af gassers opløselighed i polymermaterialer består af følgende:

- Højtryksvægt fra (Sartorius Supermicro, S3D-P) fra Sartorius AG, Tyskland, med tilhørende interface og display. Vægten må anvendes ved forsøg op til 150 bar og ved temperaturer mellem 0 ºC og 150 ºC.
- Vakuumpumpe (Drytel 30) med tilhørende manometer (CFA 212), begge fra Alcatel. Vakuumpumpen når typisk ned omkring 10-3 hPa (10-3 mbar). Manometret kan måle ned til 10-7 hPa (10-7 mbar).
- En tranducer (EPXO-P02-200B) fra Entran Sensors & Electronics. Denne måler trykket og omsætter det til en spændingsforskel over en modstand i en ”Wheatstones bro”.
- Dødvægt til kalibrering af transducer af mærket Desgranges et Hudt model 26000.
- Der er brugt CO2 gas med en renhed > 99,99 %.

I figur 8 - figur 9 ses anlægget.

Figur 8: Til venstre - Højtryksvægt; til højre – Vakuumpumpe.

Figur 9: Til venstre - Vægt til kalibrering af transducer, til højre – Transducer.

På figur 10 ses en skematisk tegning over anlægget.

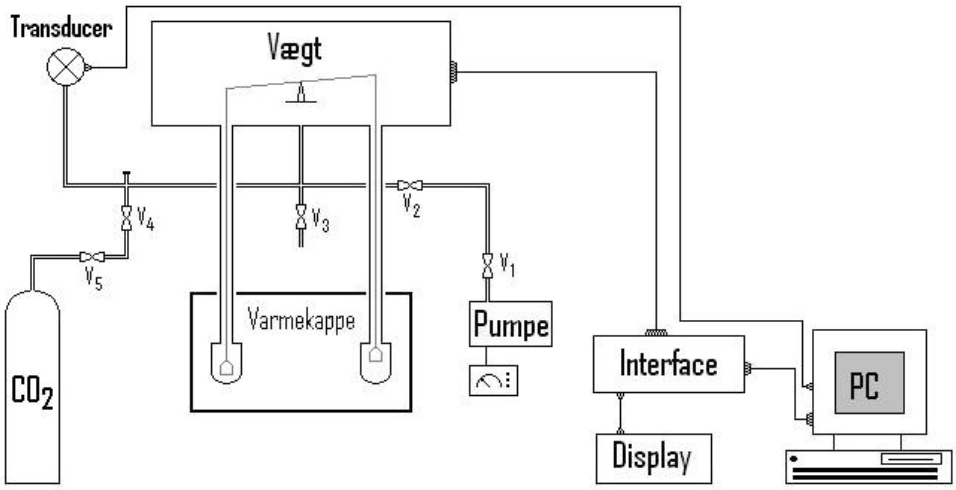

Figur 10: Skitse af anlæg.

V1, V2 og V4 er almindelige åben/lukke ventiler. V3 er en overtryksventil, som åbner ved tryk > 150 bar. V5 er en reduktionsventil. Denne udskiftes alt efter, hvilket tryk, der ønskes i systemet. Selve vægten består af 2 tynde glastråde, hvor der i enden hænger et lille bæger af glas/polymer. Vægtforskellen mellem de to tråde + bæger registreres og vises på displayet.

2.1.4 Fremgangsmåde

I det efterfølgende er det beskrevet, hvorledes laboratorieforsøgene er udført. Inden start er det vigtigt, at glasholderne er rene og tørre, og at hele anlægget står i vatter. Inden da er det også en god ide at undersøge, om anlægget er tæt overalt. Polymerprøverne, der skal bruges, er diske, der er banket ud af en ca. 1 mm tyk polymerplade. Diskenes størrelse bestemmes vha. et digitalt skydelærred og overfladearealet udregnes heraf. Densiteten er bestemt af de virksomheder, der har leveret polymerprøverne. Til alle forsøgene er der brugt 6 diske, og det samlede overfladeareal er derfor ikke udregnet pr. disk men samlet. I tabel 1 er relevante data samlet.

Polymer	Tykkelse [cm]	Diameter [cm]	Overfladeareal (6 stk) [cm^2]	Densitet [mg/cm^3]
E3804-90	0,107-0,109	0,85-0,88	8,52-9,11	1190
N8805-90	0,096-0,098	0,85-0,88	8,35-8,92	1210

Tabel 1 Prøvernes størrelse mm.

Det er vigtigt at diskene, når de skal placeres i glasholderne, placeres således, at et så stort overfladeareal som muligt er tilgængeligt. Pga. tidsbegrænsningen har det kun været muligt at undersøge opløseligheden af CO_2 i 2 polymerer. Det drejer sig om N8805-90, som er en hydreret nitril med hårdhedsgraden 90 shore A og E3804-90, som er EPDM ligeledes med en hårdhedsgrad på 90 shore A. Begge disse polymerer er forholdsvis bløde polymerer, der bruges som tætningsmateriale. På figur 11 og figur 12 ses den kemiske struktur for

polymererne E3804-90 og N8805-90.

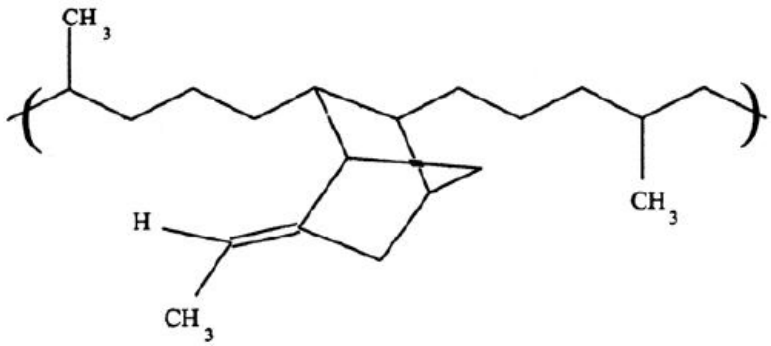

Figur 11: Strukturformel for E3804-90.

$$[CH_2\text{-}CH{=}CH\text{-}CH_2]_z\text{-}[CH_2\text{-}CH_2\text{-}CH_2\text{-}CH_2]_{x\text{-}z}\text{-}[CH_2\text{-}C(CN)H]_y$$

Figur 12: Strukturformel for N8805-90.

Opløseligheden af CO_2 i disse polymerer er blevet undersøgt ved 3 forskellige temperaturer (20 ºC, 60 ºC, og 80 ºC) og ved 3 forskellige tryk (10 bar, 40 bar og 50 bar).

Der blev lavet forsøg på opløseligheden af CO_2 ved 20 ºC og hhv. 10 og 40 bar. Disse forsøg blev udført, da der på det pågældende tidspunkt ikke var modtaget andre prøver.

2.1.5 Behandling af forsøgsresultater

I dette afsnit er det vist, hvordan data fra de eksperimentelle forsøg bruges til at bestemme opløselighed og diffusion. Som tidligere beskrevet er der lavet forsøg med de 2 polymerer E3804-90 og N8805-90 ved 3 forskellige temperaturer og 3 forskellige tryk. Dette giver 9 forskellige kombinationer. Til hver kombination er der lavet en 4-dobbelt bestemmelse. 2 gange har prøven været under tryk og 2 gange under vakuum. Det må forventes, at den mængde CO_2, der tilføres polymeren under tryk, er den samme, som frigives under vakuum. Derfor kaldes det en 4-dobbelt bestemmelse, selvom de 4 forsøg kun er udført fuldstændig ens i par af 2 go 2. Det samme gør sig naturligvis gældende for diffusion. Inden forsøgets startes, evakueres systemet, for at fjerne den atmosfæriske luft, der er til stede i systemet.

2.1.6 Resultater - Opløselighed

På figur 13 er der vist et eksempel på et forsøg, der er kørt under tryk

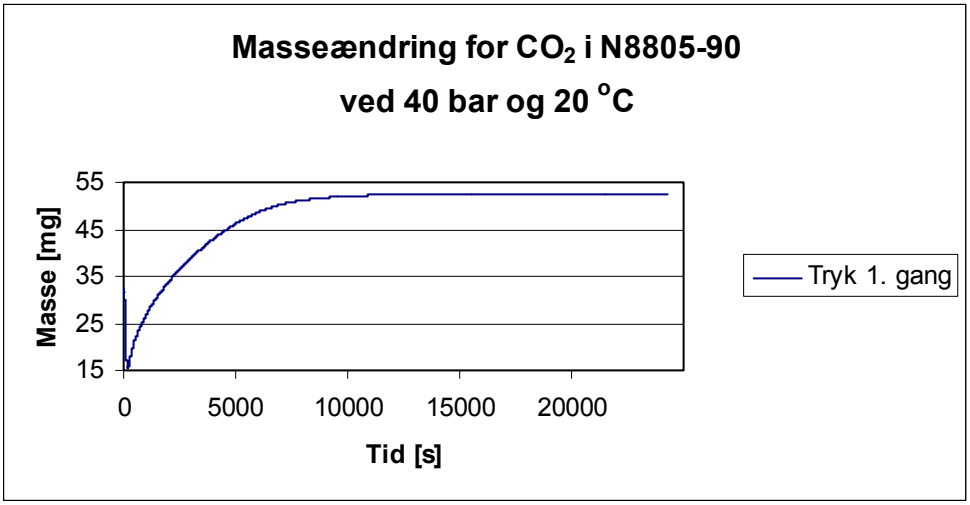

Figur 13: Eksempel fra forsøg, hvor en polymerprøve (N8805-90) er kørt ved 40 bar og 20 ºC.

Masseændringen bestemmes som forskellen mellem massen ved "toppunktet" og massen ved ligevægt. I det ovenstående tilfælde er masseændringen bestemt til at være 37,209 mg. Inden forsøgets start er massen af polymeren målt til 0,4355 g (435,5 mg). Af ligning (1) bestemmes opløseligheden til 0,085 [mg/mg]. Det har vist sig, at værdierne for opløseligheden passer sammen i par. De 2 forløb under tryk er næsten ens, og de 2 forløb med vakuum passer sammen. Opløseligheden i E3804 og N8805 er lidt større, når der køres forsøg under vakuum. Masseændringen her er simpelthen en lille smule større. Da der naturligvis ikke kan fjernes mere CO_2 fra prøven under vakuum, end der er tilført under tryk, og der ikke er nogen masseændring af betydning af hele polymeren efter afslutning af de 4 forsøg, må det skyldes opdriftseffekten. Opdriftseffekten er mere markant ved at ændre trykket fra f.eks. 40 bar til 0 bar end den modsatte vej. Dette kan skyldes, at det går hurtigere at opnå stabilt vakuum end at opnå stabilt tryk. Det observeres også, at forskellen i opløseligheden også er mest markant ved højt tryk. Dette styrker teorien om, at det skyldes en forskel i opdriftseffekten, da denne jo er trykafhængig. Af samme grund har man ikke valgt at bestemme opløseligheden som en gennemsnitsværdi af de 4 forløb, men derimod i par. Tryk for sig og vakuum for sig. Opløseligheden under tryk bestemmes så som en gennemsnitsværdi af de 2 forløb. Det samme er gældende for vakuum. På samme måde bestemmes opløseligheden ved andre forhold af tryk og temperatur. På figur 14 – figur 15 ses resultaterne for opløseligheden for hhv. E3804-90 og N8805-90.

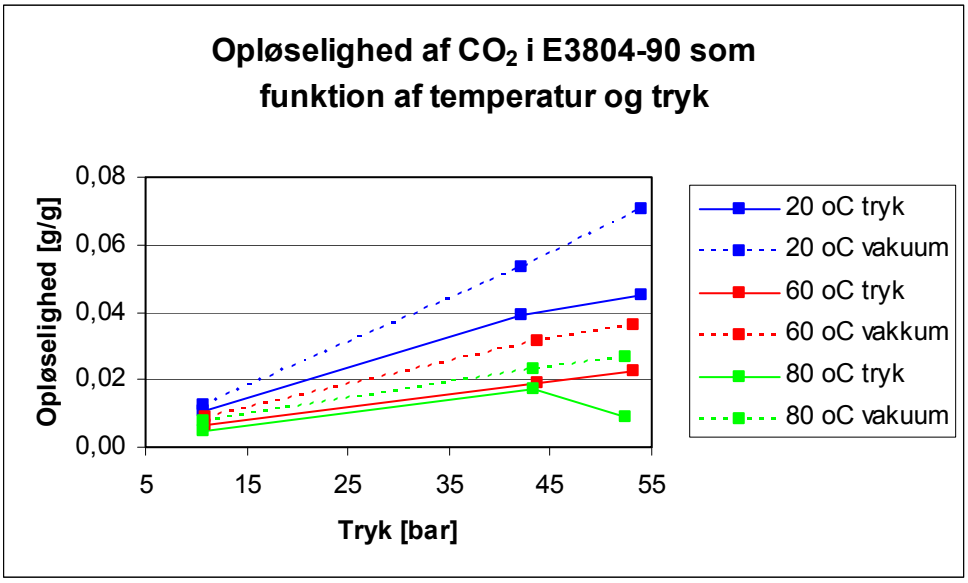

Figur 14: Opløseligheden af CO_2 i E3804-90 som funktion af tryk og temperatur.

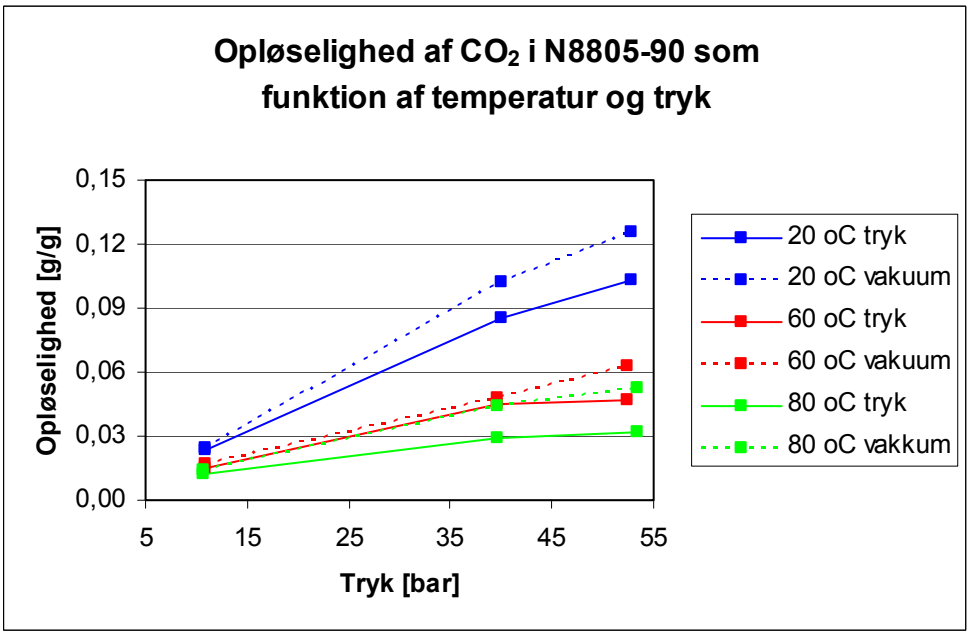

Figur 15: Opløseligheden af CO_2 i N8805-90 som funktion af tryk og temperatur.

Af overstående 2 figurer ses det, at opløseligheden er stigende med stigende tryk og faldende temperatur. Tidligere studier [3]-[8] af CO_2´s opløselighed i diverse polymerer har vist samme mønster.

2.1.7 Resultater - Diffusion

Som tidligere beskrevet, er diffusionskoefficienten lineært afhængig af kvadratroden af t. På figur 16 ses den lineære sammenhæng for det forsøg, der også er vist på figur 13

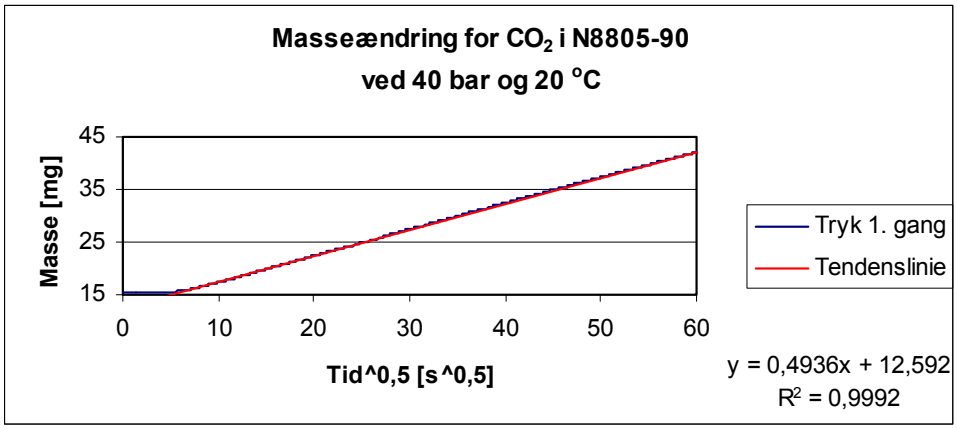

Figur 16: Masseændringen som funktion af $t^{0,5}$ for den tidlige del af forsøget. Eksempel er fra forsøget, hvor polymerprøven (N8805-90) er kørt ved 40 bar og 20 ºC.

Det bemærkes, at der næsten ikke er nogen masseændring i den allerførste del af kurven. Dette er tilfældet ved alle de forsøg, der er kørt under tryk. Dette skyldes, at absorptionen af CO_2 under tryk fra starten er lidt langsommere end desorptionen under vakuum. Det er ikke muligt at se på kurverne for opløselighed, da forsøgene er kørt over en lang tidsperiode. Hvis man ønsker det, kan man nærstudere området omkring "toppunktet" ved at tilpasse akserne, således at man zoomer ind på grafen. Her vil det ses, at "toppunktet" er meget mere spidst under vakuum end under tryk. Ifølge ligning (4) kan hældningen af den rette linie udtrykkes som

$$(c_{græn,0} - c_{cent,0}) \cdot 2A\sqrt{\frac{D}{\pi}}$$

Ved omskrivning fås diffusionskoefficienten som:

$$D = \left(\frac{hældning}{2 \cdot A \cdot (c_{græn,0} - c_{cent,0})} \right)^2 \cdot \pi \qquad (8)$$

Hældningen findes i Excel ved at tilføje en tendenslinie. I tilfældet på figur 16 er hældningen bestemt som 0,4936 [mg/(t½)]. Overfladearealet er bestemt af prøvens diameter og tykkelse. Diameteren og tykkelsen afviger lidt fra prøve til prøve, så overfladearealet og dermed diffusionskoefficienten er opgivet som et interval. Når værdierne plottes i et diagram, er der dog valgt et gennemsnit for overskuelighedens skyld. Da opløseligheden er medbestemmende for diffusionskoefficienten, er der ved præsentationen af disse resultater også taget hensyn til forskellen i værdierne for forsøg kørt under tryk og forsøg kørt under vakuum. Overfladearealet er udregnet til mellem 8,35 [cm^2] og 8,92 [cm^2], og diffusionskoefficienten er udregnet til mellem 2,25·10-7 [cm^2/s] og 2,57·10-7 [cm^2/s]. På figur 17 – figur 18 ses resultaterne for diffusionskoefficienten for hhv. E3804-90 og N8805-90.

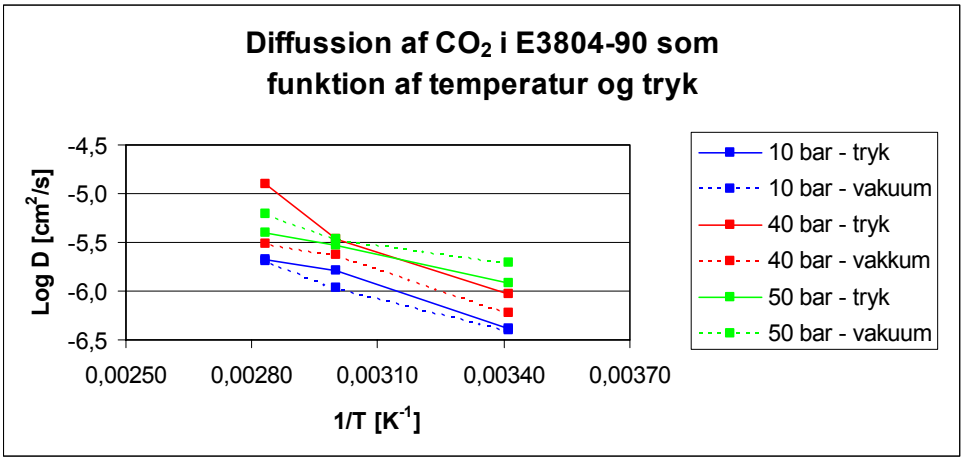

Figur 17: Diffusionskoefficienten for CO_2 i E3804-90 som funktion af tryk og temperatur.

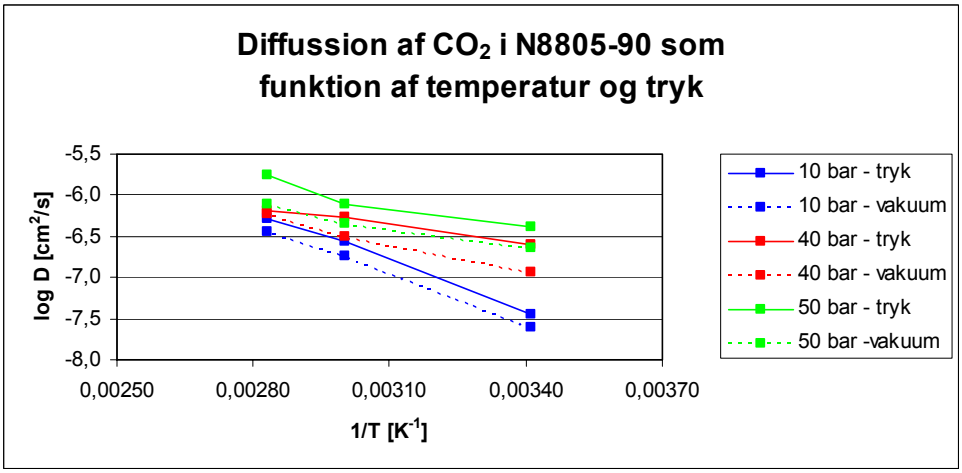

Figur 18: Diffusionskoefficienten for CO_2 i N8805-90 som funktion af tryk og temperatur.

Det bemærkes, at log D er nogenlunde lineært afhængig af den reciprokke temperatur. Det bemærkes desuden, at diffusionskoefficienten også afhænger af trykket. Det ses, at større tryk giver større diffusionskoefficient og større præeksponentiel faktor D_0. Det ses også, at diffusionskoefficienten for N8805 og E3804 er størst ved forsøg, der er kørt under tryk. Dette er også forventet, da D er reciprokt afhængig af opløseligheden, som jo var størst ved forsøg, der var kørt under vakuum. Hældningerne på figur 17 og figur 18 ser ud til at være nogenlunde konstante. Dvs. at aktiveringsenergien ikke er trykafhængig. Dette lyder fornuftigt, da aktiveringsenergien er en intramolekylær størrelse. Da kurverne ikke ligger oven i hinanden, er den præeksponentielle faktor D_0 til gengæld trykafhængig.

2.1.8 Observationer

Efter endt forsøg er polymerprøverne blevet vejet for at se, om de har ændret vægt. Der har ikke vist sig nogen bemærkelsesværdige ændringer i massen. De fleste har ændret sig en smule, men kun ude på 4. decimal af vægten (målt i g.). Denne lille ændring kan skyldes måleusikkerhed. Nogle få prøver har haft en lidt større masseændring. Op til ca. 0,45 % og altid negativ. Det er stadigvæk en meget lille masseændring, men da den altid er negativ, kan det skyldes, at den mængde atmosfæriske luft, der er til stede i polymeren, fra start ikke er diffunderet tilbage i polymeren efter sidste forsøg og inden den afsluttende vejning. Der er som regel gået mellem 4 og 5 døgn, efter prøven er

fjernet fra forsøgsopstillingen og til den sidste vejning. Måske er der på dette tidspunkt endnu ikke indtrådt ligevægt, og det er derfor nødvendigt at vente længere tid. En anden mulighed kan være, at CO_2 har opløst en lille del af polymeren, som derefter er trykket ud under vakuum. Dette er heller ikke utænkeligt, da det er velkendt, at CO_2 er ødelæggende for nogle elastomerer. En anden observation der er gjort er ved forsøget som er vist på figur 19.

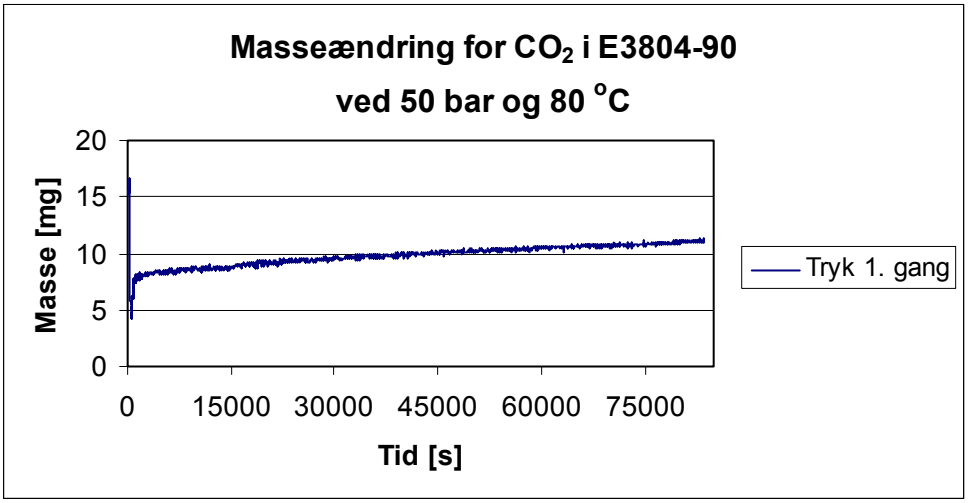

Figur 19: Masseændringen for CO_2 i E3804-90 som funktion af tryk og temperatur.

På figur 19 ses et lidt specielt tilfælde. Det bemærkes, at der først er sket et opløselighedsforløb, men i stedet for at opnå ligevægt er massen konstant stigende. Først til allersidst viser der sig en lille smule stabilitet. Da der ikke er observeret nogen trykstigning, som kan forklare masseforøgelsen, skyldes det muligvis at polymeren svulmer op. Pga. af den da faldende densitet er opløseligheden stigende, og deraf stiger vægten. Lignende observationer [6] er gjort for CO_2 i HDPE. Der er dog ikke nogen synlige ændringer af polymeren efter endt forsøg. Det er der til gengæld på det forsøg, hvor N8805-90 er kørt ved 50 [bar] og 20 ºC. På figur 20 ses et billede af polymeren efter endt forsøg.

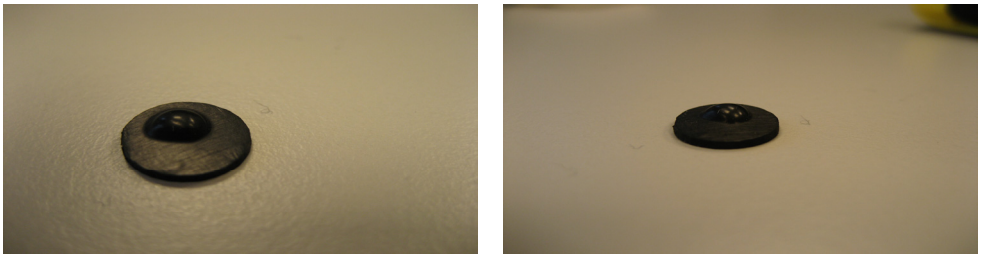

Figur 20: N8805-90 efter forsøg under 50 [bar] og 20 ºC.

Den observerede boble er ca. 1 mm høj (ligesom selve skiven) og ca. 3 mm i diameter. Det er tydeligt, at der er sket en opsvulmning. Den aftog dog i løbet af nogle timer, og efter 2 døgn var den helt væk. Det var kun denne ene skive, hvor der var sket en opsvulmning, og det er heller ikke observeret efter andre forsøg. Selvom det er bemærkelsesværdigt, er det ikke underligt, at det lige sker ved dette forsøg. Det er det forsøg, hvor opløseligheden i polymeren er størst. Dvs. den udsættes for mest transport af CO_2 ind og ud af polymeren. Den afsluttende afvejning har ikke vist nogen masseændring. Der er en difference på 0,0001 g, som lige så godt kan skyldes vægtens usikkerhed.

2.1.9 Konklusion

Eksperimenter til bestemmelse af opløselighed og diffusion af CO_2 i E3804-90 (EPDM) og N8805-90 (HNBR) er udført ved tryk mellem 10 [bar] og 50 [bar] og temperaturer mellem 20 ºC og 80 ºC. Overordnet må det siges, at resultaterne stemmer godt overens med tidligere lignende eksperimenter, og at resultaterne også viser den rigtige tendens mht. tryk og temperatur. Det kan tydeligt konkluderes, at det har været muligt at måle og bestemme hhv. opløselighed og diffusionskoefficienten af CO_2 i de forskellige polymerer. Der har vist sig en meget tydelig tendens. Opløseligheden stiger ved højere tryk og lavere temperatur.

Generel opløselighed af CO_2 i HNBR er omkring dobbelt så stor som i EPDM, derimod er diffusion ca. en størrelsesorden mindre. Dermed for alle temperatur og trykspænd er permeabiliteten af CO_2 mindre i HNBR end i EPDM (dvs. selvom opløselighed er højere i HNBR, så er diffusionskoefficienten betydelig mindre). Dette medfører, at permeabiliteten er mindre i HNBR).

2.2 Permeabilitet

Permeabilitet og diffusivitet af CO_2 var målt i en række polymerer, som er brugt som paknings- og tætningsmaterialer i køleanlæg. Målingerne er blevet udført ved hjælp af højtrykspermeationscelle. Alle målinger er udført ved 45-50 bar og temperaturspænd fra 40 – 80ºC. Det følgende er et kort opsummering af en større afhandling, som er vedhæftet i Bilag A.

2.2.1 Beskrivelse af forsøgsudstyret

Permeabilitetsmålinger er blevet udført ved hjælp af en højtrykspermaetionscelle, som er designet og fremstillet af Institut for kemiteknik ved Denmarks Tekniske Universitet. Permaetionscellen består af to kamre; højtrykskammer (primær) og lavtrykskammer (sekundær), jævnfør figur 21. Polymerprøven placeres imellem disse to kamre. De to kamre er isolerede for at opretholde en konstant temperatur. Ved test opsamles temperaturen samt tryk i de to kamre som funktion af tiden. For flere informationer se Bilag A.

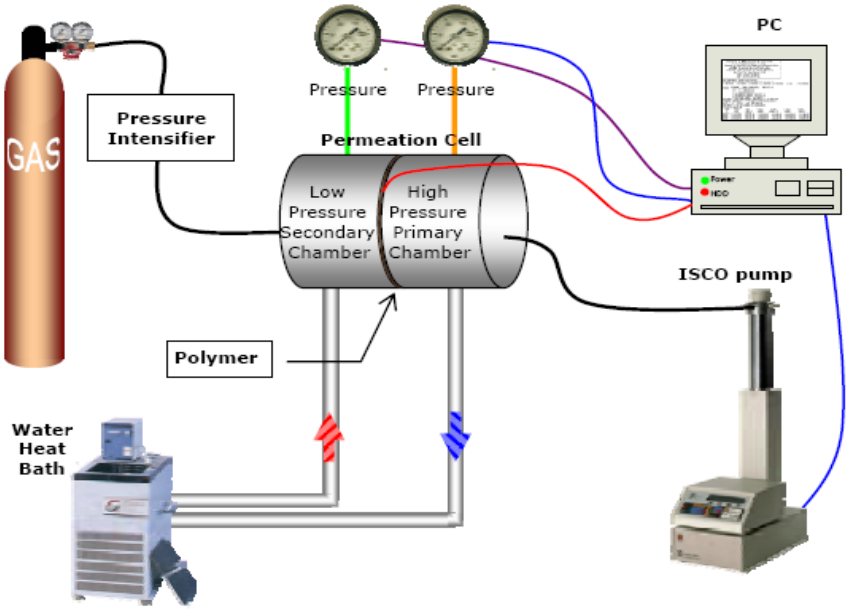

Figur 21: Forsøgsopstilling til opmåling af permeabiliteten af CO_2 i polymermaterialer.

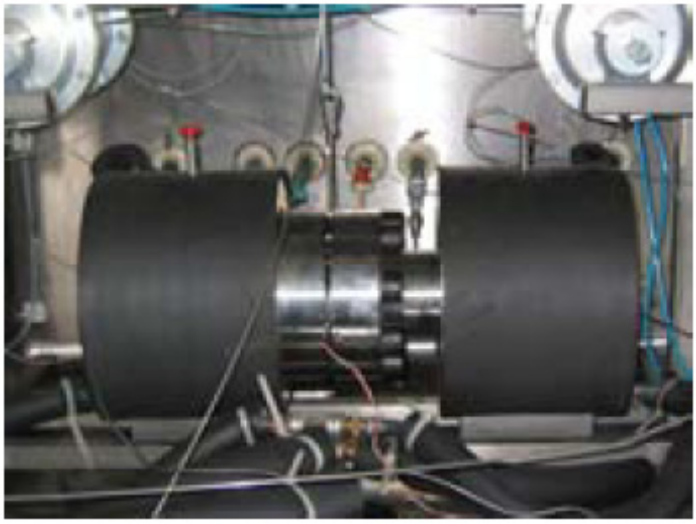

Figur 22: Billede af en isoleret permaetionscelle.

2.2.2 Fremgangsmåde

Permeabilitetsmålingerne er blevet udført på følgende polymermaterialer:

- TFM
- TFM + 20% glass
- PTFE
- PTFE + $PPSO_2$ + Graphite
- PTFE + 10% Ekonol
- FKM

Deres størrelser er blevet ændret til at passe ind imellem de to trykkamre i permeationscellen, se tabel 2.

Polymer	Udformning	Tykkelse (l) [cm]	Diameter (d) [cm]
TFM	Cirkulær	0,104	10,00
TFM+20%Glass	Cirkulær	0,105	10,10
PTFE	Cirkulær	0,105	10,05
PTFE+PPSO$_2$+Graphite	Cirkulær	0,098	10,10
PTFE+10%Ekonol	Cirkulær	0,098	10,05
FKM	Cirkulær	0,270	10,05

Tabel 2: Dimensioner af polymerprøver.

Efter anbringelse af testmaterialet i permeationscelle, suges der vakuum. Dette tager gennemsnitligt 24 timer for hvert forsøg. Herefter fyldes begge kamre med CO_2-gas til et ønskeligt tryk opnås i begge kammer (dvs. 50bar i primærkammer og 45bar i sekundærkammer). Temperaturen i cellen opretholdes på et bestemt niveau ved hjælp af cirkulation af varm glycerin.

Trykforøgelse i det sekundære kammer er et udtryk for gasdiffusion og permeabilitet gennem den testede polymer. Tryk og temperatur opsamles, og trykdata er derefter brugt til at bestemme diffusion og permeabilitet af CO_2 i polymeren.

2.2.3 Behandling af forsøgsresultater

Diffusionskoefficienten (D) er målt ved hjælp af time lag metoden. I denne metode er permeabiliteten beregnet ud fra trykforøgning i det sekundære kammer.

Indledningsvis var trykket af CO_2-gassen typisk; 50bar i det primære kammer og 45bar i det sekundære kammer. Gassen når efter et stykke tid gennem polymermaterialet til lavtrykssiden. Dette observeres som trykforøgning i det sekundære kammer. I figur 23 ses trykforøgning i den sekundære kammer som funktion af tiden for CO_2-TFM system ved 40ºC. Tiden der går, inden steady state flux er opnået, er kendt som time lag θ.

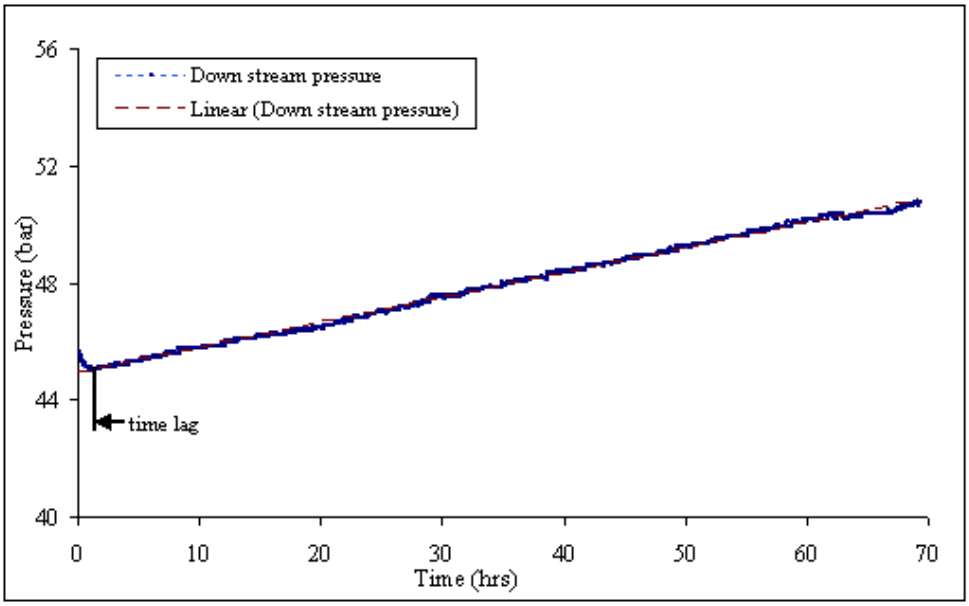

Figur 23: Trykforøgning i det sekundære kammer for CO_2-TFM system ved 40ºC.

For CO_2-TFM system er time lag bestemt til 1,51h. Når time lag er kendt, kan diffusiviteten bestemmes ved hjælp af følgende ligning:

$$D = \frac{l^2}{6\theta}$$

hvor l er polymertykkelsen (for TFM, l = 0,104cm). Permeabiliteten er bestemt ved hjælp af følgende ligning:

$$Pe = \frac{l[cm]}{A[cm^2]} \cdot \frac{(\rho_{end} - \rho_{start})\left[\frac{mol}{l}\right]}{\rho_{STP}\left[\frac{mol}{l}\right]} \cdot \frac{V[cm^3]}{\Delta P[bar] \cdot t[\sec]}$$

hvor:

ρ_{STP}	Specifik molar volumen ved normale betingelser
V	Volumen af sekundært kammer
ΔP	Trykforskellen mellem primær og sekundær kammer
A	Tværsnitareal af polymermaterialet
l	Polymertykkelse
ρ_{start}	Molardensitet ved start
ρ_{end}	Molardensitet ved slut

For yderligere informationer omkring databehandling se Bilag A.

I tabel 3 ses et gennemregnet eksempel for CO_2-TFM systemet.

CO_2-TFM system ved 40C	
CO_2 Mw [g/mol]	44,009
Densitet af CO_2 [Kg/m^3]	1,977
Densitet af CO_2 [mol/cm^3] ved STP	4,49 x 10^{-5}
Volumen af sekundært kammer (V_{cell}) i [cm^3]	22,057
Polymertykkelse (l) i [cm]	0,104
Tværsnitareal af polymermaterialet (A) i [cm^2]	38,480
$P1_{start}$ [bar]	45,655
$P1_{end}$ [bar]	50,764
$T1_{start}$ [ºC]	40,62
$T1_{end}$[ºC]	39,91
1_{start} [mol/l]	2,254
1_{end} [mol/l]	2,626
P [bar]	5,135
Tid [sec]	249461,8
Permeability (Pe) i [cm^3 STP/cm. Sec. bar]	***3,8601 x 10^{-7}***
Time lag [h] - fra Figur 23	1,510
Diffusivitet (D) i [cm^2/sec]	***3,3162 x 10^{-7}***

Tabel 3: Beregnet permeabilitet og diffusivitet for CO_2-TFM system ved 40ºC.

2.2.4 Resultater og diskussion

Permeabilitet og diffusivitet er målt på 6 forskellige polymermaterialer. Resultaterne af eksperimenterne er opsummerede i tabel 4, hvor permeabilitet, diffusivitet og opløselighed er opgivet. Forsøgene er udført ved tre forskellige temperatur 40ºC, 60ºC og 80ºC. Indledningsvis var trykket af CO_2-gassen typisk 50bar i det primære kammer og 45bar i det sekundære kammer.

Polymer	Tryk [bar]	Temperatur [°C]	Permeabilitet $\left[\frac{cm^3(STP)}{cm \cdot bar.\sec}\right]$	Diffusivitet $\left[cm^2/\sec\right]$	Opløselighed $\left[\frac{cm^3(STP)}{cm^3 \cdot bar}\right]$
TFM	48,21	40,26	$3,86 \times 10^{-7}$	$3,32 \times 10^{-7}$	1,162
	48,16	59,92	$3,91 \times 10^{-7}$	$5,09 \times 10^{-7}$	0,768
	51,25	77,65	$4,68 \times 10^{-7}$	$7,08 \times 10^{-7}$	0,660
TFM+20%Glass	48,05	40,21	$6,25 \times 10^{-7}$	$3,05 \times 10^{-7}$	2,047
	48,64	59,83	$5,75 \times 10^{-7}$	$4,57 \times 10^{-7}$	1,257
	49,25	79,41	$5,80 \times 10^{-7}$	$7,24 \times 10^{-7}$	0,802
PTFE	47,99	40,23	$5,49 \times 10^{-7}$	$3,90 \times 10^{-7}$	1,409
	48,64	59,83	$4,78 \times 10^{-7}$	$5,22 \times 10^{-7}$	0,915
	49,09	79,98	$5,08 \times 10^{-7}$	$7,82 \times 10^{-7}$	0,649
PTFE+10% Ekonol	48,23	40,57	$1,28 \times 10^{-6}$	$4,90 \times 10^{-7}$	2,612
	48,51	60,15	$1,06 \times 10^{-6}$	$6,38 \times 10^{-7}$	1,662
	48,96	49,97	$1,09 \times 10^{-6}$	$9,37 \times 10^{-7}$	1,164
PTFE+PPSO$_2$+ Graphite	49,30	40,81	$6,21 \times 10^{-5}$	-	-
	48,09	60,50	$4,07 \times 10^{-5}$	-	-
	48,42	49,75	$2,78 \times 10^{-5}$	-	-
FKM	48,16	40,06	$9,50 \times 10^{-7}$	$7,21 \times 10^{-7}$	1,317
	48,03	60,22	$8,04 \times 10^{-7}$	$8,42 \times 10^{-7}$	0,955
	48,42	80,44	$7,71 \times 10^{-7}$	$1,03 \times 10^{-7}$	0,748

Tabel 4: Permeabilitet, diffusivitet og opløselighed af CO_2 i polymererne ved forskellige temperatur.

I figuren 24 er permeabiliteten vist som funktion af 1/T for alle testede polymertyper.

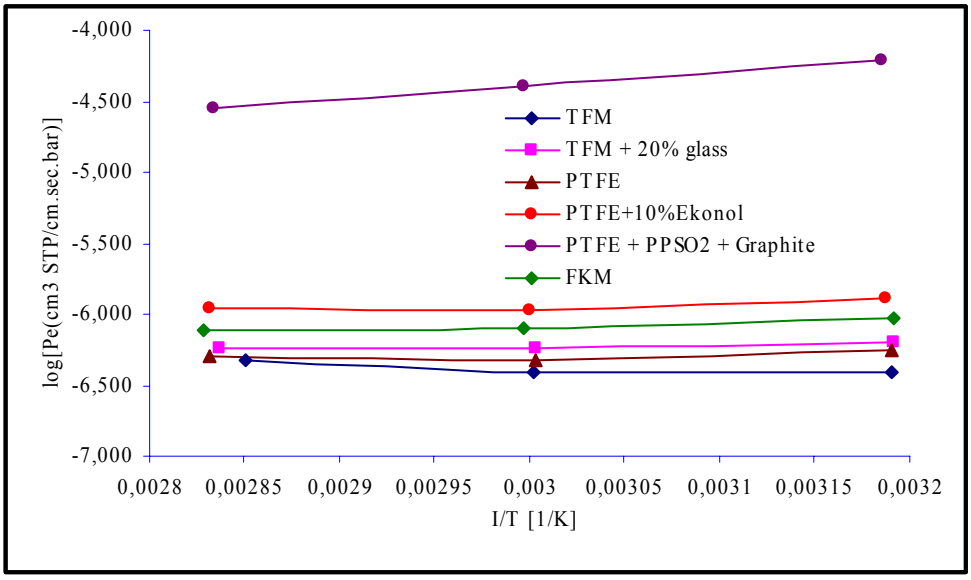

Figur 24: Permeabilitet af CO_2 i polymer3erne som funktion af 1/T.

Man kan sige, at polymererne ligger i følgende rækkefølge fra "bedst" til "værst", dvs. mindst permeabel til mest:

- TFM
- PTFE
- TFM + 10% glas
- FKM

- PTFE + 10% Ekonol
- PTFE + $PPSO_2$ + grafit.

Der er dog ikke en stor forskel mellem de første fem. Den sidste (PTFE + $PPSO_2$ + grafit) er væsentligt værre end de øvrige fem. Endvidere kan man sige, at polymererne bliver mere permeable, når man tilsætter noget (fx glas, ekonol, grafit, $PPSO_2$). For yderligere informationer se Bilag A.

3 Polymerernes mekaniske egenskaber

I dette afsnit gives der en kort introduktion til den opbyggede forsøgsopstilling, samt en beskrivelse af testproceduren for forsøgsrækken, der har til formål at måle polymerernes styrke, mens de er udsat for et CO_2 miljø. Efterfølgende præsenteres og diskuteres resultaterne.

3.1 Testserien

For at repræsentere forholdene i køleanlæggene bedst muligt er der valgt i alt 6 målepunkter i både det underkritiske og overkritiske område jævnfør tabel 5 og Figur 25. Det var ikke muligt at foretage målinger ved lav temperatur med den opbyggede forsøgsopstilling.

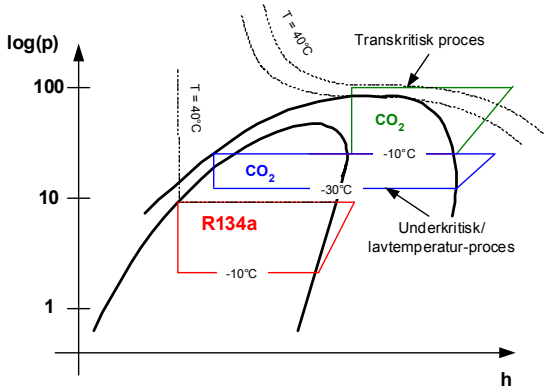

Figur 25: Kredsprocessen for R134a og CO_2.

Tryk	Temperatur	
10 bar	20 °C	80 °C
50 bar	20 °C	80 °C
80 bar	100 °C	
100 bar	100 °C	

Tabel 5 Udvalgte målepunkter

Følgende polymermaterialer testes:

Plast: PVDF; PTFE; PEEK
Elastomer: EPDM; Viton (FKM); Nitril (HNBR)

Trækforsøgene skal ideelt udføres i henhold til ISO 527-1 for plast og DIN 53 504 for elastomerer, der er de standarder, der anvendes ved bestemmelse af mekaniske egenskaber. Ud fra dette er det valgt, at samtlige test skal udføres med en prøvestang af standardiseret størrelse S2, som ses i figur 26.

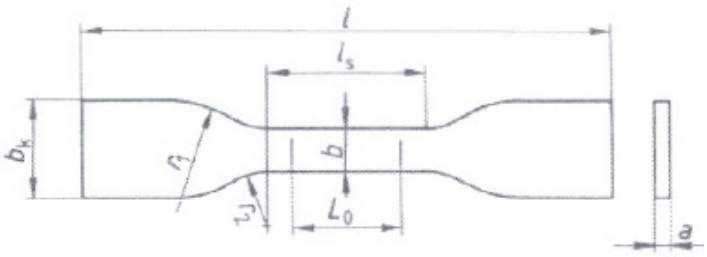

Bild 3: Schulterstab

Tabelle 3: Maße der Schulterstäbe

	Schulterstab			
	S 1	S 2	S 3	S 3A
Gesamtlänge l min.	115	75	35	50
Breite der Köpfe b_k	25	12,5	6	8,5
Länge des Stegs l_s	33	25	12	16
Breite des Stegs b ± 0,05	6	4	2	4
Übergangshalbmesser, innen r_1	25	12,5	3	10
Übergangshalbmesser, außen r_2	14	8	3	7,5
Dicke a	2 ± 0,2	2 ± 0,2	1 ± 0,1	2 ± 0,2
Anfangsmeßlänge L_0	25	20	10	10

Die Maße beziehen sich auf die Schneidwerkzeuge. Die Maße für die Köpfe der Schulterstäbe und die Übergangshalbmesser vom Steg zu den Köpfen können von den vorgeschriebenen Maßen abweichen, die Symmetrie ist jedoch einzuhalten.
Vorzugsweise soll Schulterstab S 2 verwendet werden.

Figur 26: Prøvedimensioner.

3.2 Beskrivelse af forsøgsudstyr

Formålet med forsøgsopstillingen er at kunne måle polymerernes brudstyrke, mens de er udsat for CO_2. Vitalt for forsøgsopstilling var at CO_2-trykket og temperaturen skulle kunne reguleres, så polymerernes brudstyrke kunne bestemmes ved forskellige CO_2-påvirkninger. Til dette formål er der opbygget en forsøgsopstilling, som består af følgende hovedkomponenter:

- Tryktank
- Trækmaskine
- Varmekabel
- CO_2-flaske
- Stempel.

I det følgende gives en kort beskrivelse af de enkelte komponenter samt det overordnede forsøgsdiagram.

Tryktank
Til projektet var der fremstillet en tryktank, som var specialdesignet til at klare høje temperaturer og tryk. Tryktanken er designet til at kunne klare 150 bar ved 250°C. Formålet med tanken var at placere testmaterialer i tanken, hvorefter tanken fyldes med CO_2 ved et forudbestemt tryk og temperatur. I tanken er der opbygget en anordning, hvor polymerprøverne kan fastmonteres. Desuden er tryktanken udstyret med i alt 4 skueglas for visuel indgang. Tryktanken er udstyret med en temperaturmåler PT1000 fra Danfoss, trykmåler af type MBS fra Danfoss, samt en sikkerhedsventil af fabrikatet Leser Tryktanken, som kan ses i figur 27.

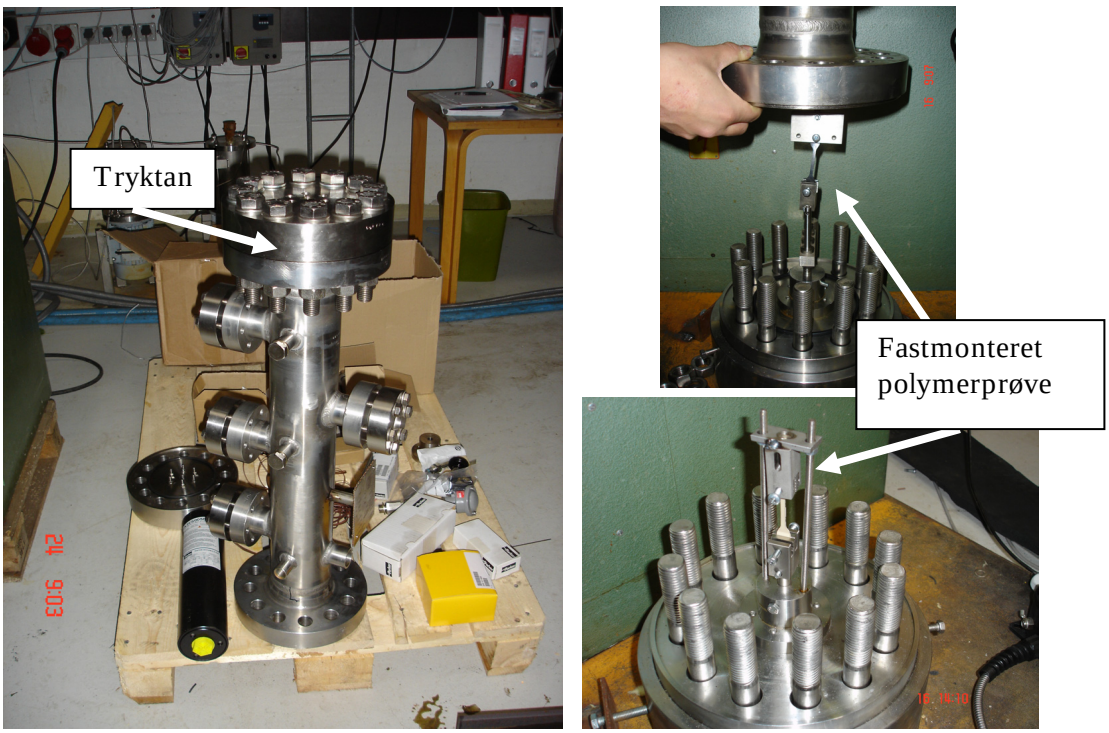

Figur 27: Til venstre tryktanken; til højre anordningen, hvor polymerprøverne fastmonteres.

Trækmaskine
Til projektet var der lånt en trækmaskine af type Zwick 1461, W.Nr.60113. Trækmekanismen har forbindelse til polymererne i tryktanken via en akselstang, som går ind i tanken via åbningen i toppen, se figur 28. Spændingen og vandringen måles eksternt ved hjælp af en vejecelle TCTN-9110-3kN og en længdetransducer HPS-M1-075-420-F-S104.

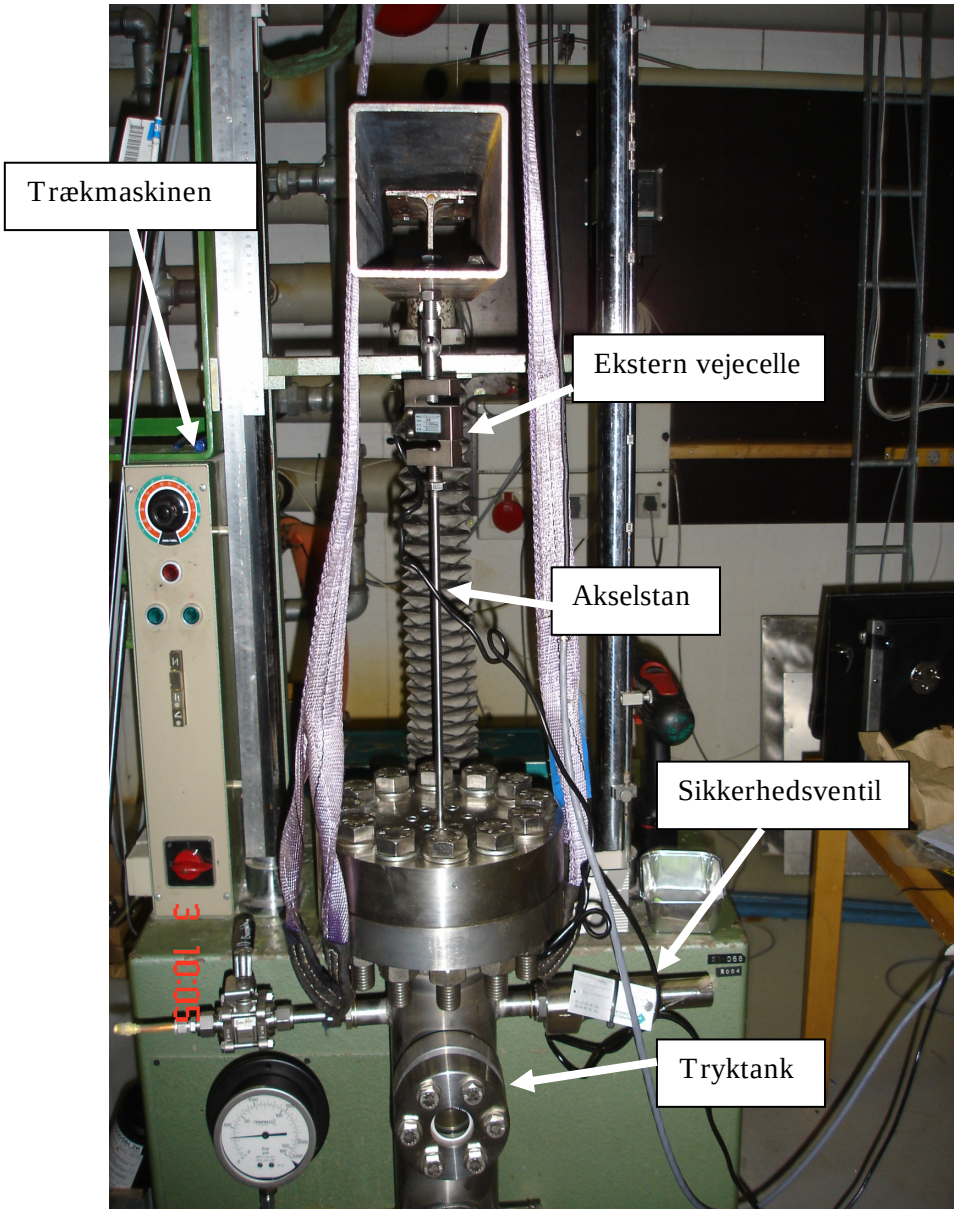

Figur 28: Trækmaskine.

Varmekabel
Temperaturen i tanken reguleres ved hjælp af et selvregulerende varmekabel, type 90FSU, som er viklet rundt omkring tryktanken. Varmekabelet styres af en termostat, type CT-C 20-300 ºC, hvis setpunkt er blevet sat manuelt ved at observere den indvendige temperatur i tanken.

CO_2-flaske
Tryktanken fyldes med CO_2 direkte fra CO_2-flasken.

Stempel
For de overkritiske forsøg er trykket i tanken øget vha. en stempelakkumulator fra Parket. Stemplet på den ene side forbindes med CO_2-flasken og på den anden side med nitrogenflasken, hvis tryk kan reguleres.

Forsøgsdiagram
Billede af hele forsøgsopstillingen kan ses i figur 29.

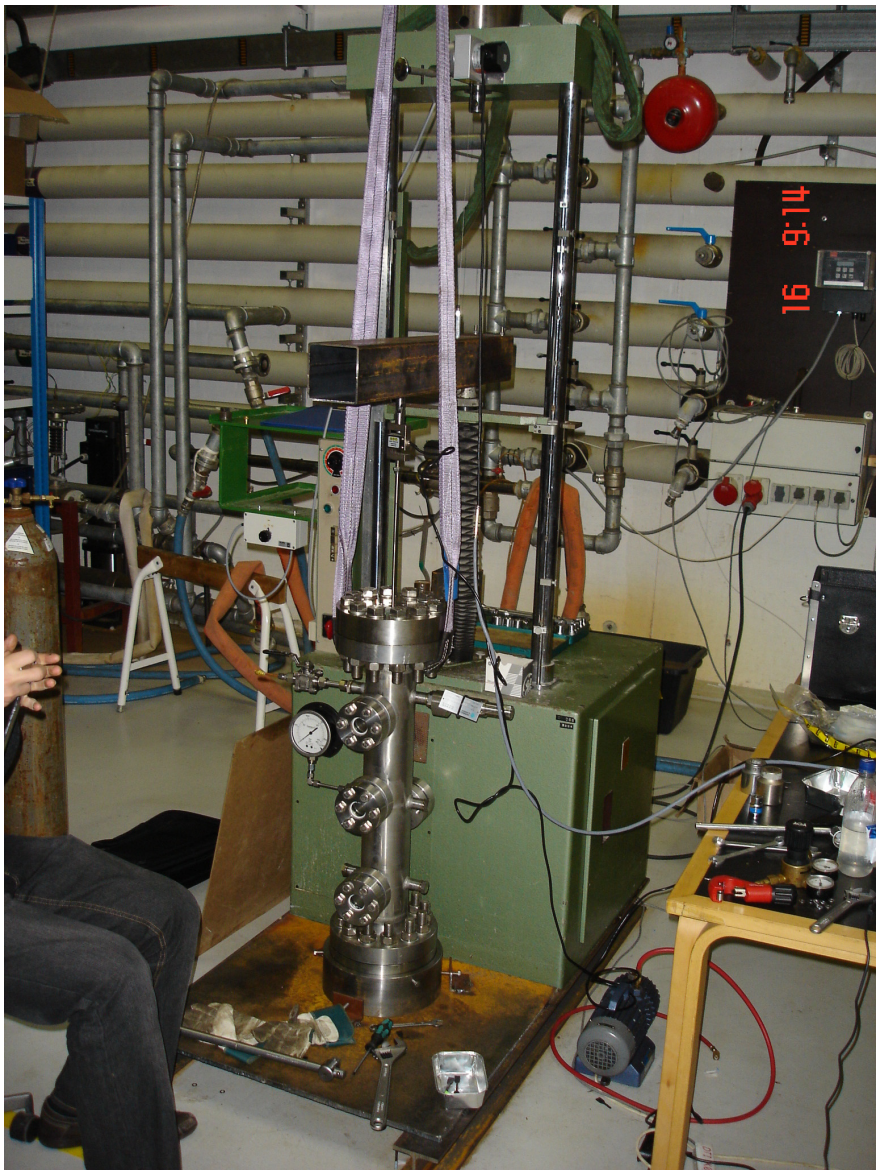

Figur 29: Forsøgsopstilling.

Under forsøgene opstår der problemer med lækager. Det viste sig, at det blev nødvendigt at efterfylde tanken kontinuerligt for at undgå trykfald i tanken. For underkritiske forsøg blev dette problem løst ved at koble tryktanken direkte med CO_2 flasken over en trykreguleringsventil. På den måde kunne trykket i tanken holdes konstant op til 50 bar, se også procesdiagram 30.

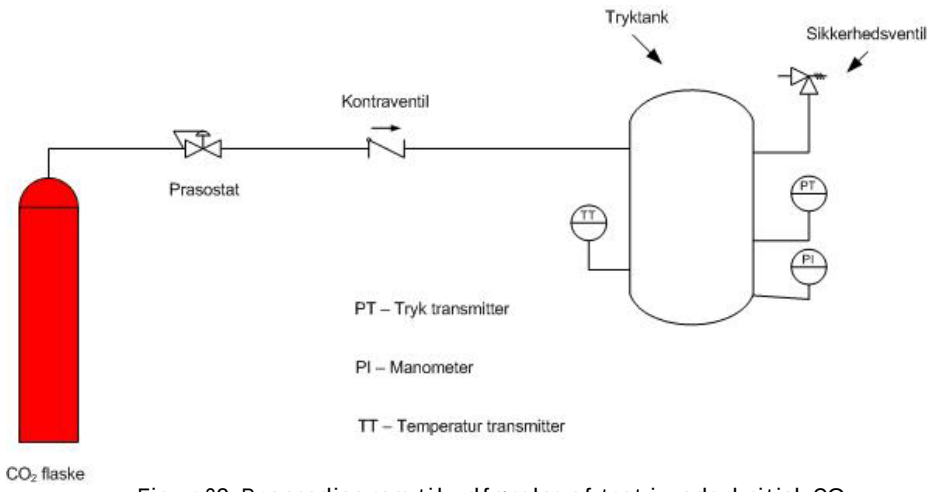

Figur 30: Procesdiagram til udførelse af test i underkritisk CO_2.

For overkritiske forsøg ser procesdiagrammet ud som vist på figur 31. Der kobles en nitrogenflaske samt et stempel på tryktanken. Stemplet fyldes med CO_2. Stemplet påvirkes af trykket fra nitrogenflasken, som reguleres ved hjælp af trykreguleringsventil. Såfremt trykket i tanken falder pga. lækagen, vil tryktanken blive efterfyldt med CO_2 fra stemplet.

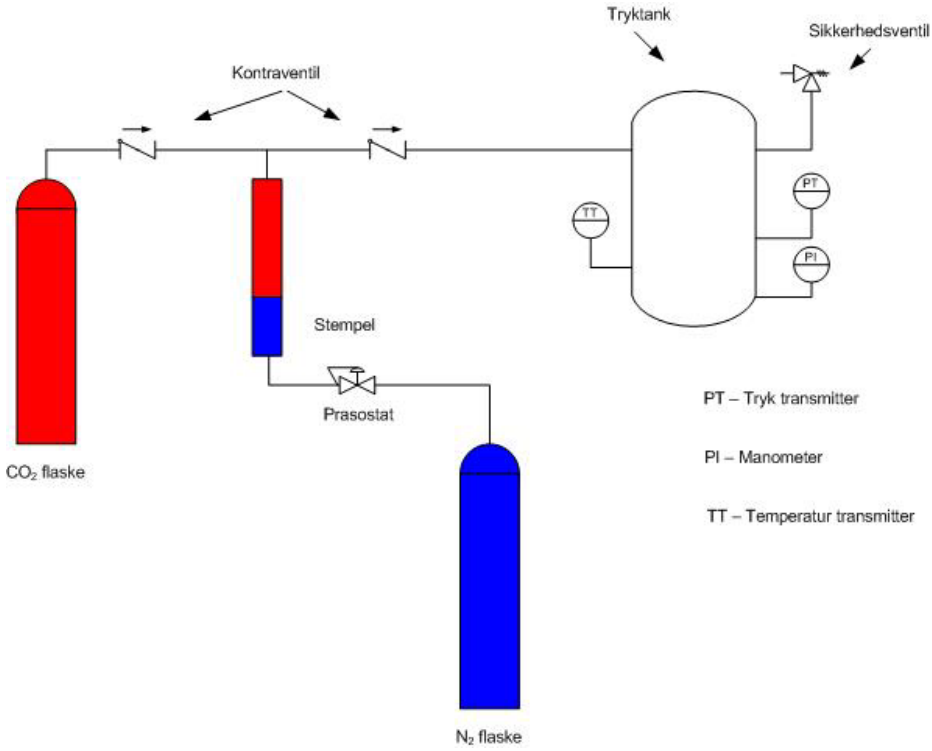

Figur 31: Procesdiagram til udførelse af test i overkritisk CO_2.

3.3 Fremgangsmåde

Hvert forsøg udføres ved at følge proceduren, som vist i diagrammet forneden. Efter anbringelse af testmaterialet i tryktanken suges der vakuum, hvorefter tanken fyldes med CO_2. Der ventes 24 timer efter påfyldning af CO_2, før træktesten foretages for at være sikker på at den testede polymer er mættet med CO_2.

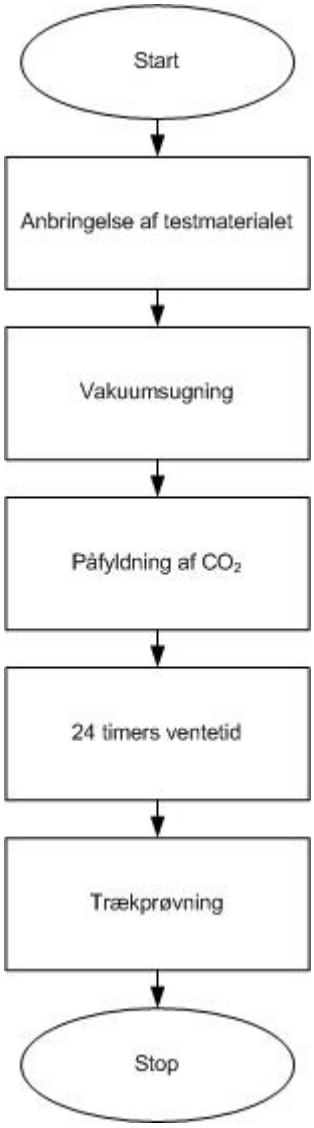

Figur 32: Testproceduren.

3.4 Validering af forsøgsstanden

Før endelig test udføres, sammenlignes en trækprøve udført i teststanden med en trækprøve udført på en trækmaskine, der normalt bruges til at foretage akkrediteret træktest. Dette er gjort for at validere forsøgsstanden. Begge trækprøver er udført ved samme konditioner dvs. i luft ved 20 °C. Resultaterne ses i figur 33 og 34 for EPDM og HNBR.

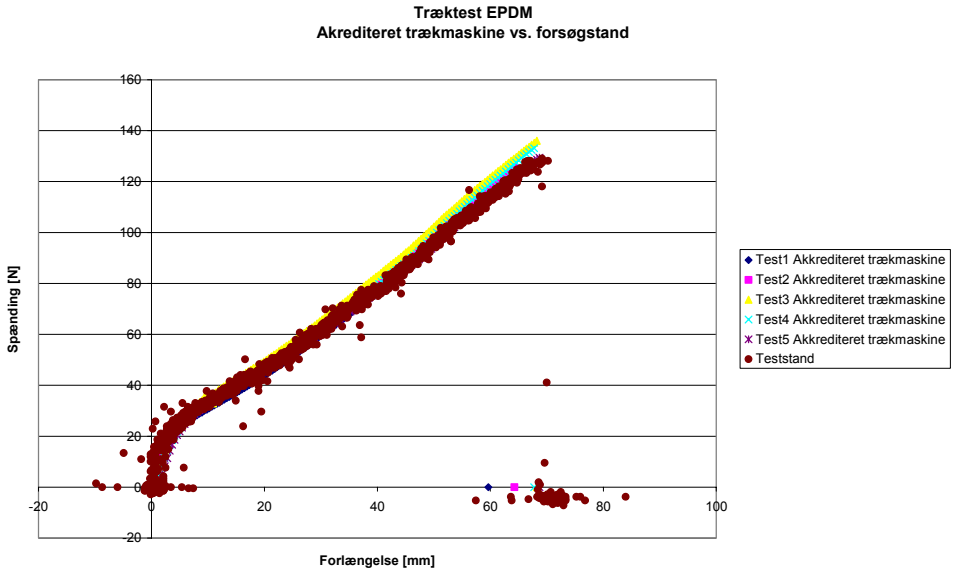

Figur 33: Træktest af EPDM i luft.

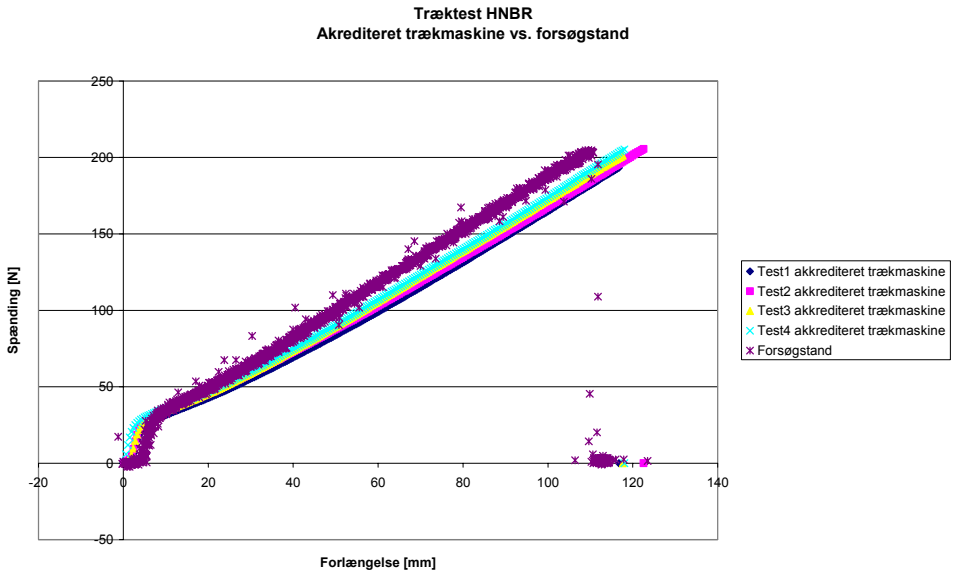

Figur 34: Træktest af HNBR i luft.

Der er foretaget henholdsvis 5 EPDM-test og 4 HNBR-test på en akkrediteret trækmaskine. Selvom teststykker er udtaget af det samme materialestykke, er der afvigelser i forhold til den målte brudstyrke, se tabel 6. Brudstyrken og brudforlængelsen fundet i forsøget, udført på teststanden, stemmer dog fint overens med gennemsnittet af testene, foretaget på den akkrediterede maskine.

	EPDM	
	Brudforlængelse [mm]	Brudstyrke [N]
Test 1	59	113
Test 2	64	125
Test 3	68	136
Test 4	68	133
Test 5	69	129
Forsøgsstand	69	129
	HNBR	
	Brudforlængelse [mm]	Brudstyrke [N]
Test 1	116	193,3
Test 2	122	205,6
Test 3	117	201,3
Test 4	118	205,3
Forsøgsstand	110	204

Tabel 6: Brudspænding og brudforlængelse af EPDM og HNBR.

3.5 Resultater og diskussion

Resultaterne præsenteres og diskuteres i det følgende afsnit.

3.5.1 Databehandling og usikkerheder

En typisk samplingsprøve ser ud som vist i figur 35. Data opsamles med en frekvens på 50 gange i sekundet, og trækprøvemaskinen kører med en konstant hastighed på 500mm/min. Det er valgt at sample data, også efter at prøven er trukket over. Det niveau, som findes, når maskinen trækker, selvom prøven er trukket i stykker, er det niveau, resultaterne nulstilles efter. Det færdigbehandlede resultat ses i figur 35 nederst.

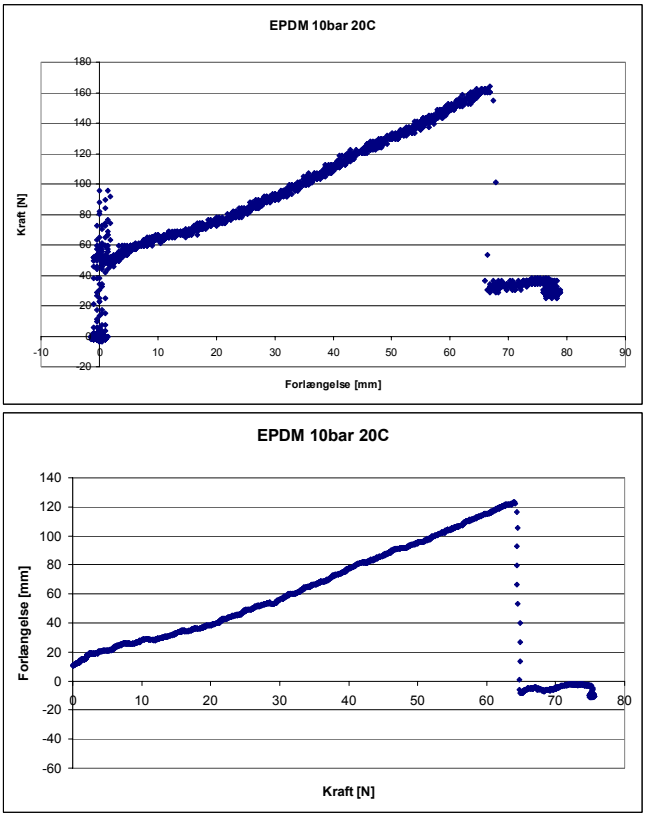

Figur 35: Øverst: Ubehandlede prøvedata. Nederst: Behandlede prøvedata.

I alle forsøgene opmåles kraften ved en ekstern vejecelle. Vejecellen har en opløsning på 0,91 N over et spænd på 3000 N, så det vurderes ikke, at denne har nogen betydning som fejlkilde. Fejlkilder på kraftmåling ligger i de kræfter, som trækstangen bliver udsat for, som ikke stammer fra materialeprøven.

Vejecellen udsættes for vibrationer og dermed udslag på målingen ved start og slut af trækprøveforsøg, og når prøven trækkes over. Vejecellen måler modstanden igennem pakningen. Denne modstand er afhængig af trykket i beholderen og dermed på pakningen, og endvidere er den afhængig af, om trækstangen trækkes helt præcist gennem pakningshuset. For at undgå skæv oplejring af beholderen i forhold til trækprøvemaskinen er et fleksibelt led mellem trækstang og vejecelle introduceret på trækprøvemaskinen.
Trykket i beholderen vil også forsøge at presse trækstangen op og ud af beholderen, og påvirker således også kraftmålingen.

I bunden af beholderen er prøven monteret mellem 2 greb, og det øverste greb er monteret således, at det holder prøven gennem de 24 timer, prøven varer. Trækstangen ned i beholderen trækker altså ikke i prøven, før trækmaskinen startes. Dette sikres med en lille notgang i det øverste greb. At prøven skal løftes fri fra de 2 stænger, der holder prøven, kan formentlig betyde, at der kan opstå en fejlmåling der. Det vurderes, at denne fejl er minimal.

Det viste sig at være problematisk med den opbyggede forsøgsopstilling at ramme det nøjagtige tryk og temperaturniveau hver gang, især for overkritiske forsøg. Trykket over 50 bar er opnået ved at fylde en bestemt mængde CO_2 i tryktanken og øge trykket ved at øge temperaturen. Selvom temperaturen kunne holdes konstant +/-3 ºC og trykket +/-5 bar efter ligevægtsbalancen blev nået, gav det problemer med hensyn til at opnå det præcise tryk- og temperaturniveau. Det kan altså blive problematisk at sammenligne på tværs af materialetyper, hvis testene ikke har fundet sted ved de samme konditioner. For et enkelt materiale kan resultater stadigvæk sammenlignes ved forskellige konditioner.

Der er altså usikkerheder på den målte kraft og på CO_2 konditionerne. Disse 2 usikkerheder vurderes umiddelbart at have den største indflydelse på forsøgenes resultater. Af andre usikkerhed, der kan overvejes, bør nævnes:

Usikkerhed på længdemålingen. Denne usikkerhed ligger både i selve måleenheden, men også i den måde, som denne vha. en metaltråd er sat på stangen, hvorfra trækket udgår. Måleenheden har en opløselighed på 0,22 mm, og dette skønnes ikke at påvirke resultaterne. Da alle prøver er foretaget med den samme opsætning af længdetransduceren og metaltråden, kan man konstatere, at en eventuel konstant fejlmåling fx pga. en lille skævhed i metaltråden må blive gentaget igennem alle forsøg, og derfor (og så længe resultaterne kun bruges til sammenligning med hinanden) elimineres fejlen. Det skønnes altså ikke, at usikkerheden på længdemålingen påvirker resultatet nævneværdigt.

Usikkerhed på hastigheden, hvormed prøven trækkes over skønnes ikke at have betydning, da trækprøvemaskinen er en maskine, der også anvendes til kalibrerede test.

Usikkerheden for nedbøjning af den stang, hvormed trækket overføres fra trækprøvemaskinen til stangen, er udregnet til 0,05 mm i punktet, hvor trækstangen er monteret, og betyder således intet.

Usikkerheden for, hvorvidt prøven er helt rigtigt monteret, er naturligvis til stede. Prøven er således monteret manuelt i beholderen, hvorefter beholderen er lukket. Prøven er natuligvis forsøgt monteret fuldstændig præcis hver gang, og der er således monteret 2 stænger i bunden af beholderen. De 2 stænger holder prøven præcis hver gang, og således udsættes prøven ikke for kræfter under de 24 timer i beholderen. En usikkerhed i denne forbindelse er, om der trækkes helt lige på polymeren. Trækkes denne skæv, kan det ændre dens styrkeforhold. Dette er forsøgt forhindret ved forud for hvert forsøg at sikre, at trækstangen er præcist monteret. Endvidere er trækstangen monteret på vejecellen vha. et fleksibelt led, der sikrer, at trækstangen står præcist, også selv om beholder og trækprøvemaskine ikke er præcist linet op. Trækstangen styres i pakningshuset af 2 føringsbånd. Dette er usikkerheder, der er svære at

gøre noget ved. Der kan eventuelt udføres flere test med samme materiale og konditioner, men det har ikke været en mulighed her.

Usikkerheden omkring materialet er ikke væsentligt, fordi alle materialeprøver er taget ud fra det samme identiske stykke råmateriale. Dog har PEEK-plasten muligvis lidt varierende tykkelse i pladen, hvorfra prøverne er taget. Dette skønnes dog ikke at udgøre en væsentlig fejlkilde, da der er tale om meget små forskelle.

Opsummering

De største usikkerhedskilder er målingen af kraften, som prøven optager, og så usikkerheden på temperatur og tryk i beholderen. Som beskrevet i ovenstående, er disse fejlkilder klart de væsentligste. Hvilken betydning, fejlkilderne har haft, er svært at sige, men det, at kraftmålingen er behæftet med usikkerhed, er nok den mest alvorlige. Kraftmålingen foregår med præcis samme hastighed på trækstangen hver gang, og er således til stede på alle målinger, men den er forskellig fra gang til gang alt efter hvilket tryk, der findes i tanken. Dog vurderes usikkerheden ikke at påvirke tendenserne, som forsøgene viser.

Problemet med at fastholde et præcist tryk og en præcis temperatur betyder som sådan ikke noget for den enkelte prøve isoleret set. Ved hver enkel test har trykket og temperaturen været konstant.

Prøven kan derfor sammenlignes med prøver af samme materiale ved andre konditioner.

Det er dog svært at sammenligne med andre polymerer, når konditionerne er forskellige, men det vurderes trods alt, at værdierne godt kan sammenlignes på tværs af materialetype, hvis man kun anser resultatet som vejledende.

Yderligere usikkerheder anses ikke for betydelige.

3.5.2 Elastomer i CO_2

EPDM

Resultaterne af forsøgene, udført på EPDM i underkritisk CO_2, er vist i figur 36. I tabel 7 vises brudstyrken ved de enkelte målepunkter.

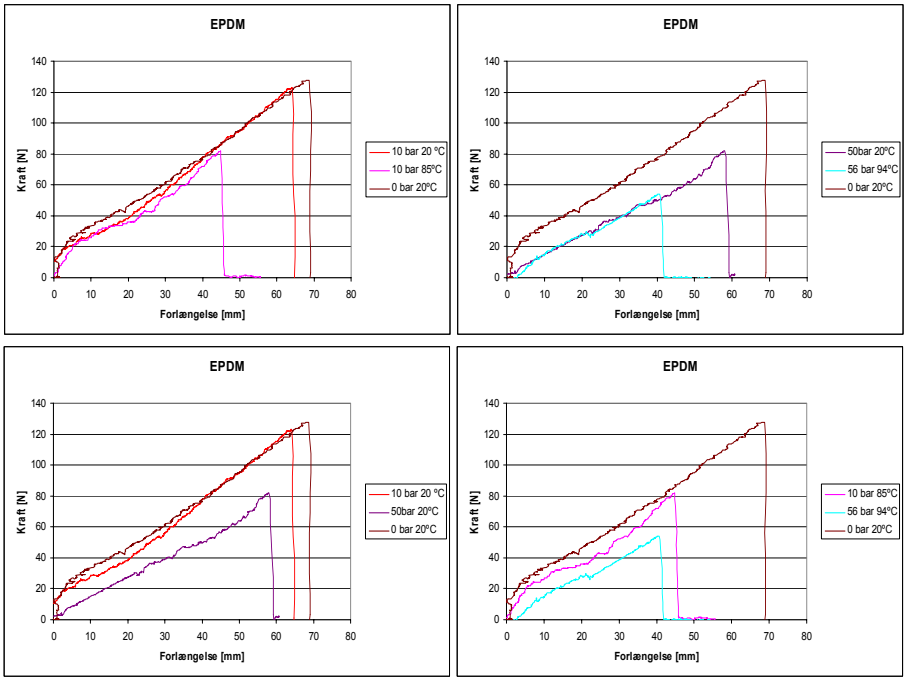

Figur 36: Mekaniske egenskaber af EPDM i underkritisk CO_2. Øverste to grafer viser EPDM temperaturafhængighed ved 10 og 50 bar; nederste to grafer viser EPDM-trykafhængighed ved 20 og 80 ºC.

	EPDM	
	Brudstyrke [N]	Styrke i forhold til luft [%]
Luft (0bar, 20C)	127	100
10 bar, 20C	122	96
10 bar, 85C	82	65
50 bar, 20C	82	65
50 bar, 94C	54	43

Tabel 7: EPDM brudstyrke i underkritisk CO2.

EPDM viste sig at være afhængig af både CO_2-tryk og temperatur. EPDM-styrke falder kraftigt selv i det underkritiske område. Ved 50 bar og 80 ºC faldt styrken til 43% af den oprindelige.

Tendensen med den faldende brudstyrke fortsætter i overkritisk CO_2, se figur 37 samt tabel 8. Brudstyrken af EPDM i overkritisk CO_2 falder til 1/3 del af dens oprindelige styrke.

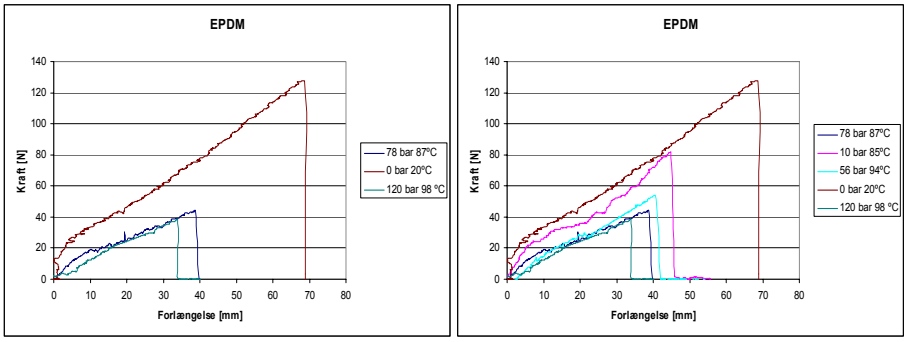

Figur 37: Mekaniske egenskaber af EPDM i overkritisk CO_2. Til venstre vises resultater i overkritisk CO_2 til højre vises resultater af alle forsøgene, hvor temperaturen er over 80 ºC i både over- og underkritisk CO_2.

	EPDM	
	Brudstyrke [N]	Styrke i forhold til luft [%]
Luft (0bar, 20 ºC)	127	100
78 bar, 87 ºC	44	35
120 bar, 98 ºC	39	31

Tabel 8: EPDM brudstyrke i overkritisk CO_2.

FKM Vitton

Resultaterne af forsøgene, udført på FKM (mens udsat for underkritisk CO_2) er vist i figur 38. I tabel 9 vises brudstyrken ved de enkelte målepunkter. Det var ikke muligt at få en brugbar måling ved 50bar og 80°C selv ved flere forsøg. Prøven brækkede ved fastmonteringsmekanismen, selvom flere mulige løsninger er blevet afprøvet.

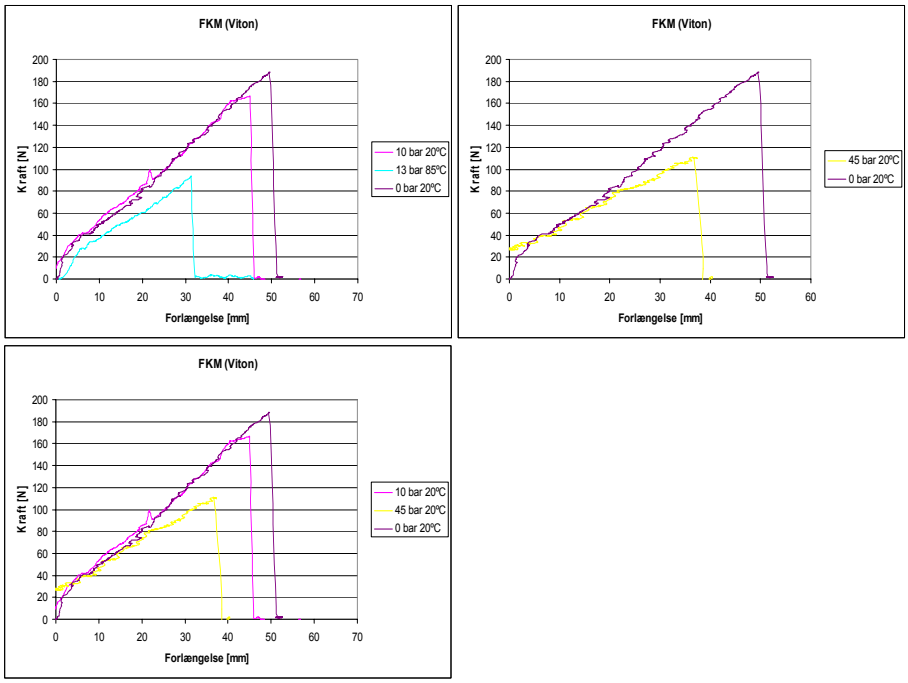

Figur 38: Mekaniske egenskaber af FKM i underkritisk CO_2. Øverste to grafer viser temperatur afhængighed ved 10 og 50bar, nederste graf viser FKM trykafhængighed ved 20 ºC.

	FKM	
	Brudstyrke [N]	Styrke i forhold til luft [%]
Luft (0bar, 20 ºC)	188	100
10 bar, 20 ºC	166	88
13 bar, 85 ºC	93	49
45 bar, 20 ºC	110	58
50 bar, 80 ºC	mangler	

Tabel 9: FKM brudstyrke i underkritisk CO_2.

FKM ser ud til at være både tryk- og temperaturafhængig. FKM styrke falder kraftigt, og allerede ved 10 bar og 80 ºC er den målte brudstyrke under halvdelen af den oprindelige.

I overkritisk CO_2 falder styrken ned til under halvdelen af den oprindelige, se figur 39 og tabel 10.

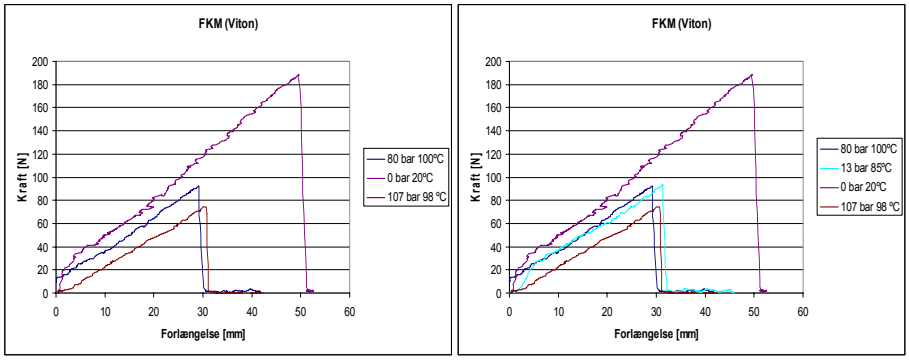

Figur 39: Mekaniske egenskaber af FKM i overkritisk CO_2. Til venstre vises resultater i overkritisk CO_2 til højre vises resultater af alle forsøgene, hvor temperatur er over 80 ºC i både over- og underkritisk CO_2.

	FKM	
	Brudstyrke [N]	Styrke i forhold til luft [%]
Luft (0bar, 20 ºC)	188	100
80 bar, 100 ºC	92	49
107 bar, 98 ºC	74	39

T

Tabel 10: FKM brudstyrke i overkritisk CO_2.

HNBR Nitril

Resultaterne af forsøgene udført på HNBR (mens udsat for underkritisk CO_2) er vist i figur 40. I tabel 11 vises brudstyrken ved de enkelte målepunkter.

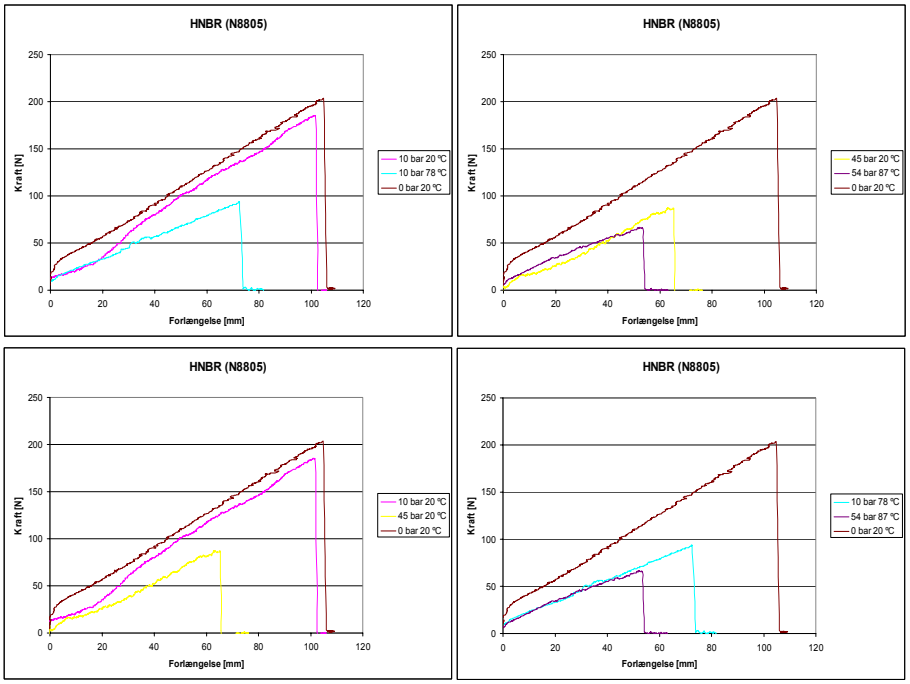

Figur 40: Mekaniske egenskaber af HNBR i underkritisk CO_2. Øverste to grafer viser HNBR temperaturafhængighed ved 10 og 50 bar; nederste to grafer viser HNBR tryk afhængighed ved 20 ºC og 80 ºC.

	HNBR	
	Brudstyrke [N]	Styrke i forhold til luft [%]
Luft (0bar, 20 ºC)	204	100
10 bar, 20 ºC	185	91
10 bar, 78 ºC	93	45
45 bar, 20 ºC	87	43
54 bar, 87 ºC	65	32

Tabel 11: HNBR brudstyrke i underkritisk CO_2.

Også HNBR ser ud til at være kraftigt påvirket af både tryk og temperatur. Brudstyrken ved 50 bar og 80 °C er faldet ned til 32% af HNBR styrke i luften.

Brudstyrken af HNBR faldt yderligere i den overkritiske CO_2, se figur 41 samt tabel 12. Ved 100 bar og 100 ºC er brudstyrket faldet ned til omkring 23% af den oprindelige styrke.

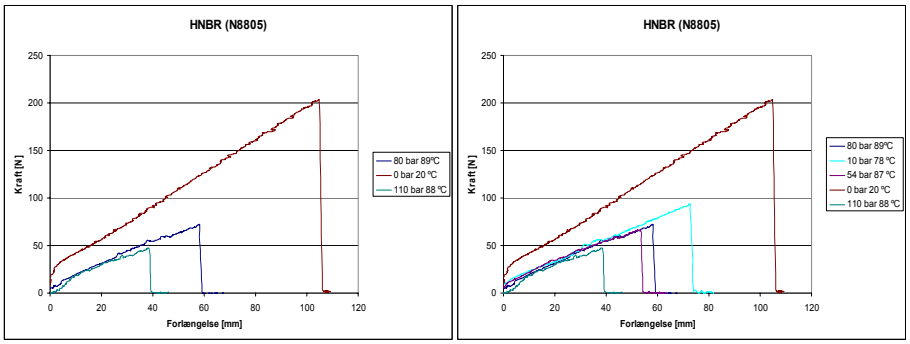

Figur 41: Mekaniske egenskaber af HNBR i overkritisk CO_2. Til venstre vises resultater i overkritisk CO_2. Til højre vises resultater af alle forsøgene, hvor temperaturen er over 80 ºC i både over- og underkritisk CO_2.

	HNBR	
	Brudstyrke [N]	Styrke i forhold til luft [%]
Luft (0bar, 20 ºC)	204	100
80bar, 89 ºC	72	35
110bar, 88 ºC	47	23

Tabel 12: HNBR brudstyrke i overkritisk CO2

3.5.3 Plast i CO_2

PTFE

Resultaterne af forsøgene, udført på PTFE er vist i figur 42. I tabel 13 vises brudstyrken ved de enkelte målepunkter.

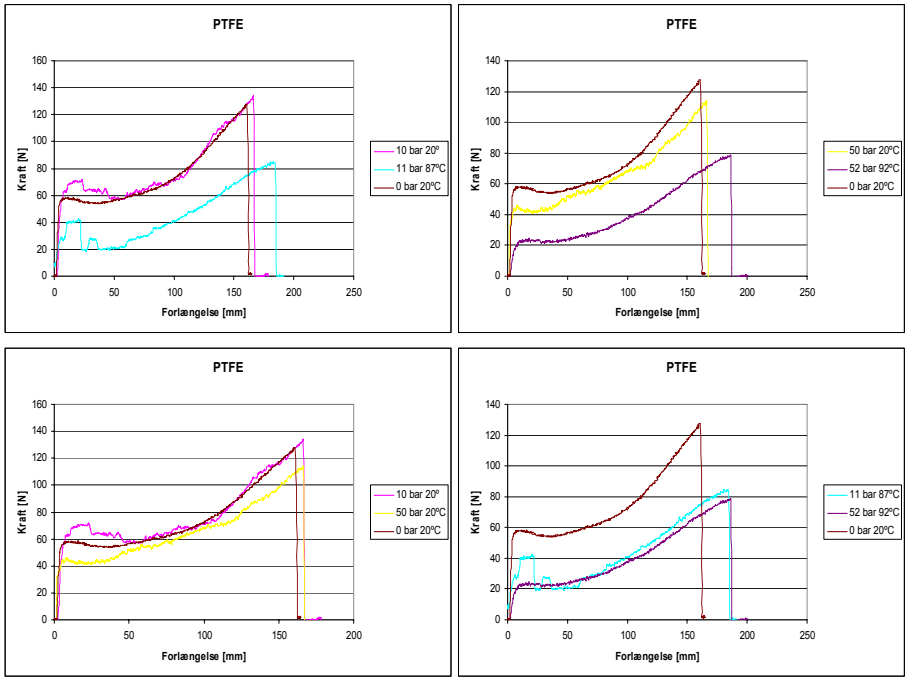

Figur 42: Mekaniske egenskaber af PTFE i underkritisk CO_2. Øverste to grafer viser PTFE temperaturafhængighed ved 10 og 50 bar. Nederste to grafer viser PTFE tryk afhængighed ved 20 og 80 ºC.

	PTFE	
	Brudstyrke [N]	Styrke i forhold til luft [%]
Luft (0bar, 20 ºC)	128	100
10 bar, 20 ºC	134	104
11 bar, 87 ºC	84	66
50 bar, 20 ºC	114	89
50 bar, 92 ºC	78	61

Tabel 13: PTFE brudstyrke i underkritisk CO_2.

Af figurerne samt tabellen kan man tydeligt se, at PTFE viser gode tendenser. PTFE brudstyrke ændres stort set ikke i forhold til ændring af CO_2-trykket, dog viser PTFE stadig afhængighed i forhold til temperaturændring. Ved 80°C faldt brudstyrken ned til 61 %-65 %, af hvad den var ved 20 ºC.

PTFE ser ud til at fastholde samme tendenser i overkritisk CO_2 dvs. PTFE brudstyrke ser ud til at afhænge af temperaturen og kun i et mindre grad af trykket, jævnfør figur 43 og tabel 14.

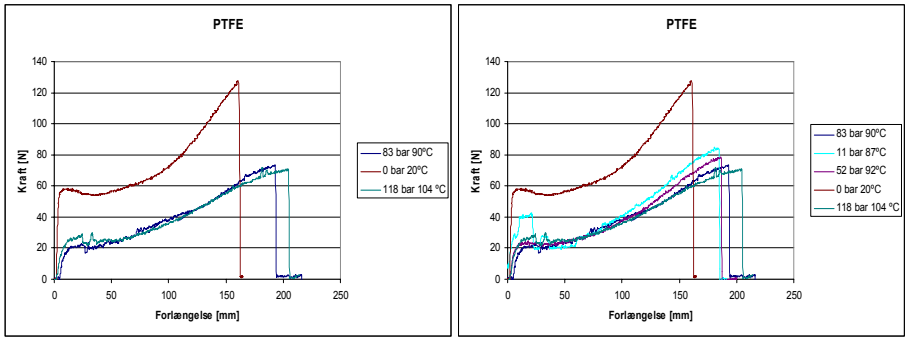

Figur 43: Mekaniske egenskaber af PTFE i overkritisk CO_2. Til venstre vises resultater i overkritisk CO_2. Til højre vises resultater af alle forsøgene, hvor temperaturen er over 80C i både over- og underkritisk CO_2.

	PTFE	
	Brudstyrke [N]	Styrke i forhold til luft [%]
Luft (0bar, 20 ºC)	128	100
83 bar, 90 ºC	73	57
118 bar, 104 ºC	69	54

Tabel 14: PTFE brudstyrke i overkritisk CO_2.

PVDF

Resultaterne af forsøgene udført på PVDF i underkritisk CO_2 er vist i figur 44. I tabel 15 vises brudstyrken ved de enkelte målepunkter.

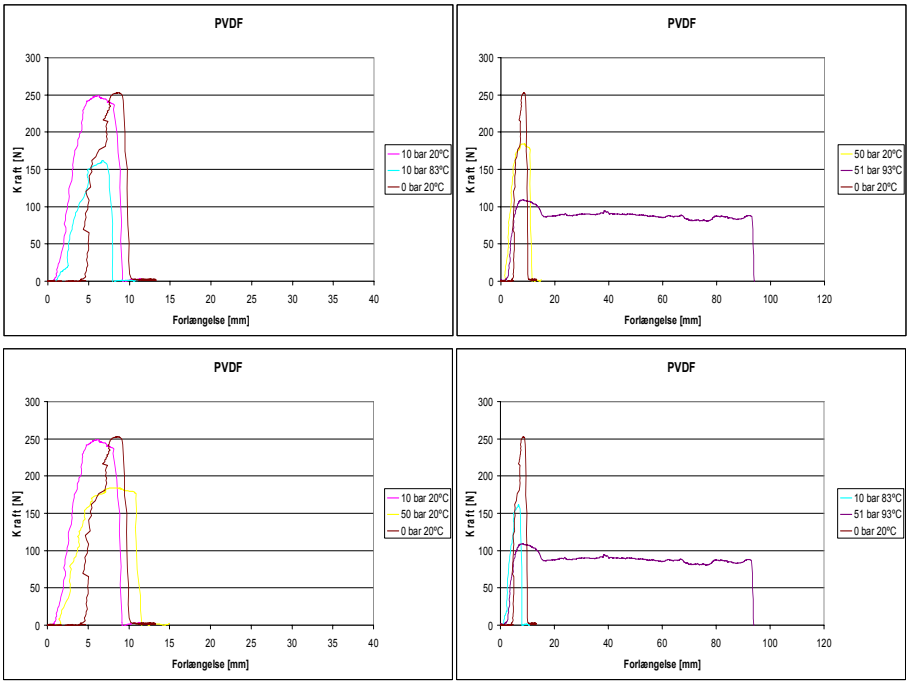

Figur 44: Mekaniske egenskaber af PVDF i underkritisk CO_2. Øverste to grafer viser PVDF temperatur afhængighed ved 10 og 50 bar. Nederste to grafer viser PVDF trykafhængighed ved 20 og 80 ºC.

	PVDF	
	Brudstyrke [N]	Styrke i forhold til luft [%]
Luft (0bar, 20 ºC)	252	100
10 bar, 20 ºC	247	98
10 bar, 83 ºC	159	63
50 bar, 20 ºC	184	73
51 bar, 93 ºC	(108)	43

Tabel 15: PVDF-brudstyrke i underkritisk CO2.

Resultaterne tyder på, at PVDF er afhængig af både CO_2-tryk og temperatur. PVDF brudstyrke ved 50 bar og 80 ºC faldt kraftig ned til 43% af dens brudstyrke i luften.

PVDF ser ud til at ændre egenskaber, når man kommer højere op i temperatur og tryk. PVDF mister lidt af styrken (under halvdelen i forhold til oprindelig brudstyrke i luft ved 20 °C), men brudforlængelse ser ud til at blive forøget kraftigt, jævnført figur 45 og tabel 16.

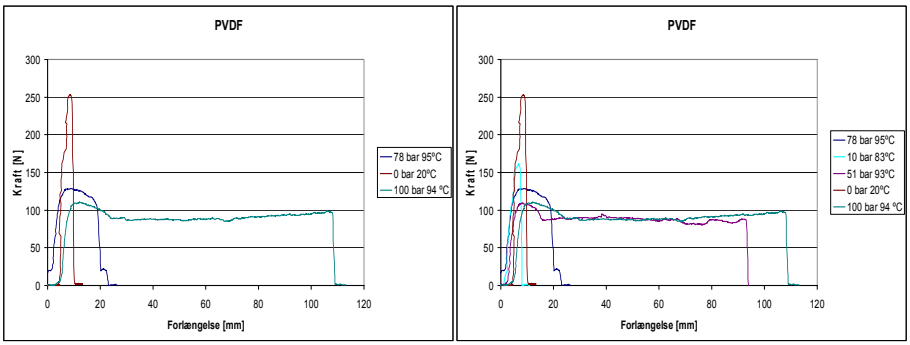

F

Figur 45: Mekaniske egenskaber af PVDF i overkritisk CO_2. Til venstre vises resultater i overkritisk CO_2 til højre vises resultater af alle forsøgene, hvor temperaturen er over 80C i både over- og underkritisk CO_2.

	PVDF	
	Brudstyrke [N]	Styrke i forhold til luft [%]
Luft (0bar, 20 °C)	252	100
78 bar, 95 °C	(127)	50
100 bar, 94 °C	(109)	43

Tabel 16: PVDF-brudstyrke i overkritisk CO_2.

PEEK

Resultaterne af forsøgene udført på PEEK i underkritisk CO_2 er vist i figur 46. I tabel 17 vises brudstyrken ved de enkelte målepunkter.

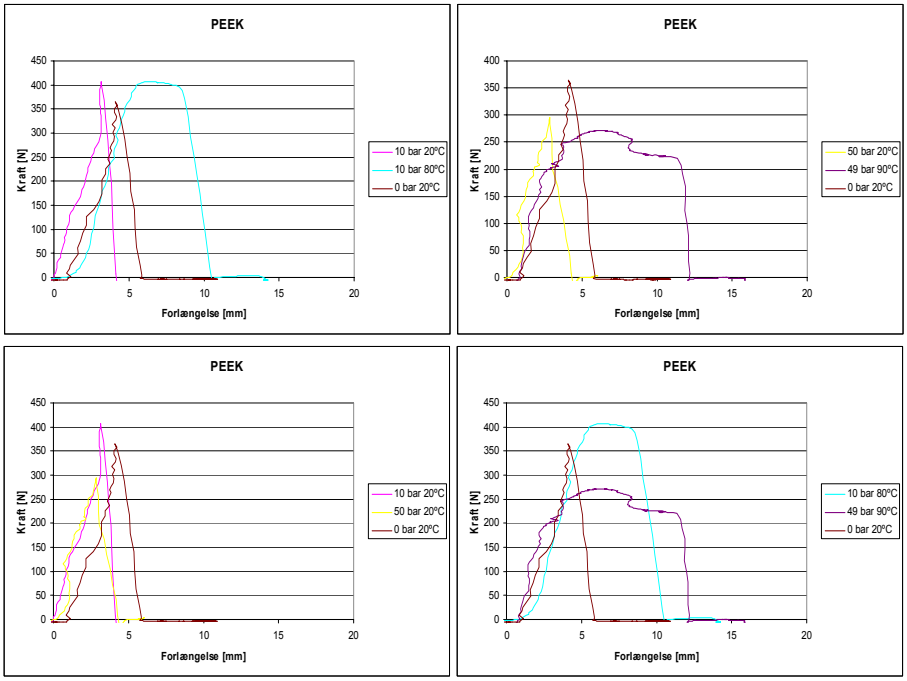

Figur 46: Mekaniske egenskaber af PEEK i underkritisk CO_2. Øverste to grafer viser PEEK temperaturafhængighed ved 10 og 50 bar, nederste to grafer viser PEEK trykafhængighed ved 20 og 80 ºC.

	PEEK	
	Brudstyrke [N]	Styrke i forhold til luft [%]
Luft (0bar, 20 ºC)	365	100
10 bar, 20 ºC	402	110
10 bar, 80 ºC	405	111
50 bar, 20 ºC	295	81
49 bar, 90 ºC	271	74

Tabel 17: PEEK-brudstyrke i underkritisk CO_2.

PEEKs meget korte brudforlængelse har gjort det meget svært at få gode måleresultater ved den opbyggede forsøgsopstilling. Derfor skal resultater betragtes som vejledende. PEEK viser dog gode tendenser med lav temperatur- og trykpåvirkning i CO_2.

PEEK ser ligesom PVDF ud til at ændre egenskaber, når man kommer højere op i temperatur og tryk. PEEK mister styrke til omkring 70 % af den oprindelige brudstyrke ved 20 ºC, mens brudforlængelse ser ud til at blive forøget kraftigt, jævnfør figur 47 og tabel 18.

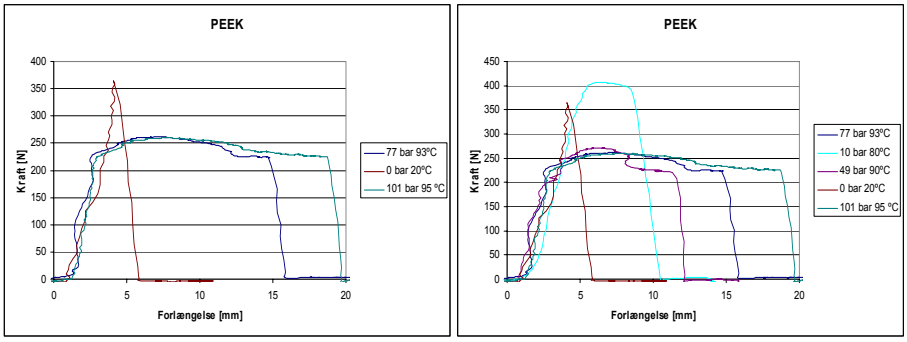

Figur 47: Mekaniske egenskaber af PEEK i overkritisk CO_2. Til venstre vises resultater i overkritisk CO_2. Til højre vises resultater af alle forsøgene, hvor temperaturen er over 80 ºC i både over- og underkritisk CO_2.

	PEEK	
	Brudstyrke [N]	Styrke i forhold til luft [%]
Luft (0bar, 20 ºC)	365	100
77 bar, 93 ºC	261	71
101 bar, 95 ºC	260	71

Tabel 18: PEEK brudstyrke i overkritisk CO_2

3.6 Opsummering

Alle valgte elastomertyper (EPDM, FKM, HNBR) ser ud til at være kraftigt påvirket af CO2. Fælles for dem alle var, at deres brudstyrke viste en stor afhængighed af både CO_2 temperatur og tryk. Brudforlængelse falder også. Ved overkritisk drift skal man forvente styrke reduktion med over 60 %, se tabel 19.

	EPDM	FKM	HNBR
	Styrke i forhold til luft [%]	Styrke i forhold til luft [%]	Styrke i forhold til luft [%]
10 bar, 20 ºC	96	88	91
10 bar, 80 ºC	65	49	45
50 bar, 20 ºC	65	58	43
50 bar, 80 ºC	43	Mangler	32
80 bar, 80 ºC	35	49	35
100 bar, 100 ºC	31	39	23

Tabel 19: Brudstyrke i CO_2 i forhold brudstyrken i luften ved 20 ºC - Elastomer.

Plastmaterialerne (PTFE, PVDF, PEEK) så ud til at være påvirket i mindre grad af CO_2. Brudstyrken af PTFE så ud til at være stort set uafhængig af trykket, derimod faldt brudstyrken, når CO_2-temperaturen blev øget, se tabel 20. Det har været svært at få gode resultater i hus for de to andre plastmaterialer pga. deres meget korte brudforlængelse især for PEEK. Betegnende for de to materialer PVDF og PEEK var, at deres egenskaber ændres ved højere tryk og temperatur, hvor brudforlængelsen blev betydelig længere.

	PTFE	PVDF	PEEK
	Styrke i forhold til luft [%]	Styrke i forhold til luft [%]	Styrke i forhold til luft [%]
10 bar, 20 ºC	104	98	110
10 bar, 80 ºC	66	63	111
50 bar, 20 ºC	89	73	81
50 bar, 80 ºC	61	43	74
80 bar, 80 ºC	57	50	71
100 bar, 100 ºC	54	43	71

Tabel 20: Brudstyrke i CO_2 i forhold brudstyrken i luften ved 20 ºC - Plast.

4 Litteraturliste

[1] J. M. Smith, H. C. Van Ness and M. M. Abbott, "Introduction to Chemical Engineering Thermodynamics, sixth edition," McGraw-Hill, 2001

[2] Peter Atkins and Julio de Paula, Atkins´ Physical Chemistry, seventh edition.
Oxford University Press, 2002

[3] Johannes K. Nielsen, "Permeation and solubility experiments performed at DTU, Danish Polymer Centre, Department of Chemical Engineering, DTU, 2001

[4] A. Y. Dandekar, N. Lindeloff, S. I. Andersen, E. L. Jakobsen and E. H. Stenby
„Measurement of gas solubility in polymers using a high-pressure microbalance" Department of Chemical Engineering, Technical University of Denmark

[5] Nicolas von Solms, Michael L. Michelsen and Georgios M. Kontogeorgis
"Prediction and correlation of high-pressure gas solubility in polymers with simplified PC-SAFT" Centre for Phase Equilibria and Separation Processes (IVC-SEP) Department of Chemical Engineering, Technical University of Denmark

[6] N. von Solms, J. K. Nielsen, O Hassager, A. Rubin, A. Y. Dandekar, S. I. Andersen and E. H. Stenby, „Direct measurement of gas solubilities in polymers with a high-pressure microbalance" IVC-SEP and Danish Polymer Centre, Department of Chemical Engineering, Technical University of Denmark og NKT Flexibles I/S, DK-2605, Denmark

[7] N. von Solms, A. Rubin, S. I. Andersen and E. H. Stenby, „Direct measurement of high temperature / high pressure solubility of methane and carbon dioxide in polyamid (PA-11) using a high-pressure microbalance,"
Centre for Phase Equilibria and Separation Processes (IVC-SEP) Department of Chemical Engineering, Technical University of Denmark, DK-2800 Lyngby og NKT Flexibles I/S, DK-2605, Denmark

[8] Nicolas von Solms, Nicoletta Zecchin, Adam Rubin, Simon I. Andersen and Erling H. Stenby, "Direct measurement of gas solubility and diffusivity in poly(vinylidene fluoride) with a high pressure microbalance," Centre for Phase Equilibria and Separation Processes (IVC-SEP) Department of Chemical Engineering, Technical University of Denmark, DK-2800 Lyngby.
NKT Flexibles I/S, DK-2605, Denmark

[9] Nicolas von Solms, Michael L. Michelsen and Georgios M. Kontogeorgis, "Computational and physical performance of a modified PC-SAFT equation of state for highly asymmetric and associating mixtures," Centre for Phase Equilibria and Separation Processes (IVC-SEP) Department of Chemical Engineering, Technical University of Denmark

[10] Abhijit Dandekar, "Operating instructions for the high-pressure Sartorius microbalance," Department of Chemical Engineering, DTU, juni 2000

[11] M. Bellstedt, F. Elefsen and Stefan S. Jensen ''Application of carbon dioxide refrigerant in industrial cold storage refrigeration plant'' Journal of Airah, June 2002.

[12] Jesse N. Lawrence ''Refrigeration fundamentals throughout History: methods used to obtain colder temperatures, and principles governing them'' Dept. of chemistry, Univ. of Alabama, A literature seminar, Feb'25th 2003.

[13] http://www.cartage.org.lb/en/themes/sciences/physics/Thermodynamics/Basic Thermodynamics/Refrigeration/Refrigeration.htm

[14] Amir F, David S. K. Ting, Wendy W. Yang ''Second law analysis of the transcritical CO_2 refrigeration cycle'' Energy conversion and Management,
Vol. 45, pp. 2269-2281, 2004.

[15] B. Flaconneche, J. Martin and M.H .Klopffer ''Transport properties of gases in polymers: experimental methods'' Oil & Gas Science and Technology-Rev. IFP, Vol.56, No. 3, pp. 223-244, 2001.

[16] M.H Klopffer and B. Flaconneche ''Transport properties of gases in polymers: Bibliographic Review'' Oil & Gas Science and Technology-Rev. IFP, Vol.56, No.3, pp. 245-259, 2001.

[17] H.Lin, B.D. Freeman ''Gas solubility, diffusivity and permeability in poly (ethylene oxide)'' Journal of Membrane Science 239, pp. 105-117, 2004.

[18] Yoshiharu Tsujita ''Gas sorption and permeability of glassy polymers with micro voids'' et. al, Polym. Sci. Vol.28, pp. 1377-1401, 2003.

[19] Vaibhav Kulshrestha, K Awasthi, N K Acharya, M Singh and Y K Vijay ''Effect of temperature and α-irradiation on gas permeability for polymeric membrane'' Bull. Mater. Sci., Vol. 28, No. 7, pp. 643-646, December 2005.

[20] C.K Yeom, J.M. Lee, Y.T.Hong, K.Y. Choi, S.C. Kim ''Analysis of permeation transient of pure gases through dense polymeric membranes measured by anew permeation apparatus'' Journal of Membrane Science 166, pp. 71-83, 2000.

[21] Frisch, H. L. Pressure dependence of diffusion in polymers. J. Elastoplastics, pp. 130-132, 1970.

[22] Koros, W. J.; Chern, R. T. Separation of gaseous mixtures using polymer membranes. In Handbook of Separation Process Technology; R. W. Rousseau, Ed.; John Wiley & Sons, Inc.: New York, pp. 862-953, 1987.

[23] V.R. Gowariker, N. V. Viswanathan, Jayadev Sreedhar "Polymer Science" Published by New Age International (P) Ltd., pp. 173-198.

[24] Paula Hubbard and Thomas Blong, Dyneon "A primer on high-purity fluoro polymers offered for wet bench processes" Material Fluorpolymers: May 2004.

[25] http://www.plasticsmag.com

[26] http://www.amicon.com/ptfeproperties.htm

[27] http://www.boedeker.com/ptfe_p.htm

[28] Douglas R. Robello, Abraham Ulman and Edward J. Urankar ''Poly (p-phenylene sulfone)'' Macromolecules, Vol.26, pp. 6718-6721, 1993.

[29] Nicolas von Solms, Michelsen, M. L.; Kontogeorgis, G. M. ''Computational and physical performance of a modified PC-SAFT

equation of state for highly asymmetric and associating mixtures." Ind. Eng. Chem. Res. Vol. 42, pp. 1098-1105, 2003.
[30] Kouskoumvekaki I.A., von Solms N., Lindvig T., Michelsen M.L., and Kontogeorgis G.M., A novel method for estimating pure component parameters for polymers, Application to the PC-SAFT Equation of state, Industrial and Engineering Chemistry Research, Vol. 43, pp. 2830-2838, 2004.
[31] DIPPR Information and Data Evaluation Manager (DIPPR 801 Database 2007)
[32]. Sako, T.; Wu, A. H.; Prausnitz, J. M. ''A Cubic Equation of State for High- Pressure Phase - Equilibria of Mixtures Containing Polymers and Volatile Fluids'' J. Appl. Polym. Sci. Vol. 38, 18-39, 1989.
[33] Patrik A. Rodgers ''Pressure-Volume-Temperature relationships for polymeric liquids: A Review of Equations of state and their Characteristic Parameters for 56 Polymers'' Journal of Applied Polymer Science, Vol. 48, pp. 1061-1080, 1993.
[34] N. von Solms, K.Y. Koo, Y.C.Chiew ''Mixing rules for binary Lennard Jones chains: theory and Monte Carlo simulation'' Fluid Phase Equilibria 180 pp. 71-85, 2001.
[35] Douglas Henderson and Peter J. Leonard ''One-and Two-Fluid vander Waals Theories of liquid Mixtures, I Hard Sphere Mixtures'' National Academy of Sciences, Vol. 67, No. 4, pp. 1818-1823, December 1970.
[36] Frisch, H. L. ''Pressure dependence of diffusion in polymers'' J. Elastoplastics 1970, 2,130-132.
[37] Nicolas von Solms, Nicoletta Zecchin, Adam Rubin, Simon I. Andersen, and Erling H. Stenby ''Direct measurement of gas solubility and diffusivity in poly (vinylidene fluoride) with a high-pressure microbalance'' European Polymer Journal, Vol. 41 pp. 341-348, 2005.
[38] Nicolas von Solms, Michelsen, M. L. and Kontogeorgis, G. M. ''Prediction and Correlation of High-Pressure Gas Solubility in Polymers with simplified PC-SAFT '' Ind. Eng. Chem. Res., 44, pp. 3330-3335, 2005.
[39] Joachim Gross, Oliver Spuhl, Freelly Tumakaka, and Gabriele Sadowski ''Modeling copolymer systems using the perturbed-chain SAFT equation of state'' Ind. Eng. Res., 42, pp. 1266-1274, 2003.
[40] Pedro Arce, Martin Aznar ''modeling the phase behaviour of commercial biodegradable polymers and copolymer in supercritical fluids'' October 2005
[41] J. Gross, and G. Sadowski, ''Perturbed-Chain SAFT: An Equation of State Based on a Perturbation Theory for Chain Molecules'' Ind. Eng. Chem. Res., Vol. 40 (4), 1244-1260, 2001.
[42] http://www.alperton.ie/alperton/Main/Plastic_ProductsByName.htm
[43] Amra Tihic, Nicolas von Solms, Michelsen, M. L. and Kontogeorgis, G. M. ''Application of simplified Perturbed-Chain Saft Equation of state'' et al.
[44] Michaels, A.S., and Parker, R.B. ''Sorption and Flow of Gases in Polyethylene'' J. Appl. Phys., Vol.34, pp.13-20, 1959.
[45] Plast og polymere, Grete Ridder Ebbesen, Kemi forlaget 2001
[46] Plastmaterialer, Finn Monrad Rasmussen, Ingeniørhøjskolen Århus, 199

5 English Summary

Objective of the project

The objective of the project was to clarify which polymer types (for sealing elements and structure elements) are applicable in systems with CO_2 as refrigerant and which material parameters are critical in relation to CO_2.

The tested polymer types were selected on the basis of the project participants' experience in the field. The strength, solubility and diffusion of the polymers were tested with the objective to determine which polymer types are effected the least in the CO_2 environment and which parameters (such as pressure and temperature) effect the polymers the most. Although the project group has pointed out that oil (in addition to pressure and temperature) also can influence the physical polymer properties, then it was chosen to disregard that parameter.

Project results

A test rig was built and it was possible to determine the ultimate stress of the polymers in subcritical and supercritical CO_2. Ultimate stress has been determined on the following polymer materials:

EPDM, FKM, HNBR, PTFE, PVDF, PEEK

Solubility and diffusion were measured by means of high pressure weight on the following polymer materials:

EPDM, HNBR

Permeabilty was measured directly by means of 2D permeation cell on the following polymer materials:

PTFE, PTFE + 10% Ekonol, PTFE + $PPSO_2$ + graphite
FKM
TFM, TFM + 10% glass

Conclusion

Permeabilty

In the light of the permeability measurements it can be said that the polymers have the following order from "best" to "worst", meaning least permeable to most permeable:

- TFM
- PTFE
- TFM + 10% glass
- FKM
- PTFE + 10% Ekonol
- PTFE + $PPSO_2$ + graphite.

However, there is no great difference between the first five. The last one (PTFE + $PPSO_2$ + graphite) is much worse than the other five. Besides, the polymers become more permeable when something is added (e.g. glass, ekonol, graphite, $PPSO_2$).

Solubility and diffusion

General solubility of CO_2 in HNBR is app. twice as big as in EPDM. On the other hand, diffusion is app. one order of magnitude smaller. Although solubility is higher in HNBR the diffusion coefficient is substantially smaller and therefore permeability is smaller in HNBR. That goes for all temperature and pressure ranges.

Mechanical properties of polymers

All tested elastomer types (EPDM, FKM, HNBR) seem to be extremely influenced by CO_2. Common for them all is that their ultimate strength depends a lot on CO_2 temperature as well as pressure. The fracture elongation of these materials seems to decline and so does the ultimate stress. At supercritical operation an ultimate stress reduction of more than 60% should be expected. The literature study confirms the measurement results. Tests carried out in 1999 at University of Wales in Swansea in Great Britain on fluor elastomers, silicone elastomers and nitrile showed the same tendencies, meaning declining ultimate stress and fracture elongation.

PTFE showed a good tendency as its ultimate stress by and large seemed to be independent of the pressure. On the other hand, the ultimate stress declined when the CO_2 temperature increased.

PVDF and PEEK – It has been difficult to obtain good results for the two plastics materials due to very short fracture elongation especially for PEEK. However, it was characteristic for the two materials (PVDF and PEEK) that their properties change at higher pressure and temperature as fracture elongation becomes much longer. The PVDF ultimate stress also seems to be influenced by CO_2 pressure as well as temperature.

Bilag A: Permeabilitet

Center for Phase Equilibria and Separation Processes (IVC-SEP)
Department of Chemical Engineering
Technical University of Denmark

Refrigeration plants using carbon dioxide as refrigerant: Measuring and Modeling the Permeability of carbon dioxide in polymers used as packing and sealing materials

Supervisor: Nicolas von Solms

Master's thesis submitted by:
Vasu Neela
Student ID Number s041494

Acknowledgements

I would like to thank my supervisor: **Associate Professor, Nicolas von Solms** for his guidance and advice throughout this project. And also for his help in introducing lab technician Poul V. Andersen.

I would like to thank **Poul V. Andersen** and **Zacarias Tecle** for their help in familiarizing me with the apparatus and for suggestions during my experiments. I would like to thank **Karin Petersen** for giving safety instructions concerning the high pressure permeation cell.

Finally, I would like to thank my friends for their suggestions during my project

Abstract

Carbon dioxide has been studied as an alternative refrigerant for refrigerant plants and it has also been successful in replacing chlorofluorocarbons (CFCs) in refrigerant plants due to negligible ozone depletion and lower global warming potential. The use of carbon dioxide as a refrigerant requires a refrigeration cycle with greater extremes of pressure. This refrigeration system should release as little as possible gas to the atmosphere, which depends on the material used for the seals and packings.

The permeability and diffusivity of carbon dioxide was measured in polymers which are used as packing and sealing materials in refrigeration plants by using a permeation cell. The described high pressure permeation cell has been successfully used to measure the transport properties of carbon dioxide in polymers. Solubility of carbon dioxide in polymers was then calculated from the measured permeability and diffusivity data. All measurements were carried out at 45–50 bar and in the temperature range of 40-80 ^{o}C.

The solubility of carbon dioxide in polymers is then modeled with the Simplified Perturbed Chain – Statistical Associating Fluid Theory (simplified PC-SAFT) equation of state. This mixture property was correlated using a single temperature–independent value of the binary interaction parameter. Pure component parameters for the polymers are generally not available and were determined using an extrapolation method from the lower molecular weight monomers. Mixing rules were used to determine parameters for copolymers. These pure component results are accurate enough to predict and correlate the solubility results by using the simplified PC-SAFT equation of state. The experimental solubility data obtained earlier was successfully correlated using simplified PC-SAFT.

Keywords: *Permeability, diffusivity, solubility, equation of state modelling, polymers, simplified PC-SAFT, carbon dioxide*

Table of contents

List of Figures

List of Tables

List of Abbreviations

CFC	Chlorofluorocarbons
FKM	Vinylidenefluoride hexafluoropropylene
GWP	Global Warming Potential
HCFC	Hydrochlorofluorocarbons
HFC	Hydrofluorocarbons
ODP	Ozone Depletion Potential
PC-SAFT	Perturbed chain statistical associating fluid
PCTFE	Poly (chlorotetrafluoroethylene)
PEEK	Poly (ether ether ketone)
PFA	Perfluoroalkoxy
PPSO2	Poly (phenylene sulfone)
PPVE	Perfluoropropyl vinylether
PTFE	Poly (tetrafluoroethylene)
TFM	Modified poly (Tetrafluoroethylene)

Chapter 1 : Introduction

Extensive research has been conducted to replace traditional refrigerants in refrigerant plants. Two candidates that have been considered are carbon dioxide and propane. Carbon dioxide has also been successful in replacing both chlorofluorocarbons (CFCs) which deplete the ozone layer, as well as hydro fluorocarbons (HFCs), which are not ozone depleters, but which have high global warming potential [1]. In refrigeration plants, the polymer materials are in contact with gases at high pressures and high temperatures in compressors. This may cause to blistering of flexible pipe inner sheaths (gas absorption in the polymer followed by an explosive decompression), or corrosion of metal armours of flexible pipes (diffusion of corrosive gases through polymer sheath) and damage to sealing materials.

The main objective of this work is to gain a better understanding of the transport properties of gases in packing and sealing materials used in carbon dioxide refrigerant plants. The second chapter provides a short overview of refrigerants used and a comparison of different refrigeration cycles with the carbon dioxide refrigeration cycle. This section also provides a synopsis of the relevant fundamentals from literature. It includes the concepts and the theoretical models that have been proposed and developed to describe the transport mechanism of molecular species in polymers by diffusion. It will show that the permeability of gases depends strongly on the polymer structure (degree of crystallinity, thermal and mechanical properties), temperature and pressure. This chapter also gives the properties of the polymers and polymer structure which are used in these experiments.

In chapter three, the permeability and diffusivity of carbon dioxide have been determined in the following polymers or polymer/composite membranes: TFM, glass-filled TFM, PTFE, PTFE+10%Ekonol, PTFE+$PPSO_2$+graphite and FKM. All these experiments were performed in the temperature range of 40-80 ^{o}C and pressure range of 45-50 bar in permeation cell. Detail experimental descriptions and calculation procedures for the transport properties have been provided in this chapter. The solubility results were

calculated from the permeability and diffusivity results that were obtained from the permeation cell experiment.

In chapter four, the results for solubility have been modeled using a simplified PC-SAFT equation of state for polymers. The application of simplified PC-SAFT equation of state requires parameters for the pure components for polymers and copolymers which are obtained by using extrapolation method for polymers and mixing rules for copolymers and results are presented in this chapter. The measured results are successfully correlated using simplified PC-SAFT. In chapter five and six, conclusion and references are provided.

Chapter 2 : Theory

2.1 History

Refrigeration as a method of artificial cooling can be traced back to the 14th century when new methods were invented to produce cold by ice and freezing mixtures such as salt and snow. In 1780, sulfur dioxide was liquefied by J.F.Clouet and G. Monge and in 1787 ammonia was liquefied by Van Marum and van Troostwijk. In 1806 Frederick Tudor began an ice business by cutting it from the Hudson River and selling it to greater number of people. Professor of chemistry, Dr.William Cullen, demonstrated the formation of ice in water by contact with ether. By the end of the 18th century liquefying vapors through compression was used for refrigeration. [2]

The first refrigeration machine was made by Jacob Perkins where any volatile fluid could be used as refrigerant. Dimethyl ether with a normal boiling point of -23.6 ^{o}C was introduced as refrigerant by Carles Tellier in 1864. Carl von Linde was the first to introduce ammonia as a refrigerant in the 1870's. Ammonia has a boiling point of -33.3 ^{o}C and provides colder temperatures at pressures of about ten atmospheres in the condenser. Ammonia decomposes slightly under certain circumstances but has many characteristics that make it a viable refrigerant. It exhibits good working pressure (not exceeding 13.789 bar) and also possesses a large latent heat of evaporation. However, ammonia is flammable and can lead to explosions. Sulfur dioxide with a normal boiling point of -10 ^{o}C was introduced as refrigerant in 1874.

Carbon dioxide is a comparatively a good refrigerant in the context that it is not toxic or reactive to metals. It does however require high pressures - generally 82.737 bar or more - and therefore requires stronger equipment and better seals. On the other hand, carbon dioxide, methane, ethane and propane have low toxicity - as do CFCs. A carbon dioxide based system was developed for use in 1886 and was used extensively on ships until 1955 when it was replaced by chlorofluorocarbons (CFCs). Furthermore, if enough hydrogen atoms are replaced by halogens then the refrigerant will be non-flammable. CFCs are generally inert, but the presence of water in the system can lead to the formation of

hydrochloric acid when either methyl chloride (R40) or dichloro/difluoro methane (R12) is used [2].

In 1930, CFCs and HCFCs such as trichlorofluoromethane (R-11), dichloro/difluoro methane(R-12), chlorotrifluoromethane(R-13) chlorodifluoromethane (R-22) and R-502 [48.8%-R22, 51.2%-R115 (chloropentafluoroethane)] were introduced. These refrigerants replaced the old refrigerants in virtually all applications other than industrial refrigeration. Ammonia and some hydrocarbons remained in use due to their desirable characteristics in some applications [1].

The disastrous effect of the CFCs and HCFCs on the ozone layer was discovered during the 1970s, leading to the phase out of all CFCs by the 1990s, followed by the phase out of HCFCs in the early 2000's. The chemical alternatives introduced by the chemical industry for CFCs and HCFCs were various hydrofluorocarbons (HFCs) and their blends such as R-134a (1,1,1,2 tetrafluoroethane), R-507(50%pentafluoroethane, 50% tri fluoro ethane), R-407c (R-32/R-125/R-134a (23/25/52)) and R-410a (R-32/R-125 (50/50)). HFC refrigerants are not directly damaging to the ozone layer, however, they are synthetic greenhouse gases with high global warming potential - significantly higher than original natural refrigerants such as ammonia (R-717), carbon dioxide (R-744), sulfur dioxide (R-764) and hydrocarbons such as propane (R-290). Emission of these refrigerants to the atmosphere contributes greatly and disproportionately to the global warming phenomena. The Global warming potential and Ozone depletion potential for various refrigerants are shown in Table 2.1.

R-134a (1,1,1,2 tetrafluoroethane) is the first chlorinefree HFC refrigerant and is now used world wide in many refrigeration and air conditioning units world wide. The main drawbacks of this refrigerant are its high GWP value (1300 on a scale where CO_2 has a GWP of 1), larger compressor displacement and the requirement of a suitable lubricant.

The advantages of using CO_2 in refrigeration plants are that it has zero ozone depleting potential and low global warming potential (GWP=1). It is chemically inactive, non-flammable and non toxic. CO_2 is also cheaper and there is no current necessity for recovery and disposal. It has a very high volumetric refrigeration capacity compared to the chlorodifluoromethane (R-22) and ammonia.

The major drawbacks of CO_2 are low critical temperature (31 ^{o}C at 74 bar) and the high operating pressure in refrigeration and air conditioning applications. The energy efficiency is often lower compared to the classical vapor compression process (with condensation).

Table 2.1 : Global warming potential and Ozone depletion potential for various refrigerants [1]

Refrigerant type	Composition (formula)	ODP [R11=1.0]	GWP [CO_2 = 1.0]
HCFC - Refrigerants			
R22	$CHClF_2$	0.05	1500
R124	$CHClFCF_3$	0.02	470
R142b	$CClF_2CH_3$	0.06	1800
HFCFC/HFC Service-Blends			
R401A, R401B	R22/152a/124	0.03, 0.035	970, 1060
R409A, R409B	R22/142b/124	0.05, 0.05	1290, 1270
R413A	R134a/218/600a	0	1770
R402A, R402B	R22/125/290	0.02, 0.03	2250, 1960
R403a, R403B	R22/218/290	0.04, 0.03	2520, 3570
Chlorine free			
R134a	CF_3CH_2F	0	1300
R152a	CHF_2CH_3		140
R125	CF_3CHF_2		2800
R143a	CF_3CH_3		3800
R32	CH_2F_2		650
R227ea	CF_3-CHF-CF_3		2900
R236fa	CF_3-CH_2-CF_3		6300
R23	CHF_3		11700
Halogen free refrigerants			
R717	NH_3	0	0
R600a	C_4H_{10}		8
R290	C_3H_8		3
R1270	C_3H_6		3
R170	C_2H_6		3
R744	CO_2	0	1

2.2 The Refrigeration cycle and comparison with the CO_2 refrigeration cycles

Vapor compression refrigeration cycle

The ideal vapor compression cycle uses a refrigerant as the working fluid to absorb and reject heat energy. The energy transfer allows the vapor compression cycle to cool a closed environment. In the ideal vapor compression cycle, the refrigerant enters the compressor as a saturated vapor (Figure 2.1) [3]. As the refrigerant is compressed, its temperature and pressure increase. After the compressor, the refrigerant passes through the condenser. Heat energy is exchanged with the surrounding environment causing the refrigerant to cool and become a saturated liquid. Next the refrigerant passes through an expansion valve to reduce the pressure and temperature, some of the liquid evaporates and the refrigerant enters the evaporator as a saturated two-phase mixture. In the evaporator heat energy is absorbed from the environment and saturated vapor enters the compressor to begin the process again

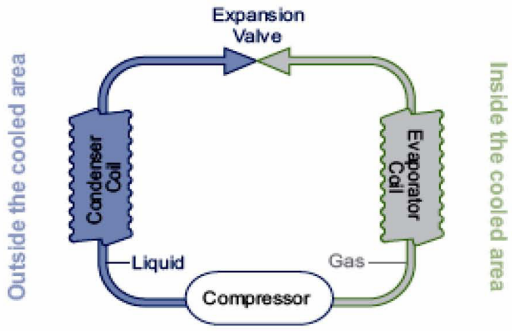

Figure 2.1: Vapor compression refrigeration cycle [3]

Carbon dioxide refrigeration cycle

The most notable property of CO_2 that relates to refrigeration applications is its low critical temperature of 31.1 ^{o}C. Refrigerants with critical temperatures lower than ambient temperature cannot use the condensation process for heat rejection. Thus the refrigeration cycle becomes transcritical as it moves between subcritical and supercritical pressures.

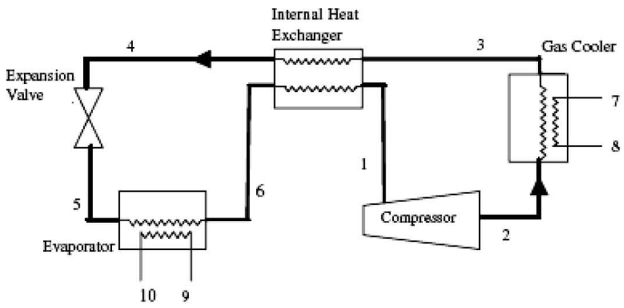

Figure 2.2 : CO_2 refrigeration cycle [4]

The main components of a transcritical CO_2 refrigeration cycle are the gas cooler (rather than condenser), compressor, evaporator, internal heat exchanger and expansion valve as shown in Figure 2.2. The hot CO_2 at supercritical pressure (state 2) enters the gas cooler where it loses heat to the ambient air (states 7 and 8). In an internal heat exchanger the high pressure CO_2 (state 3) is partially cooled by the low pressure CO_2 (state 6) coming from the evaporator. The cooled CO_2 (state 4) then passes through the expansion valve where it is throttled to become a low pressure and lower temperature refrigerant (state 5). This refrigerant flows through the evaporator where it absorbs heat from the air (states 9 and 10) as it vaporizes. After passing through the internal heat exchanger (state 1), it is compressed to high pressure at the supercritical condition before it enters the gas cooler.

Comparison with Carnot refrigeration cycle

The thermodynamic performance of a simple CO_2 refrigeration cycle is very poor compare to other refrigeration cycles. However refrigerants with poor efficiencies, such as CO_2, tend to have very good heat transfer characteristics and respond well to cycle modifications. The challenges in using CO_2 as a refrigerant revolve around system cost, efficiency and size. High pressures are about 137.89-275.79 bar in this system; it is a technical and economic challenge not only for the compressor but also for the heat exchangers. The large pressure ratio creates a challenge in the application of static and dynamic seals in the compressor with the high pressures.

Theoretically, the efficiency of the compressor is high using CO_2 as refrigerant. In reality the efficiency of the refrigeration cycle is low and approximately 40 percent of the ideal Carnot refrigeration. The coefficient of performance (COP) is 2.5 when compare to the R-134a refrigeration cycle (COP 4.2) at high temperature conditions. The system requires an additional cooler or internal heat exchanger - shown in Figure 2.2. CO_2 is less useful as a refrigerant in single stage systems but is also used as the low stage refrigerant in a cascade system. The cascade refrigeration system is that incorporating two or more refrigeration cycles in series. This is done to achieve low temperatures, which cannot be achieved with a single refrigeration cycle [4].

All these additional components lead to more complex and higher cost systems. Due to high pressure, modifications are required on the compressor shell, valves, rings, terminal and seals, as well as pressure relief valve and micro channel heat exchanger. An additional oil separator is required due to oil circulation and return problems. The low efficiency and cycle complexity are the fundamental limitations. CO_2 refrigerant is commercially viable in transport and low temperature cascade systems, as well as some heat pump applications.

2.3 Gas transport in dense polymer membranes

Mechanisms of gas transport in dense polymers depend on the structure of polymeric material, the glassy and rubbery state. The mechanism of diffusion is qualitatively different in rubbery and glassy polymers since glassy polymers are not in a true state of equilibrium. The difference in mechanism is reflected in the dependence of diffusion coefficient as well as the permeability and solubility coefficients. These are dependent on penetrate gas pressure or concentration in polymers and on the temperature. The diffusion coefficients for light gases in rubbery polymers are often independent of concentration. In glassy polymers, the diffusion coefficients are highly nonlinear functions of concentration and reach a constant value at sufficient high concentration.

The transport phenomenon can be explained in five stages, represented in Figure 2.3 [5].

- Diffusion through the limit layer of the up stream side (high pressure side)
- Absorption of the gas by the polymer
- Diffusion of the gas inside the membrane polymer
- Desertion of the gas at the lower pressure side
- Diffusion through the limit layer of the down stream side

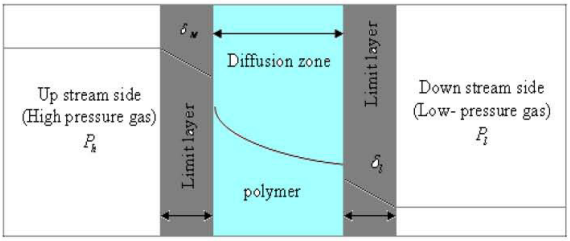

Figure 2.3 : Molecule diffusion through the polymer membrane [5]

The limiting layer of the gas staying on each side of the membrane is negligible and the resistances associated to the steps 1 and 5 are negligible.

2.4 Classic laws of the transport phenomena

Transport of gas through the polymer is defined by three transport coefficients (solubility, diffusivity and permeability) and requires some theoretical considerations.

2.4.1 Diffusion coefficient

The process of diffusion is where small molecules are transferred into the membrane. The flux J of the gas in a polymer can be defined as the quantity of gas Q, diffusing which crosses the membrane area A, during the time t [5].

$$J = \frac{Q}{A \cdot t} \tag{2.1}$$

The transfer of gas by diffusion is proportional to the gradient of the gas concentration C. The first Fick's law expresses this relation by the following equation.

$$J = -D\nabla C \tag{2.2}$$

D is called diffusion coefficient and the amount of gas by unity of membrane volume is equal to the increase of the gas concentration with respect to time.

$$-\frac{\partial J}{\partial x} = \frac{dC}{dt} \tag{2.3}$$

Combining relation(2.2) and (2.3) and assuming that D is constant in the membrane leads to Fick's second law [5]

$$\frac{dC}{dt} = -D\frac{d^2C}{dx^2} \tag{2.4}$$

The diffusion coefficient is constant and the polymer (l) is exposed to the gas then the integration of equation (2.2) gives

$$J\int_0^l dx = -D\int_{C_1}^{C_2} dC \tag{2.5}$$

Then

$$J = \frac{D(C_1 - C_2)}{l} \tag{2.6}$$

C_1 and C_2 are the gas concentrations in the membrane at high pressure side and low pressure side respectively and l is membrane thickness. In most cases D is dependent on

the sorbed penetrants concentration and is written as $D(C)$. The mean diffusion coefficient over the entire range of concentration was given as [5]

$$\overline{D} = \frac{\int_{C_1}^{C_2} D(C)dc}{\int_{C_1}^{C_2} dc} = \frac{1}{C_2 - C_1}\int_{C_1}^{C_2} D(C)dc \tag{2.7}$$

The gas penetrating through the primary high pressure chamber to low pressure chamber (secondary chamber) and diffusivity can be calculated experimentally. Figure 2.4 shows the pressure buildup (P_d) in secondary chamber versus time. The polymer is saturated with gas and then pressure gradually increases in the secondary chamber. The time lag is determined by first fitting the data to a secondary polynomial (quadratic) and subsequently drawing a tangent to this polynomial and extrapolating to the time axis. The intercept of the time axis with the extrapolated linear steady state portion of the curve is called the time lag. The diffusivity can be calculated from this time lag by assuming constant concentration gradient with in the membrane and the correlation was given by Crank in 1968 [5, 6].

$$D = \frac{l^2}{6\theta} \tag{2.8}$$

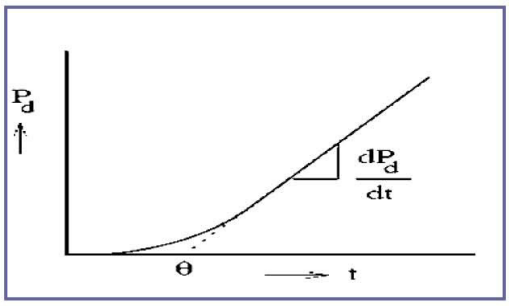

Figure 2.4 : Evaluation of diffusion and permeation coefficients by Time-lag method

2.4.2 Classification of diffusion mechanism

Diffusion of mechanism can be classified into three categories which depend on the relative mobility of the penetrant and polymer. The transport phenomena in glassy polymers were totally differing to rubbery polymers due to structure of the polymer that differs between glassy and rubbery polymers.

Fickian: The rate of diffusion is smaller than that of the relaxation modes of the polymeric matrix. In Fickian diffusion, the boundary conditions are independent of time and do not depend on swelling kinetics.

Non- Fickian: The rate of diffusion is fast compared with the simultaneous relaxation process of the polymer. In this, the sorption phenomenon depends on the swelling kinetics.

The anomalous diffusion refers to a process when the diffusion and the polymer relaxation rates are comparable. The transport molecules are affected by preexisting micro-voids in the matrix, the penetration is mainly depending on the structure of the polymer.

The polymer is highly plasticized by a penetrant, the coefficient of diffusion and solubility are calculated by non-Fickian correlations.

$$\frac{M_t}{M_\infty} = kt^n \tag{2.9}$$

M_t and M_∞ are mass uptakes of the penetrant at time t and at a long time. k is a constant. The value of $n = 0.5$ indicates Fickian diffusion where as $n = 1$ relates to the non Fickian diffusion.

2.4.3 The solubility coefficient

The solubility coefficient of small molecules in polymers is the equilibrium concentration (C) of the penetrants dissolved in the polymer matrix divided by the pressure (P) of the penetrants in the gas phase. The diffusing molecules distribution can be explained by different sorption modes. These sorption modes can be changed with the temperature, concentration, the swelling behavior of the matrix, and time. The mechanism of penetrant

solubility in a polymeric membrane depends upon the activity of the penetrant and whether the polymer is in rubbery or glassy state.

$$S = \frac{C}{P} \tag{2.10}$$

where, S is the solubility coefficient and it depends on the polymer – penetrant interactions as well as condensability.

$$C_D = k_D p \tag{2.11}$$

where, k_D is solubility coefficient and it is independent of concentration at a given temperature. This Henry's law sorption observed in low pressures and the Henry's sorption was shown in Figure 2.5. Henry's sorption is dominates in to the matrix components.

Langmuir and Dual mode sorption were proposed to describe the sorption of molecules in the micro-void region of the polymer. In Langmuir model, the diffusing molecules occupy the specific sites (pre-existing micro voids or high area inorganic fillers) in the polymer. Small quantity of diffusing molecules may dissolve and the penetrant concentration is given by the following equation

$$C_H = \frac{C'_H bp}{1+bp} \tag{2.12}$$

where, C'_H is a hole saturation and b is a hole affinity constant.

Dual mode sorption is described by the sum of Henry's sorption and Langmuir sorption. The model is valid for moderate pressures and low activity of gases in glassy polymers. It cannot describe the swelling and plasticization of the matrix by the sorbed molecules [7].

$$C = C_D + C_H = k_D p + \frac{C'_H bp}{1+bp} \tag{2.13}$$

The uptake of more soluble vapors in uncross linked rubbery polymers is frequently described using the Flory - Huggins expression [5].

$$\ln a = \ln \phi_1 + (1-\phi_1) + \chi(1-\phi_1)^2 \tag{2.14}$$

where, a represents the penetrant activity in the vapor phase, ϕ_1 is the volume fraction of penetrant in the polymer and χ is the Flory – Huggins interaction parameter.

The BET mode is a combination of Langmuir and Flory-Huggins modes. It can be representative for the sorption of water in hydrophilic polymers. The water molecules are fully absorbed in specific sites corresponding to polar groups.

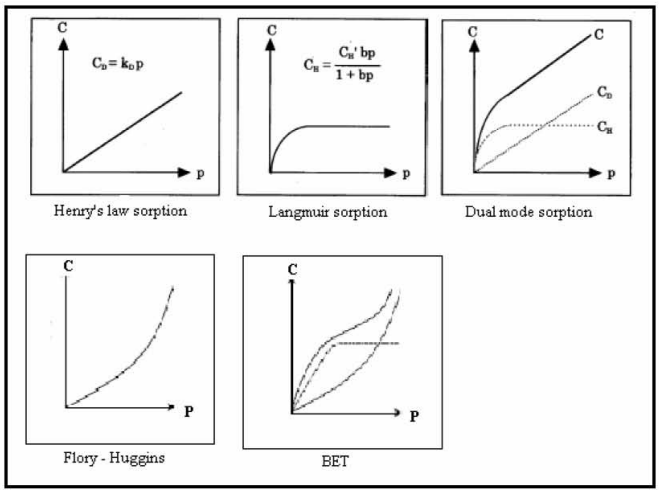

Figure 2.5 : Representation of different sorption modes [7]

2.4.4 The permeability

In a dense polymer film, the permeation is defined as the penetration of small gas molecules through the downstream side of the polymer sample. When Henry's law is satisfied then the diffusive flux at steady state is given by the following equation

$$J = DS\left(\frac{P_1 - P_2}{l}\right) \tag{2.15}$$

where, P_1 and P_2 are pressures at down stream side at time zero and time t respectively, l is thickness of the polymer sample.

The permeability coefficient Pe appears as the product of kinetic factor or diffusion coefficient (D) which reflects the dynamics of the penetrant-polymer system and of a thermodynamic term (S) which depends on the penetrant – polymer interactions.

$$Pe = D \cdot S \tag{2.16}$$

Combining equations(2.1),(2.15) and (2.16) then

$$\frac{Q}{A \cdot t} = \frac{Pe \cdot \Delta P}{d} \Rightarrow Pe = \frac{Q.d}{A \cdot t \cdot \Delta P} \tag{2.17}$$

2.5 Sorption and permeation behavior in glassy and rubbery polymers

Glassy polymers: At temperature below the glass transition temperature T_g, the polymer is in glassy state which is directly related to the restricted chain mobility. Glassy polymers are hard and maybe brittle. The intermolecular forces between the chains do not allow movement other than vibration. In glassy polymers the penetrant diffusion is low but size selectivity is very good. Below the glass transition temperature, the segment motions in a polymer are much reduced, the heat of sorption is more negative. To account for this, a dual sorption mechanism has been postulated for glassy polymers [5].

Rubbery polymers: Above the glass transition temperature the polymer is in a rubbery state. Rubbery polymers are tough and flexible and also have short relaxation times and respond very rapidly to external stresses. The temperature causes immediate adjustment for equilibrium state and immediate adjustment occurs when small penetrants are absorbed in a rubbery polymers. Larger segments of the polymer are thought to participate in the penetrate diffusion process due to internal chain motion such as chain rotation, translation and stronger vibrational motions. The penetrant diffusion is much faster than in glassy polymers but the size selectivity is lower. The glassy and rubbery polymer properties can be further modified by the presence of crystalline phases.

The sorption and permeation behavior can be understood in terms of by the structure of the membranes. If the polymer is in a glassy state, the three coefficients may not be precise as glassy polymeric membranes are in a non-equilibrium state. In this situation the diffusion coefficient obtained by time lag method from a permeation curve might not be correct due to relaxation of a non-equilibrium glassy polymeric membrane. A glassy polymeric membrane structure is composed of two components: microvoids and the matrix which is shown in Figure 2.6. Different levels of interaction between the glassy polymeric membrane and the penetrant species affect the transport phenomena considerably. The interaction of CO_2 with polycarbonate is relatively strong compared to the interaction of oxygen and nitrogen with these polymers due to the polar nature of

CO_2 [9]. It is indicative of plasticization caused by high amount of CO_2 sorption at high pressures. The relative strong interaction of a penetrant with polymeric membranes exhibits Non-Fickian diffusion or anomalous diffusion. Stronger interactions between penetrant and the polymer in the glassy polymeric membrane cause plasticization of the membrane polymer. Glassy polymeric membranes can transform to rubbery or liquid state by plasticization of penetrant even at room temperature, indicative of glass transition pressure at constant room temperature.

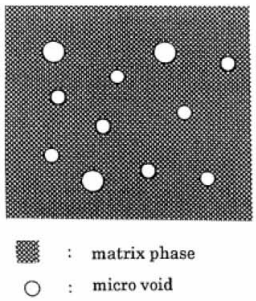

Figure 2.6 : Representation of polymeric glassy state with matrix and micro voids [8]

2.6 Free volume

Free volume usually refers to the space between the molecules. The dependence of penetrant transport properties on chain packing in polymers is often described in terms of correlation involving the fractional free volume of polymers. Fractional free volume (FFV) is the fraction of polymer that is not occupied by polymer molecules and can be estimated using the expression (2.18) [7].

$$FFV = \frac{V - V_0}{V} \tag{2.18}$$

V is the polymer specific molar volume and V_0 is an estimation of the volume occupied by polymer chains. V_0 is estimated using the equation $V_0 = 1.3V_w$. Where V_w is the Vander Waals volume and it is estimated using a group contribution method [6]. Fractional free volume (FFV) has been related to diffusion coefficients through the Doolittle equation [6].

$$D = A\exp\left(\frac{-B}{FFV}\right) \tag{2.19}$$

where, A and B are empirical constants. The fractional free volume of the system is given by

$$f = \phi_1 f_1 + \phi_2 f_2 \tag{2.20}$$

where, ϕ_i and f_i are volume fraction and volume fraction of the component i respectively.

Generally solubility is function of penetrant-polymer interactions and the evaluation of solubility was found experimentally by FFV. In 1975, Peterlin was proposed expression for the solubility coefficient as a function of interaction parameter and fractional free volume.

$$S = \frac{f}{f_1 p_1^0 \exp(1 + \chi_1)} \tag{2.21}$$

where χ_1 is the Flory-Huggins interaction parameters, p_1^0 is the liquid-vapor equilibrium pressure of the gas at temperature T (saturated vapor pressure). In the above equation(2.21), assuming that ϕ_1 is very small then the equation (2.21) becomes

$$S = \frac{f_2}{f_1 p_1^0 \exp(1+\chi_1)} \tag{2.22}$$

The free volume fraction depends on three thermodynamic variables (Frisch, 1970; Stern et al., 1972; Kulkarni and Stern, 1983): the temperature T, the hydrostatic pressure p applied to the system and the penetrant concentration which can be expressed as a volume fraction.

$$f(T, p, C) = f_{ref}(T_{ref}, p_{ref}, 0) + \alpha(T - T_{ref}) - \beta(p - p_{ref}) + \gamma C \tag{2.23}$$

The first term of this equation represents the fractional free volume of the system in a reference state, at T_{ref} and p_{ref} of the pure polymer. The second term characterizes the increase of f due to the thermal dilation with α, the thermal expansion coefficient of the free volume. The third term shows the free volume decreases during a hydrostatic compression, β being the compressibility ($\beta = \chi_l - \chi_g$, the coefficients χ are the compressibility of the liquid and glassy states). The last term is a measure of the penetrant effectiveness in increasing the free volume, γ being a coefficient of concentration.

2.7 Parameters affecting the transport characteristics

2.7.1 Influence of temperature

Generally permeation of gas through dense polymeric membrane is considered as an activated process and the permeability coefficient can be approximated by an Arrhenius expression. The following equation expresses the temperature dependency of the permeability [9].

$$P = P_0 \exp\left(\frac{-E_p}{RT}\right) \tag{2.24}$$

The permeability depends on both diffusivity and solubility. So both parameters must be involved to understand the temperature effect. Similar Arrhenius equations are shown below for the solubility and diffusivity.

$$D = D_0 \exp\left(\frac{-E_d}{RT}\right) \tag{2.25}$$

$$S = S_0 \exp\left(\frac{-\Delta H_S}{RT}\right) \tag{2.26}$$

where P_0, D_0 and S_0 are pre-exponential constants, E_P is the activation energy of permeation, E_D is the activation energy of diffusion, and ΔH_S is the enthalpy of sorption. The activation energy of permeation is the sum of activation energy of diffusion and the enthalpy of sorption.

$$E_P = E_D + \Delta H_S \tag{2.27}$$

The heat of solution can be expressed as

$$\Delta H_S = \Delta H_{cond} + \Delta H_1 \tag{2.28}$$

where ΔH_{cond} is the molar heat of condensation, this term is always negative and small for gases and ΔH_1 is the partial molar heat of mixing. The value of molar heat of mixing is small and positive which can be estimated from the cohesive energy densities of the penetrant and the polymer by using Hildebrand's theory.

$$\Delta H_1 = V_1 (\delta_1 - \delta_2)^2 \phi_2^2 \tag{2.29}$$

The parameters of solubility δ_1 and δ_2 are the square roots of the cohesive energy densities of penetrate and the polymer, V_1 is the partial molar volume of penetrate and ϕ_2 is the volume fraction of the polymer in the mixture.

These Arrhenius expressions hold mainly for the simple non-interactive gases. Especially for condensable or interactive gases the permeation parameters through a glassy membrane has more complex temperature dependency because the membrane under go morphology or a shift of glass transition by the plasticization action of the sorbed permeate molecules. The diffusion coefficient increases with increasing temperature because more energy at higher temperature produces more active chain motion resulting in formation of larger free volumes which permeate molecules can diffuse through [10]. Especially in glassy polymers all three gas transport properties decrease with increasing temperature.

2.7.2 Pressure and Concentration effects on permeability

The effect of concentration and pressure in the membrane is a major challenge in effective modeling of the gas transport process. Typical effect of gas pressure on permeability is shown in Figure 2.7. Response (a) is for the ideal case where diffusion and solubility are assumed to be independent of gas pressure. This type of behavior is observed for the case of supercritical gas permeation in amorphous polymers. Response (b) is characteristic of a gas plasticization effect on the polymer and is observed during organic vapor permeation in rubbery polymers. Response (c) corresponds to the case of highly soluble gases in glassy polymers. Response (d) is a combination of response (b) and (c) and is observed in the case of permeation of organic vapors or plasticizing gas, such as CO_2, in glassy polymers. The deviations from the ideal behavior (response (a)) are caused by the effect of pressure on either solubility or diffusion coefficient [11]. The diffusion coefficient depend on gas concentration, the permeation flux is expressed by

$$P = -D(C)\left(\frac{\partial C / \partial x}{\Delta p / h}\right) \tag{2.30}$$

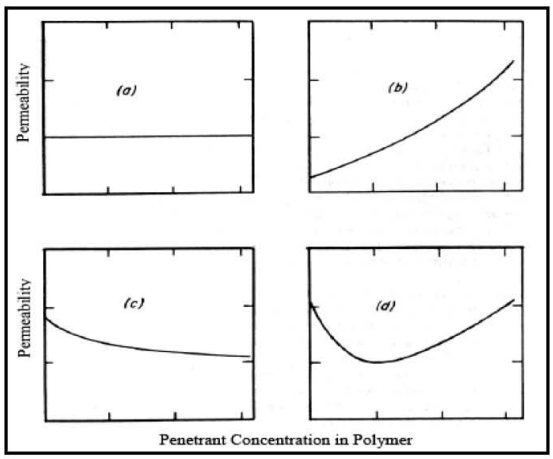

Figure 2.7: Permeability dependence on gas concentration during gas transport through the polymer [12]

Since the permeability coefficient is constant for the given upstream and downstream pressure. The product of the diffusion coefficient and $\partial C / \partial x$ is constant. So the above equation (2.30) can be expressed by using separation of variables.

$$\frac{p}{h}\int_0^h dx = \int_{C_1}^{C_2} D(C)\cdot\frac{dC}{dp}\cdot dp \qquad (2.31)$$

For the downstream pressure ($C_1 = 0$), the final permeability equation can be derived as

$$P = \left[\int_0^{C_2} D(C).\frac{dC}{C_2}\right]\left[\frac{C_2}{p_2}\right] = D.S \qquad (2.32)$$

The diffusion coefficient describes the kinetics of the transport phenomena where as the gas solubility is governed by the thermodynamic interaction between the penetrant and the membrane material. The permeation equates both the polymer-penetrant dynamics (kinetic factor), as well as the polymer-penetrant interactions (thermodynamic factor).

Sorption

The sorption behavior for any gas/vapor-polymer system is classified into four types of isotherms as shown in Figure 2.8. The concentration-dependent sorption can be expressed as

$$S(C) = S(0)e^{\sigma C} \tag{2.33}$$

where $S(0)$, the limit value of the solubility when the concentration is close to zero, which is similar to the Henry's law coefficient k_D, a characteristic parameter at given temperature and σ is a constant relating to polymer-penetrant interactions. In Figure 2.8 Response (a) represents an ideal gas-polymer system without specific interactions. This linear variation is represented by Henry's law of solubility. Response (b) is penetration of gas molecules in rubbery polymers and similar behavior also observed in polar and hydrogen bonding penetrates in rubbery polymers. Response (c) is dual mode sorption in glassy polymers. Response (d) is observed mostly highly soluble penetrates in glassy polymers. The Flory-Huggins solubility equation is used for calculating solubility of organic vapors in polymers at high pressure.

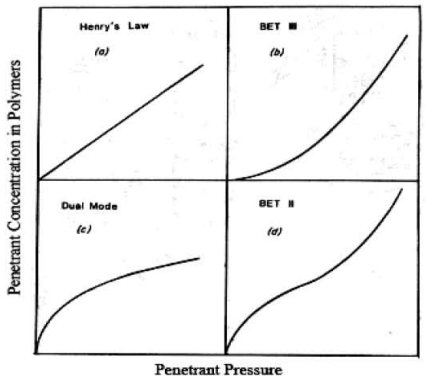

Figure 2.8 : Gas sorption in polymer membranes [12]

Diffusion

The pressure dependence on diffusion is deduced as the ratio of permeability and solubility. The four typical isotherms observed for diffusion are shown in Figure 2.9. Response (a) occurs when polymers are exposed to organic vapors or hydrophilic polymers exposed to water. Response (b) observed for plasticizing penetrants present at very low concentration. Response (c) generally observed in glassy polymers and well described in dual mode sorption model. Response (d) is characteristic of clustering penetrants [12]. Molecules with hydrogen bonding capabilities can increase in effective diameter of the gas molecules at high pressures. This leads to decrease in the effective diffusion coefficient. Chemical interactions between the polymer and penetrant have shown peculiar responses with increasing pressure. The effect of CO_2 is induce the plasticization in various polymers at different pressures.

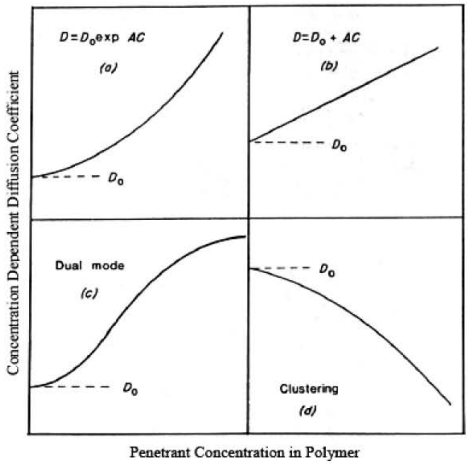

Figure 2.9 : Concentration dependence diffusion of gas in polymer membranes [12]

2.7.3 Crystallinity and chain orientation

Crystallinity is indication of the amount of crystalline region with respect to amorphous content. Crystallinity influences both solubility and diffusion coefficients. In most polymer systems crystalline region preclude penetrate sorption, there by hindering diffusion. The arrangement of polymer chain forming crystalline and amorphous regions and part of molecules are arranged in regular order, these regions are called crystalline region and some part of region molecules are arranged in random disorganized state, these are called amorphous region which was shown in Figure 2.10.

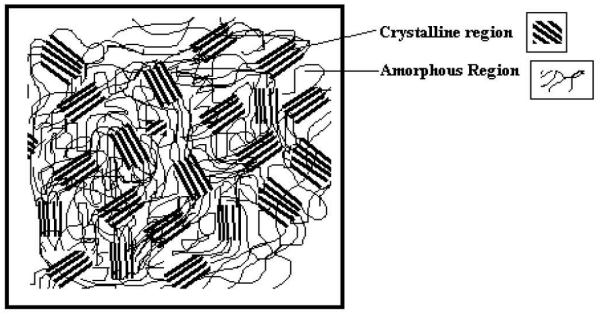

Figure 2.10 : Mixed amorphous crystalline macromolecular polymer structure [13]

Sorption and diffusion take place exclusively in the amorphous regions and the crystalline regions are impermeable barriers for the diffusion process. Crystalline zones have two effects on the gases diffusion. One of the effects is to increase the effective path length of diffusion and other one is to reduce the polymer chain mobility in the amorphous phase because chain ends are trapped to crystalline region to get higher activation energy of diffusion.

Michaels and Parker [34] used the following model to describe the effect of crystallinity on penetrant diffusion coefficients

$$D = \frac{D_a}{\tau\beta} \tag{2.34}$$

Here D_a is diffusivity in the amorphous region, τ is a geometric impedance factor and β is a chain immobilization factor. In this model, the penetrant can only diffuse through amorphous material. The crystalline regions create a tortuous path way for the penetrant by acting as impermeable barrier for diffusion. This effect is taken into account by the factor τ, which is the ratio of the distance traveled by a penetrant molecule in crossing a sample to the sample thickness. Crystallites may also restrict chain mobility in the amorphous phase by acting as virtual crosslink and reducing the volume that can be used for the penetrant to make a diffusional jump. This effect is accounted by the chain immobilization factor (β). β is equal to one in glassy polymers and is greater than one in rubbery polymers.

A two phase model is typically used to describe the sorption of penetrants in semi crystalline polymers.

$$S = S_a \phi_a \tag{2.35}$$

where S_a is the solubility of penetrants in the amorphous phase and ϕ_a is the amorphous volume fraction of the polymer.

Chain orientation also affects the transport properties and free volume of the polymer. Polymer changes the amorphous chains morphology and spatial distribution, leading to increase the density of amorphous phase. Increasing the density of amorphous phase leads to reduction of free volume in polymers. Various authors explained the effect of orientation in different polymers in different ways. Peterlin (1975) observed that drastic reduction of sorption and diffusion of organic vapors in HDPE at high draw ratio, with increasing of diffusion activation energy. Holden et al. (1985) reported same results for the permeation of He and O_2 in highly stretched PE but no considerable variation of activation energies. Wang and Porter (1984) attributed the reduction of transport parameters with the draw ratio to an increase of the orientation and degree of crystallinity. These changes are lead modifications of the amorphous chain mobility and free volume with the drawing.

2.7.4 Effect of cross linking

As the degree of cross-linking increases, the diffusion coefficient decreases and this leads to a larger the penetrant molecule. The pre-exponential term D_0 and the activation energy E_D both increase with the increasing cross-linking level but the polymer chain mobility decreases. So the combination of these effects leads to a drop of diffusivity. In polyethylene, the activation energy of diffusion increases with the degree of branching [5, 6]. Cross linking agents can be incorporated into linear polymers to improve the stiffness, surface hardness, resistance to temperature and resistance to solvent attack. Concentration of these agents is limited to 15% and if above these concentration affects the tensile strength and resistance to temperature. Higher cross-linked thermoset polymers are known to be brittle and have a low resistance to impact forces.

2.8 Polymer samples

2.8.1 Modified poly (tetrafluoro ethylene) (TFM)

TFM is a modified TFE polymer. It has a denser structure than conventional PTFE and exhibits better stress recovery in industrial applications. TFM can be utilized where PTFE and RPTFE (Reinforced PTFE) materials are currently used [14]. This modified PTFE or TFM consists of the TFE monomer polymerized with a minute amount (less than 1%) of another fully fluorinated monomer, perfluoropropyl vinyl ether (PPVE). Vinylether co-monomer integrates itself into the backbone of the chain and produces side chain branching along the polymer chain. This branching increases the entanglement of the chain and allows a slight lowering of the molecular weight (shortening the chains) while retaining good physical properties. The addition of vinylether can reduces the number of voids in the material and also improving the permeation resistance. Lower molecular weight creates a material which can flow under pressure and temperature. This vinyl ether in PTFE is greatly improving the surface smoothness of the material. This co-monomer can increase the amorphous phase without reduction of the molecular weight. Low molecular weight leads to a reduction of branching of the molecules and reduces the crystallinity. PPVE (0.1%) addition to this polymer considered as 0.1% crystallinity in solubility modeling with simplified PC-SAFT.

Chemical structure: *modified PTFE (TFM)* [PTFE + PPVE (<1%)]

Poly (tetrafluoro ethylene) $[-CF_2-CF_2-]$

Perfluoropropyl vinyl ether $[CF_3-CF_2-CF_2-O-CF=CF_2]$

Applications: Hydraulic system seals, Envelop gaskets, Compressor piston and packing rings, Bushing and bearing pads, Oil-less compressor piston cups, ‘‘V’’ packings, Ball, plug and gate valve seats, Wafer carriers, Pump and valve diaphragms, Thrust washers, Butterfly valve liners, Crank shaft rotary lip seals, Gas injection bushing, Power steering pump seals and Oxygen sensor hermetic seals.

Advantages of modified PTFE (TFM) over PTFE

- Lower deformation under load
- Lower permeability
- Smoother surfaces and Higher transparency

Modified PTFE is also used in valve industry and it is simply PTFE with addition of less than 1% per fluoro propyl vinyl ether (PPVE) and it is shown in Figure 2.11. The only difference is third fluorine atom is coming and added to the carbon atom. Modified PTFE is stronger and more durable material than PTFE. More benefits in pump and valve applications are less deformation under load and less permeability providing for longer service life in cyclic applications and better creep resistance. The applications are similar to the PTFE polymer applications.

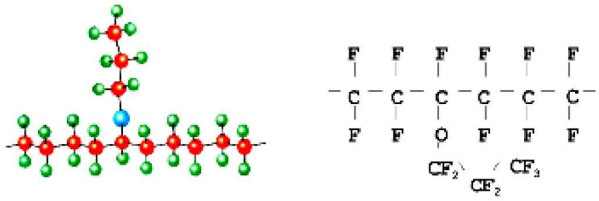

Figure 2.11 : Modified poly tetra fluoro ethylene (TFM)

2.8.2 Modified poly (tetrafluoro ethylene) with 20%glass (TFM + 20%Glass)

TFM is a modified poly (tetrafluoro ethylene) and it has a dense polymer structure than conventional PTFE. TFM with 20% glass means adding 20% of filler material (glass) to the TFM polymer. Glass fibers are often used to reinforce the polymers. An addition of filler to polymer improves the strength, stability and wears resistance. Reinforcement such as Glass fiber permits application at higher pressure and temperature. Addition of glass doesn't change the chemical structure but it improves the stress and wears resistance in polymer [15]. Filled TFM physical properties depend on addition of filler such as glass fiber, carbon, graphite, molybdenum bisulphate, bronze, ceramic powders and even mix of two or more fillers. The 20%glass addition to this polymer considered as 20% crystallinity in solubility modeling with simplified PC-SAFT.

According to filler type and quantity, it is possible to

- Increase compressive strength
- Increase wear resistance
- Reduce the thermal expansion coefficient
- Increase hardness

Chemical structure: *modified PTFE (TFM)* [PTFE + PPVE (<1%)] + *glass*

Poly (tetrafluoro ethylene) $[-CF_2-CF_2-]$

Perfluoropropyl vinyl ether $[CF_3-CF_2-CF_2-O-CF=CF_2]$

Glass $[Sio_2]$

2.8.3 Poly (tetrafluoroethylene) (PTFE)

A fluoro polymer is an organic compound consisting of fluorine and carbon atoms but can also contain hydrogen or oxygen. The atoms are held together by bonds to form monomers such as tetrafluoroethylene (TFE) as shown in Figure 2.12. When the tetra fluoro ethylene is polymerized then they form to long chain polymers like poly (tetra fluoroethylene) (PTFE) and the polymerization reaction is represented in Figure 2.12.

Poly (tetrafluoroethylene) (PTFE) is also commercially known as Teflon or fluon and is probably the most widely used fluoro polymer in the valve industry for components like seats, packing material and diaphragms. The applications include chemical, mechanical, and electrical components, bearings, tubing, and vessels for aggressive chemicals. The reasons are due to high molecular weight leading to high strength compared to other fluoro polymers and its resistance to wear from cyclic applications. PTFE also provides high chemical resistance and excellent mechanical strength [14].

Chemical structure: Poly (tetrafluoro ethylene) $\left[-CF_2-CF_2-\right]$

Fabrication of PTFE is accomplished by a press and sintering process and it can not melt. Therefore the application of PTFE is only limited to the valve components and also for larger diameter components or components with larger volumes. It differs in appearance compared to any other fluoro polymers and more of a solid white color [16, 17].

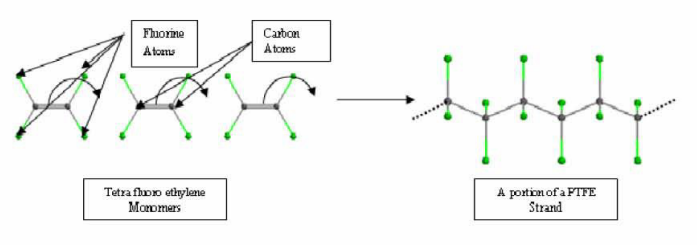

Figure 2.12 : Polymerization of tetra fluoro ethylene to poly tetra fluoro ethylene

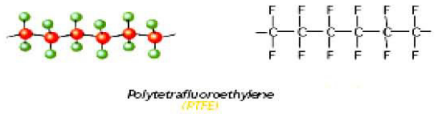

Figure 2.13 : Molecular structure of PTFE

Properties : PTFE is the best known material resistant to all known chemicals, weather and heat, has an extremely low coefficient of friction and it is non-stick. These polymers are nontoxic, nonflammable, and having a working temperature range of -270 to 260 °C.

2.8.4 Poly (tetrafluoro ethylene) with poly sulfone and graphite (PTFE + $PPSO_2$ + Graphite)

The material consists of poly tetrafluoro ethylene (PTFE) with small amount of $PPSO_2$ and graphite. PTFE is the most chemically resistant plastic but its mechanical properties are low compared to other engineered plastics. It can be improved by adding fillers such as creamer, glass fiber, carbon, graphite and similar materials. Aromatic sulfone containing polymers are widely used in high performance applications. The incorporation of polar sulfone groups into polymer backbones increases the glass transition temperature of polymers in all cases. The sulfone-containing polymers have carbon dioxide permeability coefficients at least 50 times higher than the corresponding polymers without sulfone groups.

Poly (p-phenylene sulfone): $PPSO_2$ is simply the oxidation product of poly (phenylene sulfide) (PPS). PPS is highly insoluble and most reagents cannot penetrate the solid. This high degree of crystallinity is the cause of the poor solubility behavior [18].

Chemical structure:

Poly tetra fluoro ethylene $\left[-CF_2-CF_2-\right]$

Poly (p-phenylene sulfone)

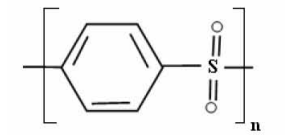

Figure 2.14 : Molecular structure of poly (phenylene sulfone)

2.8.5 Poly (chlorotrifluoro ethylene) (PCTFE)

Poly (chlorotrifluoro ethylene) is similar structure of PTFE but one of the four fluorine atoms in each monomer unit has been replaced by chlorine atom. Melting point drastically decreases from 342^{0}C for PTFE to 220^{0}C for PCTFE.

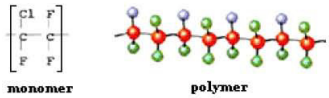

Figure 2.15 : Molecular structure of PCTFE

2.8.6 Poly (tetrafluoro ethylene) with 10% Ekonol (PTFE+10% Ekonol)

Ekonol polyester Resin is a homo-polymer based on p-oxybenzoyl repeat units and is a linear thermoplastic. Ekonol is highly crystalline polymer and thermally stable polymer. Ekonol is combined with poly (tetrafluoro ethylene), it produces a composite material and having a excellent temperature and wear resistance properties. Applications for Ekonol polyester /PTFE blends are varied and include packing sets, compressor ring sets, o-ring seals, spring-loaded seals, and self lubricating bearings.

Molecular weights of Ekonol repeat unit M_W -120.11g/mol [13]

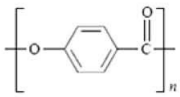

Figure 2.16 : Ekonol [poly (4-hydroxy benzoic acid)] structure

Table 2.2 : Characteristics of the PTFE+10%Ekonol polymer

Characteristics	***PTFE + 10% Ekonol***	***PTFE + 25% Ekonol***	***PTFE***
Density (g/c.c)	2.02-2.08	1.86	2.17
Min. service temperature (^0C)	-200	Not available	-190
Max. service temperature (^0C)	260	Not available	230

2.8.7 Poly (etherether ketone) (PEEK)

Poly (etherether ketone) (PEEK) is a semi-crystalline thermo-plastic with excellent thermal stability and melt processability, good mechanical properties at elevated temperatures [13].

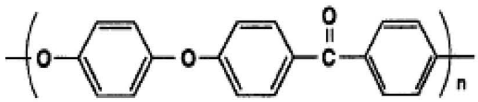

Figure 2.17 : Poly (etheretherketone) (PEEK)

Table 2.3: Characteristics of the PEEK polymer

Characteristics	***PEEK***
M_W	34700
Density (g/c.c)	1.263
$T_g(^0C)$	147.6
$T_m(^0C)$	339.1
Crystallinity (%)	32.0
$\Delta H_f(J/g)$ (Based on 100% crystalline PEEK)	41.0

2.8.8 PFA (Perfluoroalkoxy)

PFA is composed of TFE and PPVE monomer units, and has a similar structure of modified PTFE (TFM). In PFA polymer has a much larger amount of the PPVE (3-4 % for standard grades) comonomer is polymerized with TFE. Modified PTFE and PFA are fully fluorinated and exhibiting the same chemical resistance as PTFE [14].

Poly tetrafluoro ethylene $[-CF_2-CF_2-]$

Perfluoropropyl vinyl ether $[CF_3-CF_2-CF_2-O-CF=CF_2]$

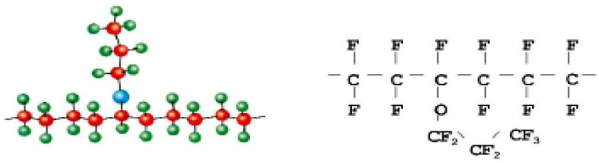

Figure 2.18 : Molecular structure of Perfluoroalkoxy (PFA)

2.8.9 Poly (Vinylidenefluoride hexafluoropropylene) (FKM)

Fluoro rubbers [i.e. fluoro elastomers (FKM)] are one of the most important classes of synthetic rubbers and uses in aerospace and automotive applications, seals, gaskets, and hoses. Fluoro elastomer was a copolymer of hexafluoropropylene (HFP) and vinylidene fluoride (VF_2). It was developed by DuPont Company in 1957 in response to high performance sealing needs in the aerospace industry. Poly (Vinylidenefluoride hexafluoropropylene) contains 30-40mol%hexafluoro propylene. The copolymer contains less than 30% of hexafluoro propylene then polymer becomes non elastic [13].

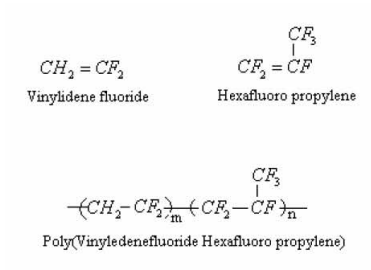

Figure 2.19 : Molecular structure of FKM –poly (Vinylidenefluoride hexafluoropropylene)

Chapter 3 : Experimental work

3.1 The high pressure permeation cell

High pressure permeation cell was designed and manufactured by the department of Chemical Engineering at the Technical University of Denmark. The operating conditions of the cell are limited to 150 °C and 700 bar.

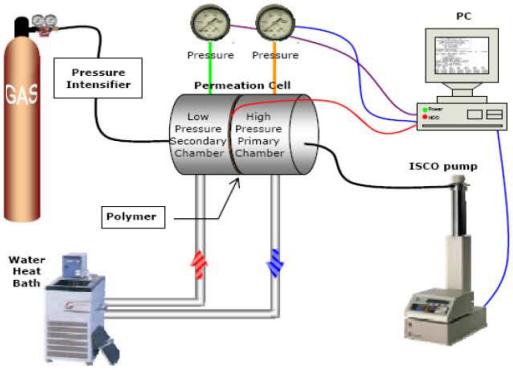

Figure 3.1 : The experimental set up for the high pressure permeation cell

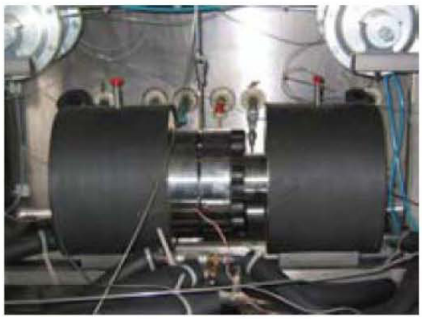

Figure 3.2 : Insulated permeation cell

The permeation cell consists of two chambers and the polymer sample is placed in between high pressure chamber (primary) and a lower pressure chamber (secondary). These two chambers are made by stainless steel and having a large hole in center of the plates. The entire combination is placed on the two equal volume chambers (each chamber having volume 22.057 cm^3) which are held together by two stainless steel flanges. The entire cell after assembly is mounted on a hook on a frame in the fume hood and shown in Figure 3.1. The hot glycerin is circulating to heat the permeation cell to get required temperature. The temperature measurement is taken by Pt-100 thermocouple and it is placed in the gap between two chambers. The two chambers are insulated to maintain temperature constant in the permeation cell and it is shown in Figure 3.2. The ice distilled water and boiling distilled water is used for calibrating temperature in the Pt-100 thermocouple. The temperature variation in the cell is estimated to be $\pm$ 0.5 ^{o}C. The pressures in the two chambers are measured by the Fisher-Rosemount pressure transducers. A Des Grange Des Huots 20000 dead weight tester is employed to calibrate the pressure transducer. A computer program is developed in-house is used to collect the data on the temperature and pressure as a function of time.

3.2 Test samples

The experiments are performed on different types of polymers using the high pressure permeation cell described above. The polymers used were modified poly (tetrafluoro ethylene) (TFM), modified poly (tetrafluoro ethylene) with 20% glass (TFM + 20% glass), poly (tetrafluoro ethylene (PTFE), poly (tetrafluoro ethylene) with polysulfone and graphite (PTFE + $PPSO_2$ + Graphite), poly (tetrafluoro ethylene) with 10% Ekonol (PTFE + 10% Ekonol) and Vinylidenefluoride hexafluoropropylene (FKM). The permeability of CO_2 was measured in these polymers at high pressure. The purity of CO_2 was better than 99.99%. All gases are directly used in the solubility measurements without any pretreatment. The test samples are modified to required dimensions and these polymers were supplied by Parker Seals.

Table 3.1 : Dimensions of polymer samples

Polymer	**Shape**	**Thickness (l) in cm**	**Diameter (d) in cm**
TFM	Circular	0.104	10.00
TFM+20%Glass	Circular	0.105	10.10
PTFE	Circular	0.105	10.05
PTFE+$PPSO_2$+Graphite	Circular	0.098	10.10
PTFE+10%Ekonol	Circular	0.098	10.05
FKM	Circular	0.270	10.05

3.3 Experimental procedure

The experimental setup is shown in Figure 3.1. The polymer membrane is placed in between the primary and secondary chambers. Before starting the experiment the two chambers are completely evacuated and this takes atleast 24 hours for each experiment. The sliding heating jackets are provided on the primary and secondary chambers. The hot glycerin is circulated through the heating jackets to maintain the required temperature in the cell. The temperature measurement is taken from the center of the permeation cell and it shown in Figure 3.1. The CO_2 gas is filled by opening the valves at the primary and secondary chambers to achieve the desired pressure setpoints (primary chamber at 50 bar and secondary chamber at 45 bar). The pressure increase in the secondary chamber is indicative of gas diffusion and permeation in the polymer sample. The pressure and temperatures are monitored as a function of time and the data collection is accomplished by the in-house developed computer program. The downstream pressure data is employed to determine the diffusivity and permeability by the time-lag and the gas flux method respectively. After completing the first experiment, the pressure is reduced by removing the carbon dioxide gas from the primary and secondary cells. Atmospheric pressure is observed on the pressure transducer before the vacuum pump is connected to the inlet valve of the cells and evacuated for 24 hours before for the next experiment occurs.

3.4 Calculation procedure

The diffusion coefficient (D) is measured by using the time lag method which was proposed by Daynes [5]. In this time lag method the permeability calculated from the increase pressure in the secondary chamber. The membrane is initially evacuated from any residual gas by applying vacuum to both sides of the membrane for several hours. Upstream and down stream side of the membranes are exposed to the desired gas at the desired pressure and temperature.

Typically the gas in the primary cell was at 50 bar and the secondary cell at 45bar initially. The gas in the primary cell comes in contact with the polymer sample and it will take some time to reach the other side. Constant temperature is maintained during the experiment by circulating hot water and the pressure build-up is recorded with time. Figure 3.3 represents the pressure build-up in the secondary chamber with time for the CO_2-TFM system at 40 °C. The time that elapses before steady state flux is achieved is known as the time lag and it is shown in Figure 3.3.

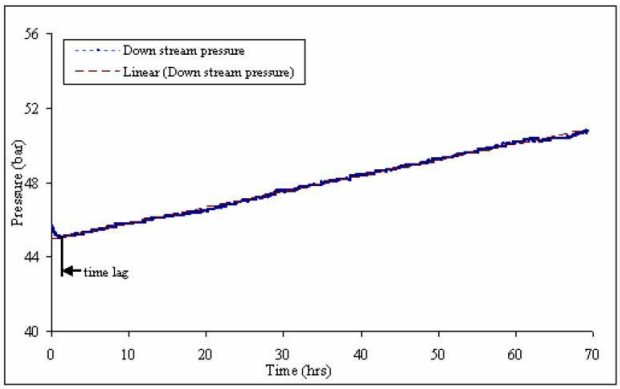

Figure 3.3 : Pressure build-up in secondary cell for the CO_2-TFM system at 45 bar and 40°C

The time lag θ is determined by drawing a tangent to the curve and extrapolating to the time axis, where it crosses the x-axis is considered as time lag. In this experiment the timelag is 1.51hrs. The diffusivity can be calculated by using the following equation(3.1).

$$D = \frac{l^2}{6\theta} \tag{3.1}$$

Where l is membrane thickness (for TFM polymer l= 0.104cm). The permeability coefficient (Pe) is calculated by using the equation (3.2). This value is more precisely known than the diffusion coefficient since it does not depend on knowing the time-lag accurately

$$Pe = \frac{Q \cdot l}{A \cdot t \cdot \Delta P} \tag{3.2}$$

The amount of gas Q permeated through the membrane can be calculated by subtracting starting quantity from the ending quantity and normalizing by dividing by a standard quantity.

$$Pe = \frac{l[cm]}{A[cm^2]} \cdot \frac{(\rho_{end} - \rho_{start})\left[\frac{mol}{l}\right]}{\rho_{STP}\left[\frac{mol}{l}\right]} \cdot \frac{V[cm^3]}{\Delta P[bar] \cdot t[\sec]} \tag{3.3}$$

ρ_{STP} Specific molar volume at standard conditions

V Volume of permeation cell at down stream side

ΔP Differential pressure between up stream pressure and down stream pressures

A Area of membrane

l Thickness of the membrane

The amount of gas permeated through the polymer can be calculated from the molar density data. The molar density (ρ_{start}) at time zero, pressure (P_{1start}) and temperature (T_{1start}) and the density (ρ_{end}) after time t, pressure (P_{1end}) and temperature (T_{1end}) (end of the experiment) are taken from NIST chemical data at desired temperature and pressure

for carbon dioxide. The molar density difference which gives the amount of gas permeated through the polymer. The membrane area is considered as area of gas exposure to the polymer sample. The differential pressure value calculated from the average of the differential pressure data from starting point to the ending point. The temperature, pressure and flow rate are continuously recorded and monitored by computer and stored in a file. The permeability Pe calculated by using equation(3.3). The density data for this particular experiment (CO_2-TFM system at 45 bar and 40 ^oC) and calculation results are shown in Table 3.2.

Table 3.2 : Calculation of Permeability and Diffusivity of CO_2-TFM system at 40 °C

CO_2-TFM system at 40 ^oC	
CO_2 Mw(g/mol)	44.009
density of CO_2 (Kg/m^3)	1.977
density of CO_2 (mol/cm^3) at STP	4.49×10^{-5}
Volume of shell(V_{cell}) in cm^3	22.057
Thickness of membrane(d) in cm	0.104
surface area of membrane(A) in cm^2	38.480
$P1_{start}$ (bar)	45.655
$P1_{end}$ (bar)	50.764
$T1_{start}$(^oC)	40.62
$T1_{end}$(^oC)	39.91
$\rho 1_{start}$ (mol/l)	2.254
$\rho 1_{end}$ (mol/l)	2.626
ΔP (bar)	5.135
Time (sec)	249461.8
Permeability (Pe) in [cm^3 STP/cm. Sec. bar]	***3.8601×10^{-7}***
volume of cell (V_{cell}) in [cm^3]	22.057
thickness of polymer (l) [cm]	0.104
Surface area of the polymer (A) [cm^2]	38.480
Time lag(t-hrs) - from ***Figure 3.3***	1.510
Diffusivity(D) in [cm^2/sec]	***3.3162×10^{-7}***

The solubility coefficient S can be calculated from the diffusion and the permeability coefficients by using the relation(3.4).

$$P = D \cdot S \tag{3.4}$$

The solubility (S) of carbon dioxide in TFM polymer at 40 ^{o}C is 1.16 cm^3 STP gas/(cm^3 polymer. bar).

Similar calculations are done for each polymer at different temperatures. The permeability and diffusivity of carbon dioxide in polymers is calculated from Figure 3.4, to Figure 3.19 by using equation (3.3) and (3.1) at different temperatures. The diffusivity is calculated by using the timelag method. The calculation of timelag by performing a regression of the curve and extending to the time axis sometimes results in a negative time, which is not physical. In this case the time that elapses before steady state flux is achieved is taken as the time lag. From this data, the solubility of CO_2 in polymers are calculated by using equation(3.4).

3.5 Experimental results and discussion

The permeability and diffusivity measurements were performed on six polymers (TFM, TFM + 20%glass, PTFE, PTFE + 10%Ekonol, PTFE + $PPSO_2$ + Graphite and FKM) at three different isotherms and one isobar. These polymers are used in refrigerant plants as either sealing or packing materials. The polymer sample is placed in between the low and high pressure permeation cells and the two cells are pressurized with CO_2 to set a required pressure in permeation cells at a fixed temperature. The experiments are carried out at temperatures 40 °C, 60 °C and 80 °C. Initially pressure in the low pressure permeation cell is 45 bar and pressure in the high pressure cell is 50 bar. The permeability, diffusivity and solubility results are shown in Table 3.3.

Table 3.3 : Permeability, diffusivity and solubility of CO_2 in polymers at different temperatures

Polymer	**Pressure** (P_{avg}) [bar]	**Temperature** (T_{avg}) [°C]	**Permeability** $\left[\frac{cm^3(STP)}{cm \cdot bar.sec}\right]$	**Diffusivity** $\left[cm^2/sec\right]$	**Solubility coefficient** $\left[\frac{cm^3(STP)}{cm^3 \cdot bar}\right]$
TFM	48.21	40.26	3.86×10^{-7}	3.32×10^{-7}	1.162
	48.16	59.92	3.91×10^{-7}	5.09×10^{-7}	0.768
	51.25	77.65	4.68×10^{-7}	7.08×10^{-7}	0.660
TFM+20%Glass	48.05	40.21	6.25×10^{-7}	3.05×10^{-7}	2.047
	48.64	59.83	5.75×10^{-7}	4.57×10^{-7}	1.257
	49.25	79.41	5.80×10^{-7}	7.24×10^{-7}	0.802
PTFE	47.99	40.23	5.49×10^{-7}	3.90×10^{-7}	1.409
	48.64	59.83	4.78×10^{-7}	5.22×10^{-7}	0.915
	49.09	79.98	5.08×10^{-7}	7.82×10^{-7}	0.649
PTFE+10% Ekonol	48.23	40.57	1.28×10^{-6}	4.90×10^{-7}	2.612
	48.51	60.15	1.06×10^{-6}	6.38×10^{-7}	1.662
	48.96	49.97	1.09×10^{-6}	9.37×10^{-7}	1.164
PTFE+PPSO₂+ Graphite	49.30	40.81	6.21×10^{-5}	-	-
	48.09	60.50	4.07×10^{-5}	-	-
	48.42	49.75	2.78×10^{-5}	-	-
FKM	48.16	40.06	9.50×10^{-7}	7.21×10^{-7}	1.317
	48.03	60.22	8.04×10^{-7}	8.42×10^{-7}	0.955
	48.42	80.44	7.71×10^{-7}	1.03×10^{-7}	0.748

TFM

The first experiment was performed on TFM polymer. The experiment was started with 50 bar in primary cell and 45 bar pressure in secondary cell. Figure 3.4 shows the pressure build up in the secondary cell (low pressure side) at 40 °C. The upper curve (in pink colour) shows the pressure build-up in primary cell (high pressure side) to maintain the constant differential pressure in the system. Pressure build-up in secondary cell refers to the penetration of carbon dioxide in TFM polymer. The permeability and diffusivity of CO_2 in polymers are measured based on pressure build-up in secondary chamber. The entire system was evacuated after completing first experiment and the sample was used for the remaining two experiments. Figure 3.5 and Figure 3.6 shows the pressure build-up in secondary cell at temperatures 60 °C and 80 °C.

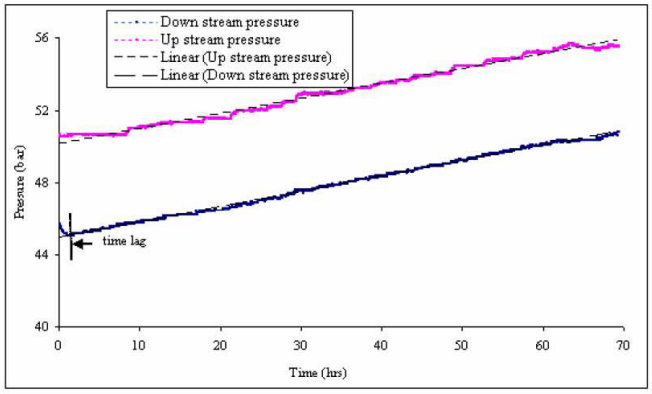

Figure 3.4 : Pressure build-up in the secondary cell for the CO_2-TFM system at 45 bar and 40 °C.

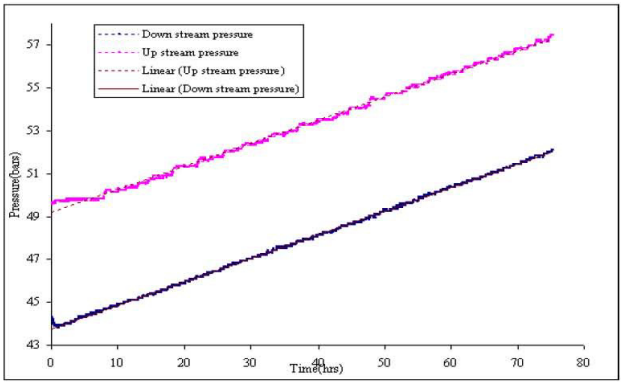

Figure 3.5 : Pressure build-up in the secondary cell for the CO_2-TFM system at 45 bar and 60 °C

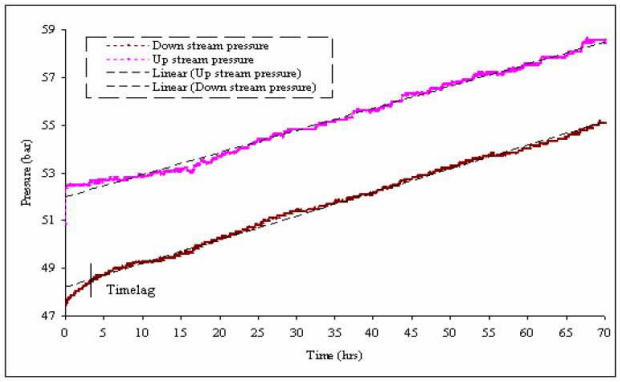

Figure 3.6 : Pressure build-up in the secondary cell for the CO_2-TFM system at 45 bar and 80 °C

TFM + 20% glass

The experiment was started with 50 bar in primary cell and 45 bar pressure in secondary cell. Figure 3.7 shows the pressure build up in the secondary cell (low pressure side) at 40 °C. The upper curve (in pink colour) shows the pressure build up in primary cell (high pressure side) to maintain the constant differential pressure in the system. Pressure build-up in secondary cell refers to the penetration of carbon dioxide in TFM+20%glass polymer. The permeability and diffusivity of CO_2 in polymers are measured based on pressure build up in secondary chamber. The entire system was evacuated after completing first experiment and the sample was used for the remaining two experiments. Figure 3.8 and Figure 3.9 shows the pressure build up in secondary cell at temperatures 60 °C and 80 °C.

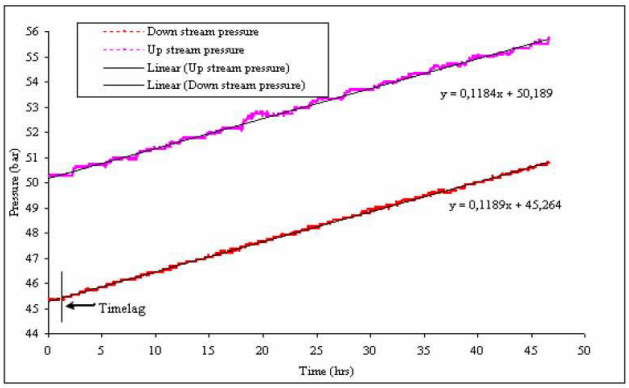

Figure 3.7 : Pressure build-up in the secondary cell for the CO_2-TFM+20% glass at 45 bar and 40 °C

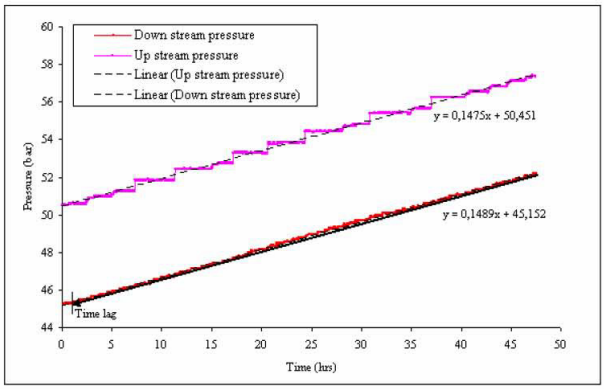

Figure 3.8 : Pressure build-up in the secondary cell for the CO_2-TFM+20% glass at 45 bar and 60 °C

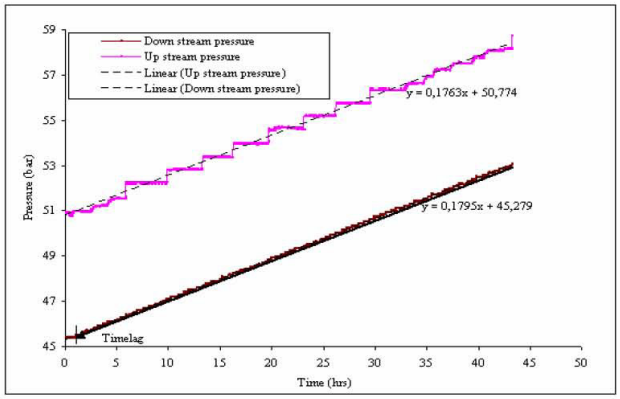

Figure 3.9 : Pressure build-up in the secondary cell for the CO_2-TFM+20% glass at 45 bar and 80 °C

PTFE

The experiment was started with 50 bar in primary cell and 45 bar pressure in secondary cell. Figure 3.10 shows the pressure build-up in the secondary cell (low pressure side) at 40 °C. The upper curve (in pink colour) shows the pressure build-up in primary cell (high pressure side) to maintain the constant differential pressure in the system. Pressure build up in secondary cell refers to the penetration of carbon dioxide in PTFE polymer. The permeability and diffusivity of CO_2 in polymers are measured based on pressure build-up in secondary chamber. The entire system was evacuated after completing first experiment and the sample was used for the remaining two experiments. Figure 3.11 and Figure 3.12 shows the pressure build-up in secondary cell at temperatures 60 °C and 80 °C.

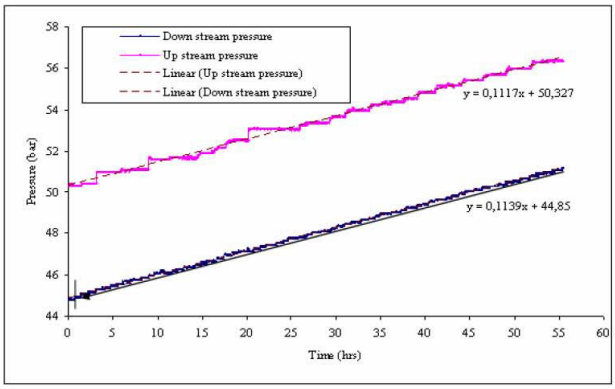

Figure 3.10 : Pressure build-up in the secondary cell for the CO_2-PTFE system at 45 bar and 40°C

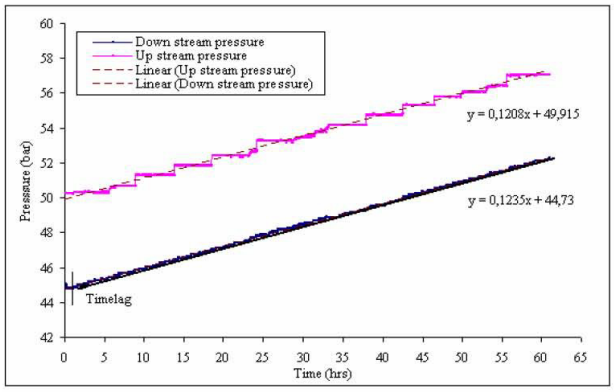

Figure 3.11 : Pressure build-up in the secondary cell for the CO_2-PTFE system at 45 bar and 60°C

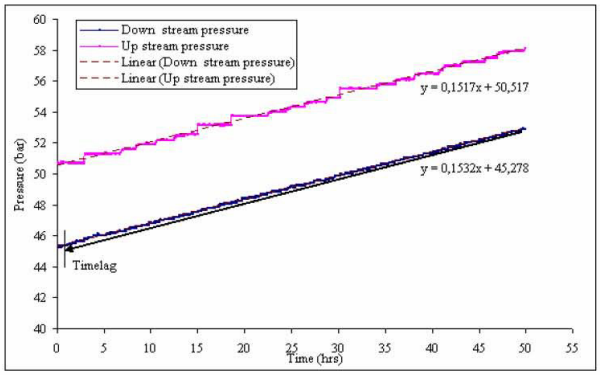

Figure 3.12 : Pressure build-up in the secondary cell for the CO_2-PTFE system at 45 bar and 80°C

PTFE + 10% Ekonol

The experiment was started with 50 bar in primary cell and 45 bar pressure in secondary cell. Figure 3.13 shows the pressure build-up in the secondary cell (low pressure side) at 40 °C. The upper curve (in pink colour) shows the pressure build up in primary cell (high pressure side) to maintain the constant differential pressure in the system. Pressure build-up in secondary cell refers to the penetration of carbon dioxide in PTFE + 10% Ekonol polymer. The permeability and diffusivity of CO_2 in polymers are measured based on pressure build up in secondary chamber. The entire system was evacuated after completing first experiment and the sample was used for the remaining two experiments. Figure 3.14 and Figure 3.15 shows the pressure build-up in secondary cell at temperatures 60 °C and 80 °C.

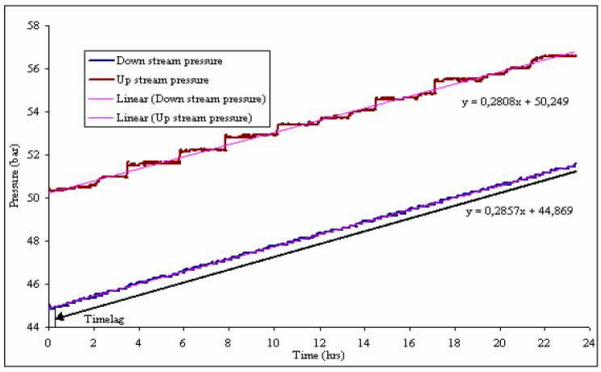

Figure 3.13 : Pressure build-up in the secondary cell for the CO_2-PTFE+10%Ekonol system at 45 bar and 40 °C

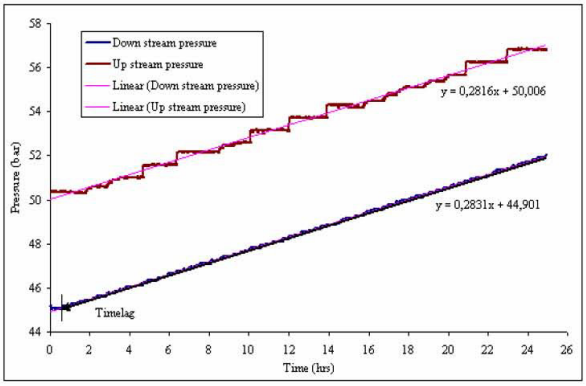

Figure 3.14 : Pressure build-up in the secondary cell for the CO_2-PTFE+10%Ekonol at 45 bar and 60°C

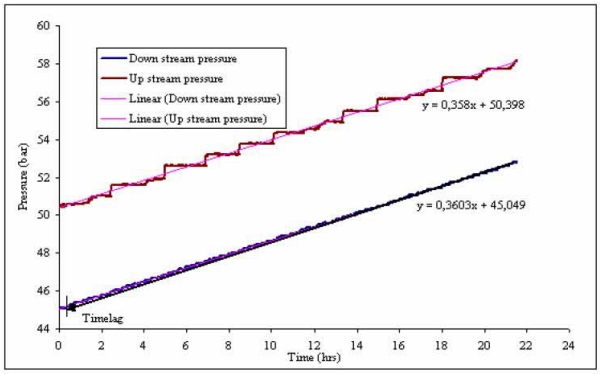

Figure 3.15 : Pressure build-up in the secondary cell for the CO_2-PTFE+10% Ekonol at 45 bar and 80°C

FKM

FKM polymer (soft polymer) thickness is high compare to the other polymers and dimensions are mentioned in Table 3.1. The experiment was started with 50 bar in primary cell and 45 bar pressure in secondary cell. Figure 3.16 shows the pressure build-up in the secondary cell (low pressure side) at 40 °C. The upper curve (in pink colour) shows the pressure build up in primary cell (high pressure side) to maintain the constant differential pressure in the system. Pressure build-up in secondary cell refers to the penetration of carbon dioxide in FKM polymer. The permeability and diffusivity of CO_2 in polymers are measured based on pressure build-up in secondary chamber. The entire system was evacuated after completing first experiment and the sample was used for the remaining two experiments. Figure 3.17 and Figure 3.18 shows the pressure build-up in secondary cell at temperatures 60 °C and 80 °C.

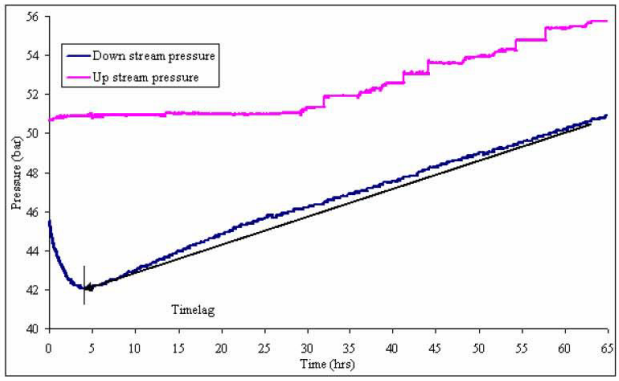

Figure 3.16 : Pressure build-up in the secondary cell for the CO_2-FKM system at 45 bar and 40 °C

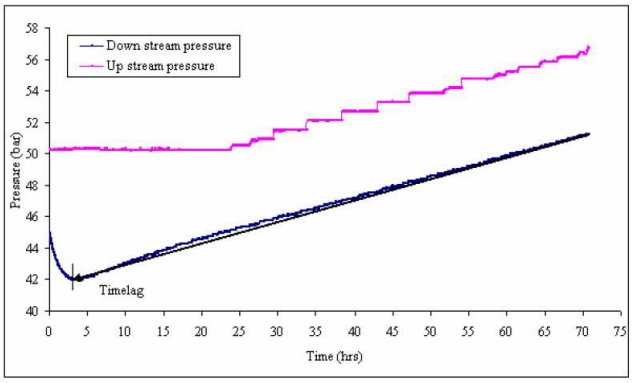

Figure 3.17 : Pressure build-up in the secondary cell for the CO_2-FKM system at 45 bar and 60 °C

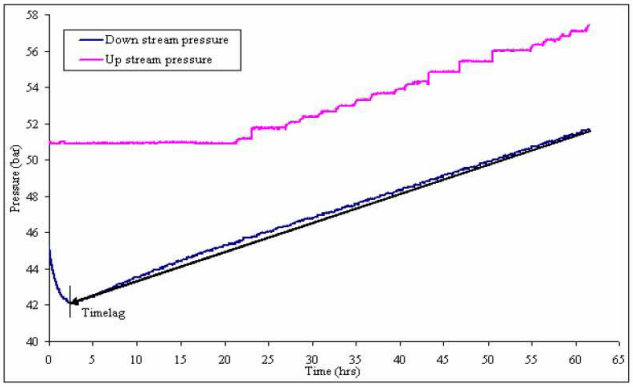

Figure 3.18 : Pressure build-up in the secondary cell for the CO_2-FKM system at 45 bar and 80 °C

PTFE + PPSO$_2$ + Graphite

The experiments are started with 50 bar in primary cell and 45 bar pressure in secondary cell. Figure 3.19 shows the pressure build-up in the secondary cell (low pressure side) at temperatures 40 °C, 60 °C and 80 °C. These three experiments are completed below 1hr. It means that polymer is highly permeable compare to other polymers. The pressure build- up in the secondary chamber is plotted against the time as shown in Figure 3.19. There is no time elapses before the steady state flux is achieved. So the timelag measurement is not possible from this Figure 3.19 . Only permeability calculations are performed by using pressure build-up in the secondary cell.

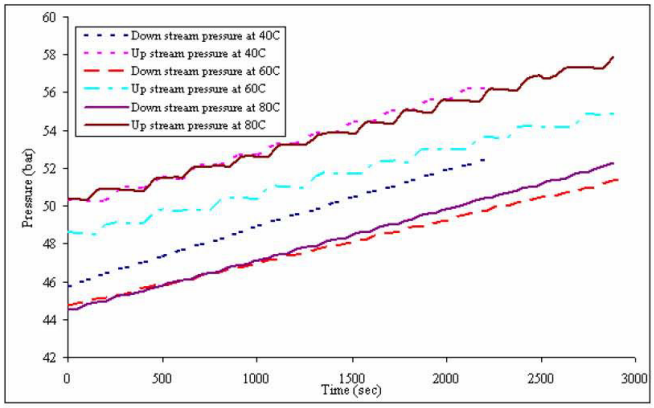

Figure 3.19 : Pressure build-up in the secondary cell for the CO_2-PTFE+PPSO2+Graphite system at 40 °C, 60 °C and 80 °C

Figure 3.20 shows the permeability ($\log Pe$) of carbon dioxide in different polymers over reciprocal temperature $1/T$ and each type polymer showing its own behavior with respect to temperature. The values tend to decrease as the temperature increases in polymers. The results shows clearly that the permeability of carbon dioxide in PTFE + PPSO2 + Graphite polymer is high compare to the original PTFE. The permeability does not seem to increase with temperature, in fact it remains constant or even decrease for certain gases. Similarly permeability of carbon dioxide in PTFE + 10% Ekonol is also very high compare to the PTFE, TFM, and TFM + 20% Glass. The permeability results for the TFM, TFM + 20% glass and PTFE polymers are very close at different temperatures. The permeability in PTFE + $PPSO_2$ + Graphite polymer is strongly temperature dependence and the permeability is decreasing when temperature is increasing. In this polymer the Poly sulfone and graphite addition changes the property (density, crystallinity) of the polymer. The carbon dioxide permeability in PTFE + 10% Ekonol (Ekonol having benzene ring structure) polymer is also very high compare to PTFE polymers.

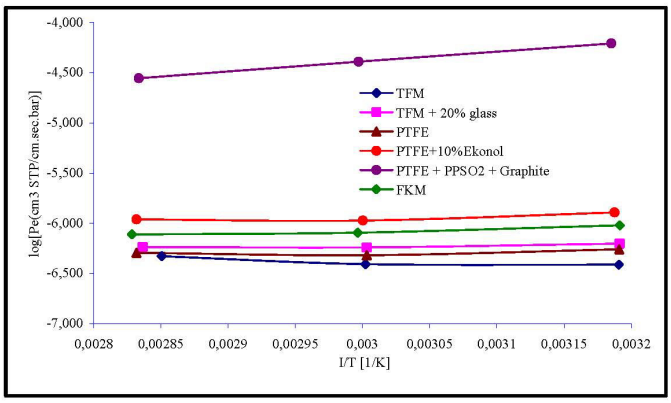

Figure 3.20 : Permeability of CO_2 in polymers as a function of inverse temperature.

The permeability of carbon dioxide in this polymer is quite different to the other polymers. Figure 3.21 shows the permeability of carbon dioxide in PTFE + PPSO2 + Graphite polymer. The permeability is high at low temperatures and low at higher temperatures. This polymer is strongly temperature and pressure dependence. The diffusivity of carbon dioxide in this polymer is very difficult to find out by time lag method. Three experimental results at different temperatures are not given exact time lag to find out the diffusivity for this polymer. So the solubility calculations are not shown for this polymer in Table 3.3 . The high permeability in this polymer is due to addition of polysulfone (having benzene ring structure) and graphite.

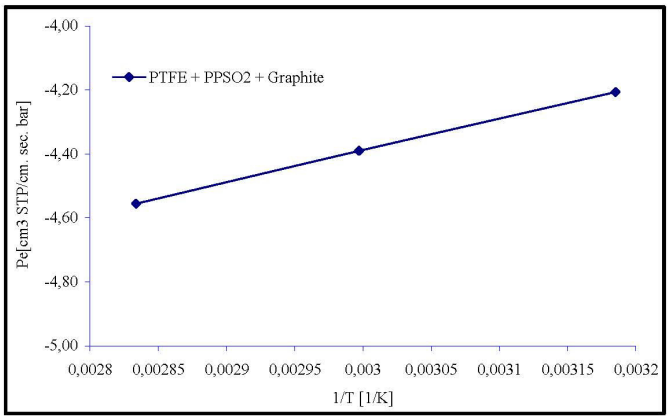

Figure 3.21 : Permeability of CO_2 in PTFE+PPSO$_2$+Graphite as a function of inverse temperature.

Figure 3.22 shows the diffusion coefficient of carbon dioxide in polymers is function of inverse temperature. The diffusion coefficient is high in PTFE+10%Ekonol polymer compare to the other polymers. The results are shown in Table 3.3. Diffusion of carbon dioxide in TFM results are very close to PTFE. Carbon dioxide diffusion in TFM+20%glass is lower compared to TFM and PTFE polymers due to the fact that glass filler added to the TFM polymer changes the free volume of the polymer. The density of the polymer also differs from the original TFM polymer. The diffusion coefficient increases with increasing temperature because more energy at higher temperature produces more active chain motion resulting in formation of larger free volumes which permeate molecules can diffuse through polymers. The slope of these lines gives the pre exponential factor (D_0) and activation energy of diffusion (E_d) for these polymers. The D_0 and E_d are represented in Arrhenius temperature dependency in equation(2.25).

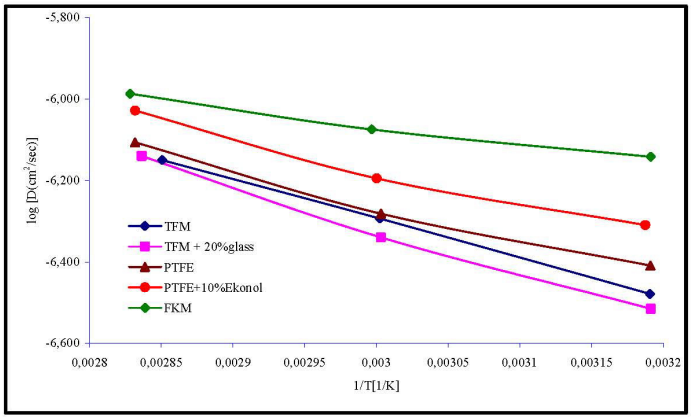

Figure 3.22 : Diffusivity of CO_2 in polymers as a function of inverse temperature

The solubility results are calculated from the permeability and diffusivity data. The solubility of carbon dioxide in polymers is given in Table 3.3. The solubility results from experiments are plotted in Figure 3.23. Polymers are showing its own behavior with respect to temperature. It shows how solubility varies with temperature at constant pressure. The glass filler to the TFM can increase the solubility of carbon dioxide to high compared with the pure TFM polymer. The solubility of PTFE+10%Ekonol is very high compared to the other polymers. The solubility data follow a Henry's law (linear) dependence on pressure, although at very high pressures, deviations from Henry's law have been observed.

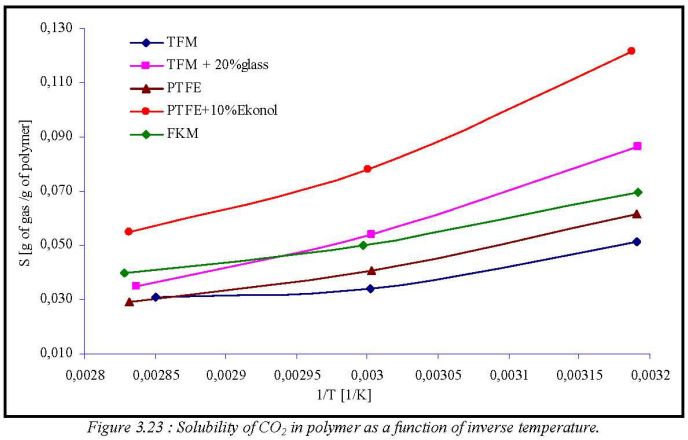

Figure 3.23 : Solubility of CO_2 in polymer as a function of inverse temperature.

The heat of solution obtained from the Arrhenius plot of solubility coefficient against reciprocal absolute temperature (Equation(2.28)), is a composite quantity containing the heat of condensation of the gas and the heat of mixing with the polymer. The heat of condensation will always be small and negative; the heat of mixing will usually be small and positive. As a result, the overall heat of solution can be positive or negative, but it will be small, reflecting the absence of strong polymer/penetrant interactions.

Finally, some of the differences we observed in the permeability of the carbon dioxide in polymers could also be attributed to the variations in the characteristics of the polymer samples. The characteristic property (like crystallinity, free volume) and structure, as well as the size and distribution of microvoids or free volume in the glassy state, and above the glass transition temperature will all affect the transport properties of the gas/polymer system.

Chapter 4 : Modeling

4.1 Simplified PC – SAFT Equation

The solubility of carbon dioxide in polymers was modeled using the Simplified PC-SAFT (Perturbed Chain – Statistical Associating Fluid Theory), a simplified version by von Solms et al. [19], based on the original equation of state (EOS) developed by Gross and Sadowski [31]. The detailed explanations and equations for this EOS is explained in the paper by von Solms et al. [19].

The general form of reduced Helmholtz energy for a mixture of associating molecules,

$$\tilde{a} \equiv \frac{A}{NkT} = \tilde{a}^{id} + \tilde{a}^{hc} + \tilde{a}^{disp} + \tilde{a}^{assoc} \tag{4.1}$$

where $\tilde{a}^{id}$ is the ideal gas contribution, $\tilde{a}^{hc}$ is the contribution of the hard-sphere chain contribution, $\tilde{a}^{disp}$ is the dispersion contribution arising from the square-well attractive potential, and $\tilde{a}^{assoc}$ is the contribution due to association. The contribution to the hard chain term is made of two contributions: the hard sphere term and chain term,

$$\tilde{a}^{hc} = \bar{m}\tilde{a}^{hs} - \sum_i x_i (m_i - 1) \ln g_{ii}^{hs}(d_{ii}^{+}) \tag{4.2}$$

where $\bar{m}$ is a mean segment length defined simply as $\bar{m} = \sum_i x_i m_i$ and the hard sphere term is given by the mixture version of the Carnahan-Starling equation of state for hard spheres.

$$\tilde{a}^{hs} = \frac{1}{\zeta_0}\left[\frac{3\zeta_1\zeta_2}{1-\zeta_3} + \frac{\zeta_2^3}{\zeta_3(1-\zeta_3)^2} + \left(\frac{\zeta_2^3}{\zeta_3^2} - \zeta_0\right)\ln(1-\zeta_3)\right] \tag{4.3}$$

The ζ_n values are defined by

$$\zeta_n = \frac{\pi\rho}{6}\sum_i x_i m_i d_i^n \tag{4.4}$$

where d_i is the individual temperature-dependent segment diameter.

The radial distribution function at contact is given in PC-SAFT by [24]

$$g_{ij}^{hs}(d_{ij}^{+}) = \frac{1}{1-\zeta_3} + \left(\frac{d_i d_j}{d_i + d_j}\right)^2 \frac{3\zeta_2}{(1-\zeta_3)^2} + \left(\frac{d_i d_j}{d_i + d_j}\right)^2 \frac{2\zeta_2^2}{(1-\zeta_3)^3} \tag{4.5}$$

It is assumed that all the segments in the mixture have a mean diameter d, which gives a mixture volume fraction identical to that of the actual mixture. Equation (4.3) and (4.5) are modified in simplified PC-SAFT equation of state. These modifications are done in the following equations of hard sphere and radial distribution functions.

$$\tilde{a}^{hs} = \frac{4\eta - 3\eta^2}{(1-\eta)^2} \tag{4.6}$$

Here x_i is the mole fraction of component i. The radial distribution function at contact is

$$g^{hs}(d^{+}) = \frac{1-\eta/2}{(1-\eta)^3} \tag{4.7}$$

The volume fraction $\eta = \pi\rho\bar{m}d^3/6$ is based on the diameter of equivalent one-component mixture

$$d = \left(\frac{\sum_i x_i m_i d_i^3}{\sum_i x_i m_i}\right)^{1/3} \tag{4.8}$$

Where the individual d_i are temperature-dependent segment diameters

$$d_i = \sigma_i \left[1 - 0.12\exp\left(-3\frac{\varepsilon_i}{kT}\right)\right] \tag{4.9}$$

This simplifications in chain term and radial distribution functions makes the simplified PC-SAFT easy to implement and faster computationally.

4.2 Modeling with equation of state (simplified PC – SAFT)

The experimental solubility results are modeled with simplified PC-SAFT (Perturbed Chain – Statistical Associating Fluid Theory). In PC-SAFT, each component is described with three parameters, a length parameter m, a segment size parameter σ, and a segment energy parameter ε (shown in Figure 4.1). Each component can be thought of as consisting of m spherical segments bonded together, with each segment having a diameter σ and dispersion energy ε. These three parameters are required to calculate the solubility of CO_2 in polymers by using PC-SAFT.

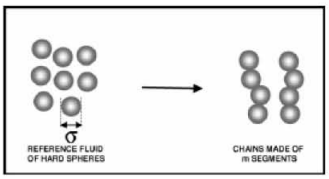

Figure 4.1 : Representation of polymer parameters

4.2.1 Polymer parameters

To utilize an EOS to model polymers requires the knowledge of all the pure component parameters for the model that are not readily available. It is imperative to determine these parameters for each polymer to use PC-SAFT. These parameters are obtained by regressing saturated liquid density and vapor pressure data for the monomers. Since, polymers are repeating units of the monomer; their parameters can be deduced from those of the monomers. For example PTFE is repeating units of tetrafluoroethylene. Tetrafluoroethylene is the monomer for the PTFE polymer. For longer chain hydrocarbon Tetrafluoroethane is chosen as the monomer for calculating monomer parameters. The parameters for the polymers are obtained by using the method developed by [Kouskoumvekaki I.A., von Solms N., Lindvig T., Michelsen M.L.] [20]. The monomer parameters are needed to find out for calculating the polymer parameters. The monomer

for the polymer was considered as compound with longer or shorter hydrocarbon tail can be selected as the monomer. Pure component parameters for the monomer (Tetrafluoroethane) are obtained by fitting the vapor pressure and the molar volume data for saturated liquid [21]. By using a parameter estimation program, the monomer (pure compounds) parameters are estimated and shown in Table 4.1.

Table 4.1 : Pure component parameters of the monomers

EoS	**Component**	**Parameters**		
		m	$\sigma(\times 10^{-8} cm)$	$\varepsilon/k\,(K)$
PC - SAFT	Tetrafluoroethane	2.3717	3.3408	206.88
	2-Chloro-1,1,1 trifluoroethane	2.4775	3.5116	223.18
	Hydroquinone	6.7283	2.7485	275.65
	Benzophenone	4.5318	3.7489	331.39
	Salicylic acid	8.5995	2.5205	234.83
	Difluoroethane	2.6957	3.1076	192.94
	Hexafluoropropane	3.7630	3.1656	175.37

The polymer parameters are calculated by extrapolating monomer parameters and the method is as follows.

The methodology is to extrapolate from the parameters of similar, lower molecular weight compounds. This method is applied for polyethylene based on parameters of the well characterized alkane series [22]. The following combinations of the pure component parameters for alkanes are linear functions of molecular weight (MW).

$$m = 0.02537MW + 0.9081 \tag{4.10}$$

$$m\varepsilon / k = 6.918MW + 127.3 \tag{4.11}$$

The above equations are obtained by plotting m and $m\varepsilon/k$ against MW for linear alkanes from ethane to eicosane [21]. These equations are assumed to be reasonable for all polymers. So the generalized equations are as follows

$$m = A_m MW + B_m \tag{4.12}$$

$$m\varepsilon/k = A_\varepsilon MW + B_\varepsilon \tag{4.13}$$

The constants B_m and B_ε are universal and can be determined for the alkane series from equations (4.12) and (4.13) at molecular weight equal to zero.

$$B_m = 0.9081 \tag{4.14}$$

$$B_\varepsilon = 127.3 \tag{4.15}$$

The remaining constants A_m and A_ε are determined from the equations (4.12) and (4.13) by using monomer pure component parameters. These monomer pure component parameters are obtained from experimental liquid density and vapor pressure data [21]. For polymer parameters, dividing equation (4.12) and (4.13) by molecular weight and considering molecular weight of polymer should be high, then the equations are as follows

$$\frac{m}{MW} = A_m \tag{4.16}$$

$$\frac{\varepsilon}{k} = \frac{A_\varepsilon}{A_m} \tag{4.17}$$

These expressions provide the chain length and energy parameter of the polymer. The remaining size parameter obtained from simplified PC-SAFT by regressing over PVT data [23]. The Above-mentioned procedure was followed for all polymers which were used in these experiments. The polymer parameters are shown in Table 4.2.

Table 4.2 : PC-SAFT parameters for the polymers

EoS	Component	Parameters		
		m/MW	$\sigma(\times 10^{-8} cm)$	$\varepsilon/k\,(K)$
PC- SAFT	PTFE	0.1434	3.169	249.042
	PCTFE	0.1325	3.725	272.136
	TFM + 20% glass	0.1434	3.169	249.042
	TFM	0.1434	3.169	249.042
	Poly(Hydroquinone)	0.0529	2.741	296.559
	Poly(Benzophenone)	0.1988	3.884	379.055
	Ekonol	0.0557	2.586	245.942

4.2.2 Copolymer parameters

The copolymer properties are determined with mixing rules that combine parameters for the two homo-polymers that comprise the copolymer. The co-polymer pure component parameters are calculated based on the assumption that the two or more polymers are mix to form a polymer chain. Copolymers are composed of different types of repeat units. Copolymers can form by adding small amount of different types of repeat units to the polymer chain. In this work simplified PC-SAFT equation of state is extended to copolymers.

Figure 4.2 : Molecular model for a copolymer
(α and β are different polymer repeat units)

Mixing rules of the copolymers

Copolymer chains are characterized by three segment parameters per species (size parameter, energy parameter and chain length). Three mixing rules are needed to determine the pure component parameters for the copolymers. The PTFE+10%Ekonol, PEEK and FKM polymers are assumed to be copolymers (PTFE +10%Ekonol consisting of 90% PTFE and 10% Ekonol, PEEK consisting of 50% poly(Hydroquinone) and 50% poly(Benzophenone) and FKM consisting of 65%poly(Difluoroethane) and 35% poly(Hexafluoropropane). All are characterized based on weight percentages. These mixing rules are equivalent to pseudo-pure component parameters based on the individual species parameters and concentrations. Initially, the following combining rules were applied [24]

$$\sigma_{ij} = \frac{\sigma_i + \sigma_j}{2} \tag{4.18}$$

$$\varepsilon_{ij} = \sqrt{\varepsilon_i \varepsilon_j} \tag{4.19}$$

Where σ_i and σ_j are individual polymer segment diameter and ε_i and ε_j are energy parameters of pure polymers.

Following the paper by von Solms [2001], we can derive the mixing rule as follows

For a mixture of hard spheres, the compressibility factor [24]

$$Z = 1 + \frac{2\pi}{3}\rho \sum_i \sum_j x_i x_j \sigma_{ij}^3 g_{ij}(\sigma_{ij}) \tag{4.20}$$

Where x_i is the mole fraction of hard spheres of species i, ρ represents the total hard sphere number density and $g_{ij}(\sigma_{ij})$ the radial distribution function at contact. If equation (4.20) is applied to a pure fluid then the equation can be reduces to

$$Z = 1 + \frac{2\pi}{3}\rho\sigma^3 g(\sigma_x) \tag{4.21}$$

$$g_{ij}(\sigma_{ij}) = g(\sigma_x) \tag{4.22}$$

Comparing equation (4.20) and(4.21), then the vdW1 mixing rule is

$$\sigma_x^3 = \sum_i \sum_j x_i x_j \sigma_{ij}^3 \tag{4.23}$$

The copolymer segment diameter was calculated by using equation(4.23).

The pressure of hard sphere chain mixtures consists of two-body, Z_2 and three body, Z_3 correlations between hard segments

$$Z = 1 + Z_2 + Z_3 \tag{4.24}$$

In this equation (4.24) involves the inter chain segment-segment correlation function $g_{ij}(r)$ and three body term involves correlation between two segments in a chain and another segment in a different chain. Then

$$Z = 1 + \frac{2\pi}{3}\rho_c \sum_i \sum_j x_i x_j m_i m_j \sigma_{ij}^3 g_{ij}(\sigma_{ij}) + Z_3 \tag{4.25}$$

Where x_i is the chain fraction of species i and ρ_c is the total chain density of copolymer. Similarly the above equation (4.25) can be applied to the pure compound then equation can be changed to

$$Z = 1 + \frac{2\pi}{3}\rho_c m_x^2 \sigma_x^2 g(\sigma_x) + Z_3 \tag{4.26}$$

Applying equation (4.22) and comparing equations (4.25) and (4.26) then the expression can be written as

$$m_x^2 \sigma_x^3 = \sum_i \sum_j x_i x_j m_i m_j \sigma_{ij}^3 \tag{4.27}$$

The segment number (m_x) for the copolymer can be calculated by using equations (4.27) and (4.23),

Calculating energy parameter by using energy equation of Henderson and Leonard [24, 25] and this equation is extended to the chain fluids. So the inter-chain internal energy is

$$\frac{U_N}{V} = \frac{1}{2}\sum_i \sum_j \rho_{ci}\rho_{cj} \sum_{\alpha=1} \sum_{\gamma=1} \int u_{ij}^{(\alpha\gamma)}(r) g_{ij}^{(\alpha\gamma)}(r) 4\pi r^2 dr \tag{4.28}$$

For a conformal solution, the pair potentials of all its binary interactions can be described by a universal function F of the reduced distance between the interacting segment centers according to

$$u_{ij}^{(\alpha\gamma)}(r) = \varepsilon_{ij} F\left(\frac{r}{\sigma_{ij}}\right) = \varepsilon_{ij} F\left(r^*\right) \tag{4.29}$$

Now substituting equation (4.29) in equation (4.28) and transforming distance r into reduced distance r^* then the energy equation can be written as

$$\frac{U_N}{V} = \frac{1}{2}\rho_c^2 \sum_i \sum_j x_i x_j m_i m_j \varepsilon_{ij} \sigma_{ij}^3 \int F(r^*) g_{ij}^{(\alpha\gamma)}(r^*) 4\pi r^{*2} dr^* \tag{4.30}$$

The equivalent one-component equation is

$$\frac{U_N}{V} = \frac{1}{2}\rho_c^2 m_x \varepsilon_x \sigma_x^3 \int F(r^*) g(r^*) 4\pi r^{*2} dr^* \tag{4.31}$$

Again making assumption similar to the equation (4.22)

$$g_{ij}^{(\alpha\gamma)}\left(\frac{r}{\sigma_{ij}}\right) = g\left(\frac{r}{\sigma_x}\right) \tag{4.32}$$

Comparing equations (4.30) and(4.31), then the final solution for the energy parameter is

$$m_x^2 \varepsilon_x \sigma_x^2 = \sum_i \sum_j x_i x_j m_i m_j \varepsilon_{ij} \sigma_{ij}^3 \tag{4.33}$$

By using equations(4.23),(4.27) and(4.33) the three parameters for the polymer mixtures are calculated and the results are shown in Table 4.3.

Table 4.3 : Pure component parameters for the copolymers

EoS	Component	Parameters		
		m/MW	$\sigma(\times 10^{-8} cm)$	$\varepsilon/k(K)$
PC-SAFT with mixing rule	PTFE + 10% Ekonol	0.017	3.1237	248.385
	PEEK	0.035	3.2179	361.156
	FKM	0.0231	3.1306	202.151

Regression method

The three pure component parameters required for non associating molecules were determined from combining rules and density data of the copolymer. The molecular structure of copolymer is shown in Figure 4.2. The molecular model is extended for copolymers by allowing different types of segments with in the polymer chain and it was shown in Figure 4.2.

The non associating copolymers need pure component parameters of the individual polymer. These polymer parameters in the copolymers were calculated by using extrapolation method from pure components which is described in the polymer parameter section. These polymer parameters are used to find out the copolymer parameters in regression method by simplified PC-SAFT equation.

The pure polymer parameters are segment diameter $\sigma_{i\alpha}$, number of segments $m_{i\alpha}$, of type α in the chain, and the energy parameter $\varepsilon_{i\alpha}/k$. The polymer mixture is comprised of different segment types and here one fluid mixing rule is used in the dispersion term. The combing rules are [23]

$$\sigma_{ij} = \frac{\sigma_i + \sigma_j}{2} \tag{4.34}$$

$$\varepsilon_{ij} = \sqrt{\varepsilon_i \varepsilon_j}(1 - K_{i\alpha i\beta}) \tag{4.35}$$

Where σ_i and σ_j are individual polymer segment diameter and ε_i and ε_j are energy parameters of pure polymers. $K_{i\alpha i\beta}$ is an internal correction parameter and it corrects the dispersive energy between different segment types. In this work $K_{i\alpha i\beta}$ is assumed to zero. Three binary interaction parameters are considered to find out the interaction parameter $K_{i\alpha i\beta}$. Two are polymer-solvent interactions and another one is polymer-polymer interactions. In this case binary data for polymer-solvent and polymer-polymer mixtures are not available so it can be assumed that $K_{i\alpha i\beta}$ is equal to zero.

Two parameters for the copolymers are calculated by using equations (4.34) and(4.35). The remaining segment number obtained from simplified PC-SAFT by regressing over density data (PVT data) of polymer mixture [23]. The results are shown in Table 4.4.

Table 4.4 : Pure component parameters for the copolymers (from PC-SAFT)

EoS	**Component**	**Parameters**		
		m/MW	$\sigma(\times 10^{-8} cm)$	$\varepsilon/k\,(K)$
PC-SAFT	PTFE + 10% Ekonol	0.0298	2.8775	247.487
	PEEK	0.0315	3.3125	335.279
	FKM	0.0225	3.2360	202.222

The pure component parameters for copolymer by regression method are quite different from mixing rule parameters due to assumption of the density of individual polymers are equal to the copolymer density (only for PEEK and FKM polymers) and also crystallinity is not considered for these copolymers.

4.2.3 Modeling with simplified PC-SAFT equation of state

Solubility of carbon dioxide in polymers is modeled with simplified PC-SAFT equation of state. The molecular weights are considered as 100000g/mol for polymers and for CO_2 44.01g/mol in simplified PC-SAFT calculations. The results are shown in Table 4.5 to Table 4.9. The Figure 4.3 shows the solubility of CO_2 in TFM, TFM+20%glass, PTFE, PTFE + 10% Ekonol and FKM as a function of inverse temperature. These results are modeled with simplified PC-SAFT at temperature 40 °C, 60 °C and 80 °C with temperature independent value $k_{ij} = -0.023$, $k_{ij} = -0.06$, $k_{ij} = -0.03$, $k_{ij} = -0.055$ and $k_{ij} = 0.023$ respectively.

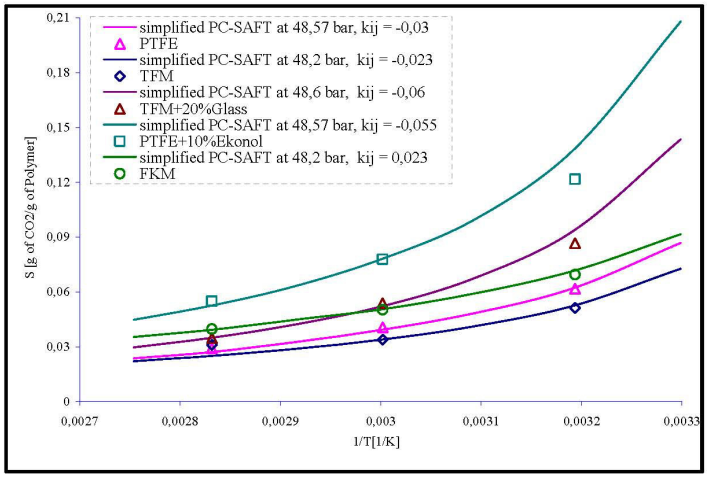

Figure 4.3 : Correlation of carbon dioxide solubility in PTFE, TFM, TFM+20%glass, PTFE+10% Ekonol and FKM at different temperatures. A temperature independent parameter K_{ij} is used at all temperatures for different polymers. Pink colour for PTFE, blue colour for TFM, violet colour for TFM+20%glass, teal colour for PTFE+10%Ekonol and green colour for FKM (solid line for model results and points are experimental results)

The model correctly predicts the observed solubility results and it decreases with increasing temperature. It is clear that using K_{ij} with small temperature independent value would improve to fit the experimental values.

CO_2- TFM polymer

Figure 4.4 shows the solubility predictions using simplified PC-SAFT for carbon dioxide-TFM polymer system as a function of inverse temperature at pressure of 48.2 bar. The correct temperature trend is observed and the carbon dioxide solubility decreases with increasing temperature. Figure 4.5 shows the solubility predictions using simplified PC-SAFT for TFM-carbon dioxide system as a function of pressure at different temperature 40 °C, 60 °C and 80 °C. The results are exactly fitted to the modeled results with temperature independent factor binary interaction parameter $k_{ij} = -0.023$. Same k_{ij} was used at all temperatures. In these solubility predictions, the crystallinity considered 0.1% for the TFM polymer (PPVE content less than 0.1%). The pure component parameters are same as PTFE polymer pure component parameters but the only difference is crystallinity considered in solubility predictions of TFM polymer. The solubility results are shown in Table 4.5.

Table 4.5 : Solubility of carbon dioxide in TFM polymer (Experimental and simplified PC-SAFT results)

(simplified PC-SAFT)				**Experimental Results**		
Temperature [°C]	**Pressure** [*bar*]	**Solubility** $\left[\frac{\text{g of gas}}{\text{g of polymer}}\right]$	K_{ij}	**Pressure** (P_{avg}) [*bar*]	**Solubility** $\left[\frac{\text{g of gas}}{\text{g of polymer}}\right]$	**AAD** (%)
30	48.2	0.073	-0.023	-	-	7.427
40	48.2	0.053	-0.023	48.20	0.0513	
50	48.2	0.041	-0.023	-	-	
60	48.2	0.034	-0.023	48.16	0.0339	
70	48.2	0.029	-0.023	-	-	
80	48.2	0.025	-0.023	51.25	0.0310	
90	48.2	0.022	-0.023	-	-	

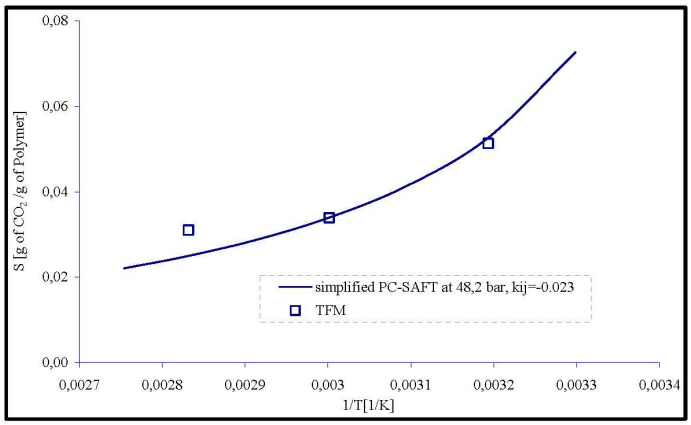

Figure 4.4 : Solubility of CO_2 in TFM polymer as a function of inverse temperature. Points are experimental data and line is from simplified PC-SAFT

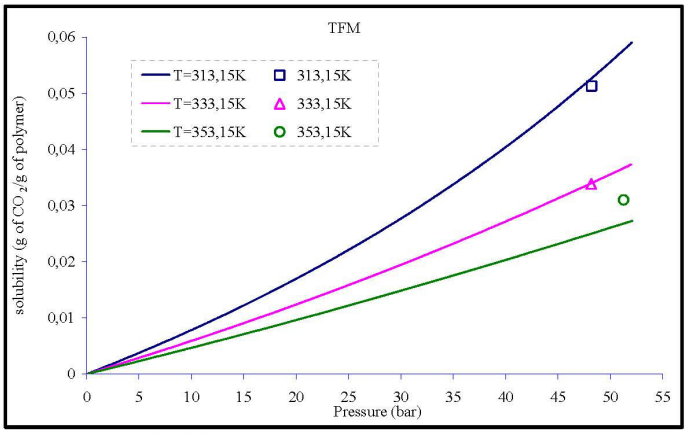

Figure 4.5 : Solubility of CO_2 in TFM polymer as a function of pressure at k_{ij} = -0,023. Points are experimental data and line is from simplified PC-SAFT at different temperatures

CO_2 - TFM +20% glass polymer

Figure 4.6 shows the solubility predictions using simplified PC-SAFT for carbon dioxide -TFM+20% glass polymer as a function of inverse temperature at pressure of 48.6 bar. The carbon dioxide solubility decreases with increasing temperature. The results are exactly fitted to the modeled results with temperature independent factor binary interaction parameter $k_{ij} = -0.06$. Same k_{ij} value was used at all temperatures. Figure 4.7 shows the solubility predictions using simplified PC-SAFT for carbon dioxide-TFM+20% glass polymer as a function of pressure at different temperature 40 ^{o}C, 60 ^{o}C and 80 ^{o}C. In these solubility predictions, the crystallinity considered 20% for the TFM+20%glass polymer (20% glass filler addition). The pure component parameters are same as PTFE polymer but the only difference is crystallinity. This figure shows that the effect of crystallinity changes the solubility of carbon dioxide in polymers. The solubility results are shown in Table 4.6.

Table 4.6: Solubility of carbon dioxide in TFM + 20% glass (Experimental and simplified PC-SAFT results)

(simplified PC-SAFT)				**Experimental Results**		
Temperature [^{o}C]	**Pressure** [bar]	**Solubility** $\left[\frac{\text{g of gas}}{\text{g of polymer}}\right]$	K_{ij}	**Pressure** (P_{avg}) [bar]	**Solubility** $\left[\frac{\text{g of gas}}{\text{g of polymer}}\right]$	**AAD** (%)
30	48.6	0.144	-0.06	-	-	4.007
40	48.6	0.094	-0.06	48.052	0.0866	
50	48.6	0.068	-0.06	-	-	
60	48.6	0.052	-0.06	48.640	0.0538	
70	48.6	0.042	-0.06	-	-	
80	48.6	0.035	-0.06	49.257	0.0347	
90	48.6	0.030	-0.06	-	-	

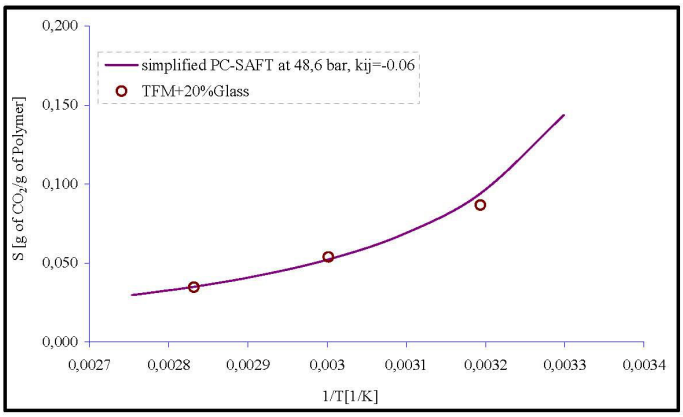

Figure 4.6 : Solubility of CO_2 in TFM+20% glass polymer as a function of inverse temperature. Points are experimental data and line is from simplified PC-SAFT

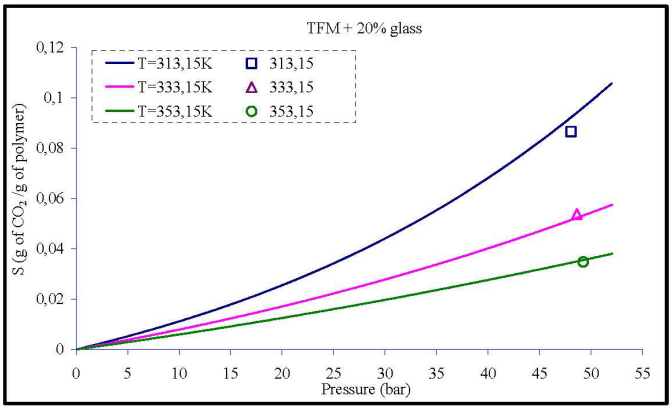

Figure 4.7 : Solubility of CO_2 in TFM+20% glass polymer as a function of pressure at k_{ij} = -0,06. Points are experimental data and line is from simplified PC-SAFT at different temperatures

CO_2- PTFE polymer

Figure 4.8 shows the solubility predictions using simplified PC-SAFT for carbon dioxide-PTFE polymer as a function of inverse temperature at pressure of 48.57bar. The carbon dioxide solubility in PTFE decreases with increasing temperature. The results are exactly fitted to the modeled results with temperature independent factor binary interaction parameter $k_{ij} = -0.03$. Same k_{ij} value was used at all temperatures. Figure 4.9 shows the solubility predictions using simplified PC-SAFT for carbon dioxide-PTFE as a function of pressure at different temperature 40 °C, 60 °C and 80 °C and solubility results are shown in Table 4.7. The solubility of carbon dioxide is high compare to the TFM polymer.

Table 4.7 : Solubility of carbon dioxide in PTFE (Experimental and simplified PC-SAFT results)

(simplified PC-SAFT)				Experimental Results		
Temperature [°C]	**Pressure** [bar]	**Solubility** $\left[\frac{\text{g of gas}}{\text{g of polymer}}\right]$	K_{ij}	**Pressure** (P_{avg}) [bar]	**Solubility** $\left[\frac{\text{g of gas}}{\text{g of polymer}}\right]$	**AAD** (%)
30	48.57	0.0868	-0.03	-	-	3.657
40	48.57	0.0623	-0.03	47.99	0.0617	
50	48.57	0.0502	-0.03	-	-	
60	48.57	0.0393	-0.03	48.64	0.0406	
70	48.57	0.0326	-0.03	-	-	
80	48.57	0.0298	-0.03	49.09	0.0291	
90	48.57	0.0266	-0.03	-	-	

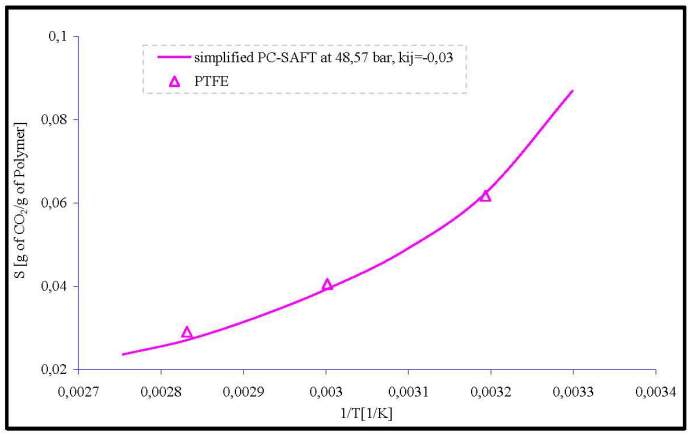

Figure 4.8 : Solubility of CO_2 in TFM and PTFE polymers as a function of inverse temperature. Points are experimental data and line is from simplified PC-SAFT

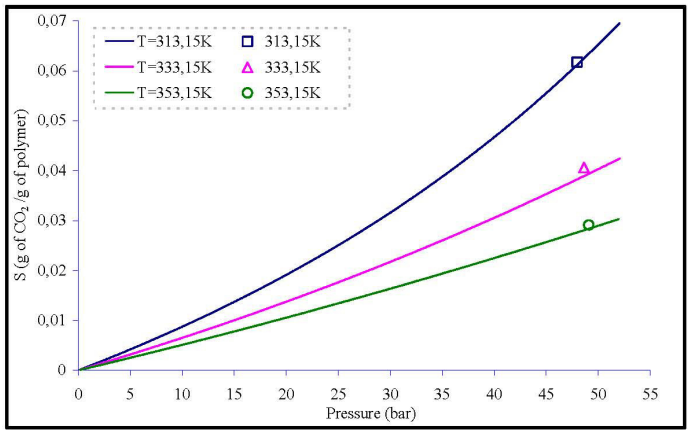

Figure 4.9 : Solubility of CO_2 in PTFE polymer as a function of pressure k_{ij} = -0,03. Points are experimental data and line is from simplified PC-SAFT at different temperatures.

CO_2 - PTFE + 10% Ekonol polymer

Figure 4.10 shows the solubility predictions using simplified PC-SAFT for CO_2-PTFE + 10%Ekonol polymer as a function of inverse temperature at pressure of 48.57bar. The carbon dioxide solubility in PTFE10%Ekonol decreases with increasing temperature. The results are exactly fitted to the modeled results with temperature independent factor binary interaction parameter $k_{ij} = -0.055$. Same k_{ij} value was used at all temperatures. Figure 4.11 shows the solubility predictions using simplified PC-SAFT for CO_2-PTFE+10%Ekonol as a function of pressure at different temperature 40 °C, 60 °C and 80 °C and solubility results are shown in Table 4.8. The solubility of carbon dioxide is high compare to the TFM polymer. The pure component parameters are calculated by using mixing rule to predict the solubility of carbon dioxide in this polymer.

Table 4.8 : Solubility of carbon dioxide in PTFE + 10% Ekonol (Experimental and simplified PC-SAFT results)

(simplified PC-SAFT)				Experimental Results		
Temperature [°C]	**Pressure** [bar]	**Solubility** $\left[\frac{\text{g of gas}}{\text{g of polymer}}\right]$	K_{ij}	**Pressure** (P_{avg}) [bar]	**Solubility** $\left[\frac{\text{g of gas}}{\text{g of polymer}}\right]$	**AAD** (%)
30	48.57	0.208	-0.055	-	-	6.219
40	48.57	0.138	-0.055	48.238	0.1217	
50	48.57	0.100	-0.055	-	-	
60	48.57	0.078	-0.055	48.511	0.0779	
70	48.57	0.063	-0.055	-	-	
80	48.57	0.052	-0.055	48.970	0.0550	
90	48.57	0.044	-0.055	-	-	

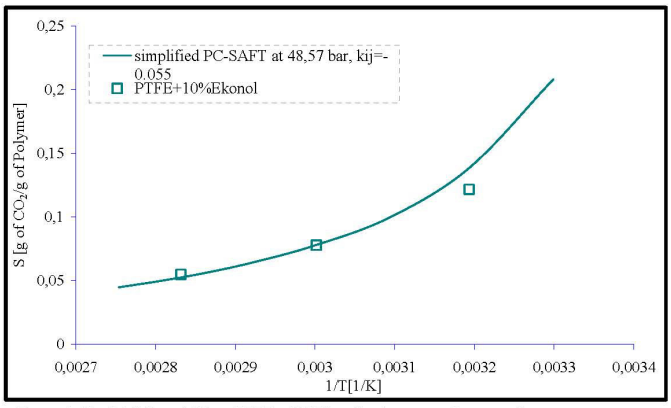

Figure 4.10 : Solubility of CO_2 in PTFE+10%Ekonol polymer as a function of inverse temperature. Points are experimental data and line is from simplified PC-SAFT

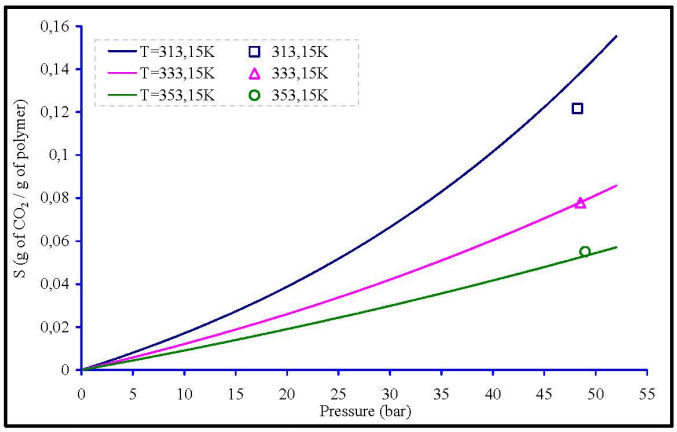

Figure 4.11 : Solubility of CO_2 in PTFE+10%Ekonol polymer as a function of pressure at k_{ij} = -0,055. Points are experimental data and line is from simplified PC-SAFT at different temperatures

CO_2- FKM polymer

FKM is composed with two polymers. It consist of 65% Poly (Difluoro ethane) and 35% Poly (Hexa fluoro propane). Figure 4.12 shows the solubility predictions using simplified PC-SAFT for CO_2- FKM polymer as a function of inverse temperature at pressure of 48.57bar. The carbon dioxide solubility in FKM decreases with increasing temperature. The results are exactly fitted to the modeled results with temperature independent factor binary interaction parameter $k_{ij} = 0.023$. Small binary interaction parameter k_{ij} is needed to fit the experimental data. Same k_{ij} value was used at all temperatures. Figure 4.13 shows the solubility predictions using simplified PC-SAFT for CO_2-FKM as a function of pressure at different temperature 40 ^oC, 60 ^oC and 80 ^oC and and solubility results are shown in Table 4.9. The pure component parameters are calculated by using mixing rule to predict the solubility of carbon dioxide in this polymer. Figure 4.13 shows that the solubility results in FKM polymer are follow a Henry's law (linear) at high pressures.

Table 4.9 : Solubility of carbon dioxide in FKM (Experimental and simplified PC-SAFT results)

(simplified PC-SAFT)				**Experimental Results**		
Temperature [^oC]	**Pressure** [bar]	**Solubility** $\left[\frac{\text{g of gas}}{\text{g of polymer}}\right]$	K_{ij}	**Pressure** (P_{avg}) [bar]	**Solubility** $\left[\frac{\text{g of gas}}{\text{g of polymer}}\right]$	**AAD** (%)
30	48.2	0.0915	0.023	-	-	1.746
40	48.2	0.0718	0.023	48.166	0.0694	
50	48.2	0.0593	0.023	-	-	
60	48.2	0.0505	0.023	48.035	0.0502	
70	48.2	0.0447	0.023	-	-	
80	48.2	0.03923	0.023	48.420	0.0397	
90	48.2	0.03535	0.023	-	-	

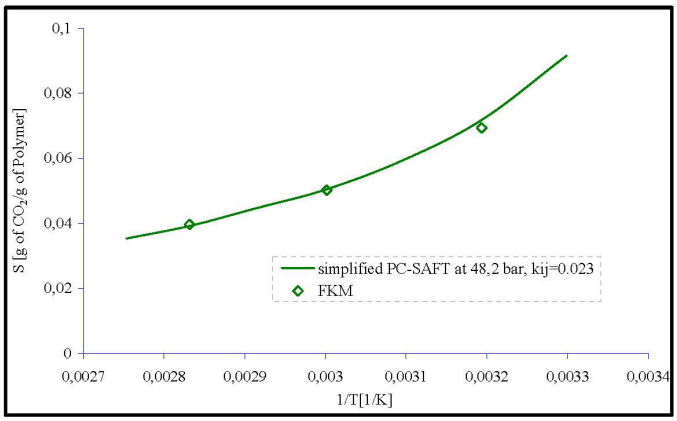

Figure 4.12 : Solubility of CO_2 in FKM polymer as a function of inverse temperature. Points are experimental data and line is from simplified PC-SAFT

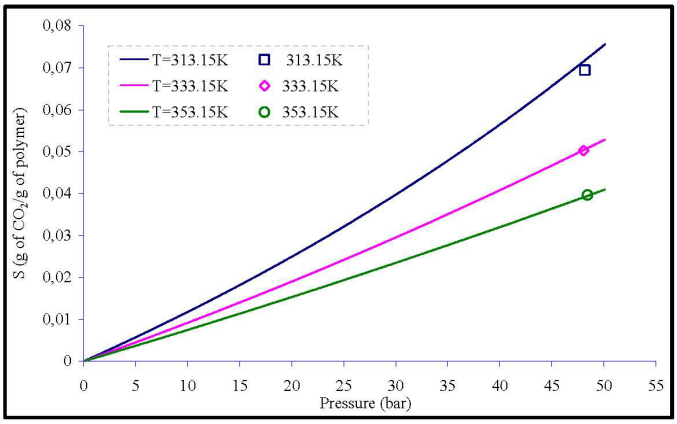

Figure 4.13 : Solubility of CO_2 in FKM polymer as a function of pressure at k_{ij} = 0,023. Points are experimental data and line is from simplified PC-SAFT at different temperatures

Chapter 5 : Conclusion

The high pressure permeation cell experimental set up was well suited for measuring the permeability of carbon dioxide gas in polymers. Permeability, Diffusivity and Solubility of carbon dioxide gas in polymers (TFM, glass filled TFM, PTFE, PTFE+10% Ekonol, PTFE with $PPSO_2$ and graphite and FKM) are measured at temperature range of 40-80 ^oC and pressure range of 45-50 bar. Carbon dioxide solubility in PTFE+10%Ekonol polymer is high compared to other polymers. The solubility of carbon dioxide in TFM is low compare to the PTFE polymer. It was observed that solubility data is linear dependence (Henry's law) on pressure at lower pressure. It was deviating at high pressures. We observed that the measurement of diffusivity by time-lag method based on extrapolation of the steady state region to the zero axis can lead to significant errors.

We have successfully modeled gas solubility in various polymers at high pressure and temperatures by using simplified PC-SAFT equation of state. A temperature-independent value k_{ij} used to correlate the experimental data successfully. In order to do this we need to find out the polymer and copolymer parameters. It was done successfully by an extrapolation method and (for copolymers) applying a mixing rule. The solubility data can improve the design of sealing and packing materials in carbon dioxide refrigeration plants.

Chapter 6 : List of References

[1] M. Bellstedt, F. Elefsen and Stefan S. Jensen ''Application of carbon dioxide refrigerant in industrial cold storage refrigeration plant'' Journal of Airah, June 2002.

[2] Jesse N. Lawrence ''Refrigeration fundamentals throughout History: methods used to obtain colder temperatures, and principles governing them'' Dept. of chemistry, Univ. of Alabama, A literature seminar, Feb'25th 2003.

[3] http://www.cartage.org.lb/en/themes/sciences/physics/Thermodynamics/Basic Thermodynamics/Refrigeration/Refrigeration.htm

[4] Amir F, David S. K. Ting, Wendy W. Yang ''Second law analysis of the transcritical CO_2 refrigeration cycle'' Energy conversion and Management, Vol. 45, pp. 2269-2281, 2004.

[5] B. Flaconneche, J. Martin and M.H .Klopffer ''Transport properties of gases in polymers: experimental methods'' Oil & Gas Science and Technology-Rev. IFP, Vol.56, No. 3, pp. 223-244, 2001.

[6] M.H Klopffer and B. Flaconneche ''Transport properties of gases in polymers: Bibliographic Review'' Oil & Gas Science and Technology-Rev. IFP, Vol.56, No.3, pp. 245-259, 2001.

[7] H.Lin, B.D. Freeman ''Gas solubility, diffusivity and permeability in poly (ethylene oxide)'' Journal of Membrane Science 239, pp. 105-117, 2004.

[8] Yoshiharu Tsujita ''Gas sorption and permeability of glassy polymers with micro voids'' et. al, Polym. Sci. Vol.28, pp. 1377-1401, 2003.

[9] Vaibhav Kulshrestha, K Awasthi, N K Acharya, M Singh and Y K Vijay ''Effect of temperature and α-irradiation on gas permeability for polymeric membrane'' Bull. Mater. Sci., Vol. 28, No. 7, pp. 643-646, December 2005.

[10] C.K Yeom, J.M. Lee, Y.T.Hong, K.Y. Choi, S.C. Kim ''Analysis of permeation transient of pure gases through dense polymeric membranes measured by anew permeation apparatus'' Journal of Membrane Science 166, pp. 71-83, 2000.

[11] Frisch, H. L. Pressure dependence of diffusion in polymers. J. Elastoplastics, pp. 130-132, 1970.

[12] Koros, W. J.; Chern, R. T. Separation of gaseous mixtures using polymer membranes. In Handbook of Separation Process Technology; R. W. Rousseau, Ed.; John Wiley & Sons, Inc.: New York, pp. 862-953, 1987.

[13] V.R. Gowariker, N. V. Viswanathan, Jayadev Sreedhar "Polymer Science" Published by New Age International (P) Ltd., pp. 173-198.

[14] Paula Hubbard and Thomas Blong, Dyneon "A primer on high-purity fluoro polymers offered for wet bench processes" Material Fluorpolymers: May 2004.

[15] http://www.plasticsmag.com

[16] http://www.amicon.com/ptfeproperties.htm

[17] http://www.boedeker.com/ptfe_p.htm

[18] Douglas R. Robello, Abraham Ulman and Edward J. Urankar ''Poly (p-phenylene sulfone)'' Macromolecules, Vol.26, pp. 6718-6721, 1993.

[19] Nicolas von Solms, Michelsen, M. L.; Kontogeorgis, G. M. ''Computational and physical performance of a modified PC-SAFT equation of state for highly asymmetric and associating mixtures." Ind. Eng. Chem. Res. Vol. 42, pp. 1098-1105, 2003.

[20] Kouskoumvekaki I.A., von Solms N., Lindvig T., Michelsen M.L., and Kontogeorgis G.M., A novel method for estimating pure component parameters for polymers, Application to the PC-SAFT Equation of state, Industrial and Engineering Chemistry Research, Vol. 43, pp. 2830-2838, 2004.

[21] DIPPR Information and Data Evaluation Manager (DIPPR 801 Database 2007)

[22]. Sako, T.; Wu, A. H.; Prausnitz, J. M. ''A Cubic Equation of State for High-Pressure Phase - Equilibria of Mixtures Containing Polymers and Volatile Fluids'' J. Appl. Polym. Sci. Vol. 38, 18-39, 1989.

[23] Patrik A. Rodgers ''Pressure-Volume-Temperature relationships for polymeric liquids: A Review of Equations of state and their Characteristic Parameters for 56 Polymers'' Journal of Applied Polymer Science, Vol. 48, pp. 1061-1080, 1993.

[24] N. von Solms, K.Y. Koo, Y.C.Chiew ''Mixing rules for binary Lennard Jones chains: theory and Monte Carlo simulation'' Fluid Phase Equilibria 180 pp. 71-85, 2001.

[25] Douglas Henderson and Peter J. Leonard ''One-and Two-Fluid vander Waals Theories of liquid Mixtures, I Hard Sphere Mixtures'' National Academy of Sciences, Vol. 67, No. 4, pp. 1818-1823, December 1970.

[26] Frisch, H. L. ''Pressure dependence of diffusion in polymers'' J. Elastoplastics 1970, 2,130-132.

[27] Nicolas von Solms, Nicoletta Zecchin, Adam Rubin, Simon I. Andersen, and Erling H. Stenby ''Direct measurement of gas solubility and diffusivity in poly (vinylidene fluoride) with a high-pressure microbalance'' European Polymer Journal, Vol. 41 pp. 341-348, 2005.

[28] Nicolas von Solms, Michelsen, M. L. and Kontogeorgis, G. M. ''Prediction and Correlation of High-Pressure Gas Solubility in Polymers with simplified PC-SAFT '' Ind. Eng. Chem. Res., 44, pp. 3330-3335, 2005.

[29] Joachim Gross, Oliver Spuhl, Freelly Tumakaka, and Gabriele Sadowski ''Modeling copolymer systems using the perturbed-chain SAFT equation of state'' Ind. Eng. Res., 42, pp. 1266-1274, 2003.

[30] Pedro Arce, Martin Aznar ''modeling the phase behaviour of commercial biodegradable polymers and copolymer in supercritical fluids'' October 2005

[31] J. Gross, and G. Sadowski, ''Perturbed-Chain SAFT: An Equation of State Based on a Perturbation Theory for Chain Molecules'' Ind. Eng. Chem. Res., Vol. 40 (4), 1244-1260, 2001.

[32] http://www.alperton.ie/alperton/Main/Plastic_ProductsByName.htm

[33] Amra Tihic, Nicolas von Solms, Michelsen, M. L. and Kontogeorgis, G. M. ''Application of simplified Perturbed-Chain Saft Equation of state'' et al.

[34] Michaels, A.S., and Parker, R.B. ''Sorption and Flow of Gases in Polyethylene'' J. Appl. Phys., Vol.34, pp.13-20, 1959.